UNIVERSITAT POLITÈCNICA DE CATALUNYA BARCELONATECH

Modelling emergent rhythmic activity in the cerebral cortex

Leonardo Dalla Porta Dornelles

UNIVERSITAT POLITÈCNICA DE CATALUNYA BARCELONATECH

IDIBAPS Institut D'Investigacions Biomèdiques August Pi i Sunyer

Modelling emergent rhythmic activity in the cerebral cortex

Author:
Leonardo Dalla Porta Dornelles, MSc

Supervisors:
Maria V. Sanchez Vives, MD, PhD
Alain Destexhe, PhD

A thesis submitted in fulfillment of the requirements for the degree of Doctor of Philosophy in Physical Science

System Neuroscience group
Cortical Networks lab
July 3, 2022

To my parents Roque Souza Dornelles and Ledir Dalla Porta Dornelles

"Educação não transforma o mundo
Educação muda pessoas
Pessoas transformam o mundo"

"Education does not change the world
Education changes people
People change the world"

Paulo Freire, Brazilian educator

Acknowledgements

First of all, I want to thank my supervisor, Mavi, for the opportunity to develop the thesis in her lab and for believing in me. Thank you for all the opportunities and the chance to participate in different projects, expanding my knowledge in neuroscience and contributing to my education. Also, thank you for the pieces of advice, professional and personal, and guidance throughout these years. I feel fortunate to have had the opportunity to work with you in such an interdisciplinary environment. Thank you!

To the co-supervisor of my thesis, Alain Destexhe, and to my thesis tutor, Toni Guillamon. Thank you for contributing to my education. To my past supervisors, Claudio Mirasso and Mauro Copelli, for proportioning me solid education to be here today, for your friendship, advice and collaboration. To Pedro Carelli and Fernanda Matias, for the wonderful collaboration and friendship throughout these years. Thank you all!

From the Sanchez-Vives lab, I want to thank all its members, past and present. Thank you all for directly or indirectly contributing to my formation during my Ph.D. journey. I feel lucky to have learned from all of you. Especially, I would like to thank Alessandra Camassa and Arnau Manasanch for being more than colleagues, for being my friends. All your support during these years significantly contributed to my professional formation and to my personal life. So, from the bottom of my heart, I thank you two! Also, during different scientific meetings, I was pleased to meet many people with whom I'm grateful for the time shared between conversations and scientific discussions.

I want to thank all my friends from Recife as well. I always remember that time with so much joy and love. I feel incredibly blessed to have had the opportunity to live with you. You have helped me expand my world vision, and I'm extremely grateful for that. Especially, I would like to thank Natalia Domingues Alves, who immensely contributed to the human being I'm today. Thank you so much for being who you are and contributing to my life. I will always be grateful to you!

To my life friends from São Borja and Santa Maria who, even physically distant, made their presence be felt on my journey. I feel blessed to count on your friendship. Canha, Carol, Guilherme, Hiti, Iuri, Jão, Lorenzo, Rafa Haas, Raul, Renanzinho, Marcelo, Gabe, Betinho, Piegas, Cabeleira, Wermuth, Gonzaga, Matheo e Luís, thank you all for standing by my side. Thank you, João, for tireless hours of gameplay. Particularly, I

would like to thank my non-blood brother Rafael Sasso. Thank you for more than a decade of company, support, and friendship and for sharing your beautiful family with me, making me feel like his brother, a sister to Ilca, and a son to his parents. Thank you for so much love and support over these years.

To my climbing family, thank you for making me feel so welcomed and loved in your presence. I couldn't be happier climbing together with you or just being in your company. Thanks Amanda Garcia Tirado, Giorgio Ballati, Gisela Guim, Gustavo Esquivias, Iñaki Beascoa, Javier *Dog* Barranco, Javier Fernandez, Jordi Sintes, Lidia Rodriguez, Paula Rivada, and Victor Cugat. Thank you, too, Pemi, for putting up with us.

I want to thank Amanda Garcia Tirando for sharing her life with me. You bring peace and calm to my world. Being at your side is a constant feeling of love and safety. Thank you so much for your unconditional support, kindness and care and for sharing your family with me.

Pai, mãe, e mano, o último e mais importante agradecimento que eu posso fazer é para vocês. Nada disso seria possível sem a estabilidade que vocês me proporcionaram ao longo da minha vida. Palavras nunca serão suficientes para expressar minha gratidão. Tenho muita sorte de ter vocês três como minha família. O apoio incondicional de vocês sempre foi o meu alicerce. Obrigado por tudo que vocês fazem e fizeram por mim. Pai, obrigado por ser esse homem exemplar, sólido e honesto. Mãe, obrigado por tanto amor, carinho, e cuidado. Pai e mãe, obrigado por cuidarem tão bem de nós, nunca deixando faltar nada em nossas vidas, especialmente amor e cuidado. Mano, muito obrigado por ser a presença física para nossos pais que eu não posso ser. Obrigado por ser quem tu és, com tua integridade e honestidade. Obrigado por trazer ao mundo, junto com Mariana, o pequeno Augusto. Família, meu amor e orgulho por vocês só crescem. Obrigado por tudo!

Abstract

The brain, a natural adaptive system, can generate a rich dynamic repertoire of spontaneous activity even in the absence of stimulation. The spatiotemporal pattern of this spontaneous activity is determined by the brain state, which can range from highly synchronized to desynchronized states. During slow wave sleep, for example, the cortex operates in synchrony, defined by low-frequency fluctuations, known as slow oscillations (< 1Hz). Conversely, during wakefulness, the cortex is characterized mainly by desynchronized activity, where low-frequency fluctuations are suppressed. Thus, an inherent property of the cerebral cortex is to transit between different states characterized by distinct spatiotemporal complexity patterns, varying in a large spectrum between synchronized and desynchronized activity. All these complex emergent patterns are the product of the interaction between tens of billions of neurons endowed with diverse ionic channels with complex biophysical properties. Nevertheless, what are the mechanisms behind these transitions? In this thesis, we sought to understand the mechanisms and properties behind slow oscillations, their modulation and their transitions towards wakefulness by employing experimental data analysis and computational models. We reveal the relevance of specific ionic channels and synaptic properties to maintaining the cortical state and also get out of it, and its spatiotemporal dynamics. Using a mean-field model, we also propose bridging neuronal spiking dynamics to a population description.

Resumen

El cerebro, un sistema adaptativo natural, es capaz de generar un amplio repertorio dinámico de actividad espontánea, incluso en ausencia de estímulos. La patrón espacio-temporal de esta actividad espontánea viene determinada por el estado cerebral, el cual puede variar de estados altamente sincronizados hasta estados muy desincronizados. Cuando en el sueño se entra en la fase de ondas lentas, por ejemplo, la corteza opera en sincronía, cuya actividad es definida por fluctuaciones de baja frecuencia, conocidas como oscilaciones lentas (< 1Hz). En cambio, durante la vigilia, el córtex se caracteriza principalmente por tener una actividad desincronizada, donde las fluctuaciones de baja frecuencia desaparecen. Por lo tanto, una propiedad inherente de la corteza cerebral es transitar entre diferentes estados caracterizados por distintos patrones de complejidad espacio-temporal, los cuales se sitúan dentro del amplio espectro marcado por la actividad sincronizada y la desincronizada. Estos patrones emergentes son el producto de la interacción entre decenas de miles de millones de neuronas dotadas de múltiples y distintos canales iónicos con complejas propiedades biofísicas. Sin embargo, ¿cuáles son los mecanismos que regulan estas transiciones? En esta tesis tratamos de entender los mecanismos, propiedades y sus transiciones hacia la vigilia, que están detrás de las oscilaciones lentas a través del uso y análisis de datos experimentales y modelos computacionales. En ella describimos la importancia de los canales iónicos específicos y sus propiedades sinápticas tanto para mantener el estado cortical como para salir de él, estudiando así su dinámica espacio-temporal. Además, mediante el uso de un modelo de campo medio, proponemos establecer un puente que pueda describir la dinámica de disparos neuronales con una descripción general de la población neuronal.

Publications

- **A mean-field approach to the dynamics of networks of complex neurons, from nonlinear Integrate-and-Fire to Hodgkin–Huxley models** [Carlu et al., 2020].
  M. Carlu, O. Chehab, **L. Dalla Porta**[†] et al.
  [†] shared first-author.
  Journal of Neurophysiology, 2020.
- **Impact of $GABA_A$ and $GABA_B$ Inhibition on Cortical Dynamics and Perturbational Complexity during Synchronous and Desynchronized States** [Barbero-Castillo et al., 2021].
  A. Barbero-Castillo, P. Mateos-Aparicio, **L. Dalla Porta** et al.
  The Journal of Neuroscience, 2021.
- **Proceedings: Fast and slow inhibition on cortical spatiotemporal complexity in a computational model of the cerebral cortex** [DALLA PORTA and Sanchez-Vives, 2021].
  L. Dalla Porta, and M. Sanchez-Vives.
  Journal of Computational Neuroscience, 2021.
- **Impact of potassium currents on the dynamics opf the cortical network**.
  L. Dalla Porta, A. Compte, and M. Sanchez-Vives
  In preparation.
- **Role of SK calcium-activated potassium current on cortical slow oscillations**.
  L. Dalla Porta, L. Kargieman, and M. Sanchez-Vives
  In preparation.
- **Modulation of M-current during spontaneous cortical slow oscillations**.
  L. Dalla Porta, A. Barbero-Castillo, and M. Sanchez-Vives
  In preparation.
- **Hyperpolarization-activated cation current modulation during cortical spontaneous activity**.
  L. Dalla Porta, A. Barbero-Castillo, A. Destexhe, and M. Sanchez-Vives
  In preparation.
- **Exploring the Phase-Locking Mechanisms Yielding Delayed and Anticipated Synchronization in Neuronal Circuits** [Dalla Porta et al., 2019].
  L. Dalla Porta et al.
  Frontiers in Systems Neuroscience, 2019. Not included in this thesis.

- **Feedforward and feedback influences through distinct frequency bands between two spiking-neuron networks** [Dalla Porta et al., 2021].
  L. Dalla Porta et al.
  Physical Review E, 2021. Not included in this thesis.

Funding

This Thesis work has been possible thanks to the following funding:

- R+D+i project CORTICOMOD PID2020 – 112947RB–I00 financed by MCIN / AEI /10.13039/501100011033.
- European Union's Horizon 2020 Framework Programme for Research and Innovation under the Specific Grant Agreement No.945539 (Human Brain Project SGA3).
- Commission for Universities and Research of the Department of Innovation, Universities, and Enterprise of the Generalitat de Catalunya -AGAUR- (IU16 – 011508) and co-financed by the European Union Regional Development Fund within the framework of the ERDF/FEDER Operational Program of Catalonia.

Contents

Chapter 1

Introduction

Synchronization is a remarkable collective phenomenon that emerges through the interaction between components of a complex system. Remember the last time you went to a concert or a theater. Usually, after a good performance, the audience starts to clap incoherently, producing a noisy sound. Suddenly, it turns out to be an almost unison phenomenon due to emergent synchronization [Néda et al., 2000]. Another example of synchronization is the famous experiment of two pendulum clocks hanging from the same beam that, after a while, start swinging in perfect synchrony [Strogatz and Stewart, 1993]. An essential key requirement for these kinds of phenomena is communication. The first example is established by auditory perception, while the second is through small forces exerted on the supporting beam. Similarly, interconnected neurons in the human brain, which communicate through action potentials, often show the emergence of spontaneous oscillations [Buzsaki, 2006, Wang, 2010]. Neuronal oscillations were first observed in 1938, through measures of electrical potentials in the human scalp [Berger, 1938]. Since then, a variety of frequencies have been described in the human brain, but not only, these periodic rhythms were also observed presently in other mammals with the same aspects, like duration or temporal evolution [Buzsáki et al., 2013]. Even more, different rhythms can coexist and interact with each other [Steriade et al., 2001, Buzsaki and Draguhn, 2004].

The synchronization of neuronal networks, in the form of oscillations of different frequencies, has been associated with different brain states, such as sleep or awake rest, and with cognitive processes, including memory formation, attention, and the processing of sensory stimuli (see for a review [Ward, 2003, Wang, 2010]). One striking pattern that can be observed in physiological NREM (non-rapid eye movement) sleep is slow oscillations (SO). This global pattern propagates through the cerebral cortex as a traveling wave [Massimini et al., 2004]. However, this pattern is not exclusive to NREM sleep, which is one of the most curious aspects. SO are an emergent pattern under conditions where the cortex has been functionally disconnected, such as during deep

anesthesia [Chauvette et al., 2011, Steriade et al., 1993c], cortical slabs [Timofeev et al., 2000], focal brain lesions [Butz et al., 2004], or white matter lesions [Gloor et al., 1977]. More recently, SO have been detailed characterized around stroke and radio-frequency thermocoagulation lesions done in surgery of epilepsy [Sarasso et al., 2020, Russo et al., 2021]. Furthermore, SO are spontaneously expressed in cortical slices without any chemical or electrical stimulation [Sanchez-Vives and McCormick, 2000]. Strikingly, slow oscillations display similar characteristics in all these cases, expressing a multiscale phenomenon. For these reasons, this emergent pattern has been suggested as the default mode of activity of the cerebral cortex [Sanchez-Vives and Mattia, 2014, Sanchez-Vives et al., 2017].

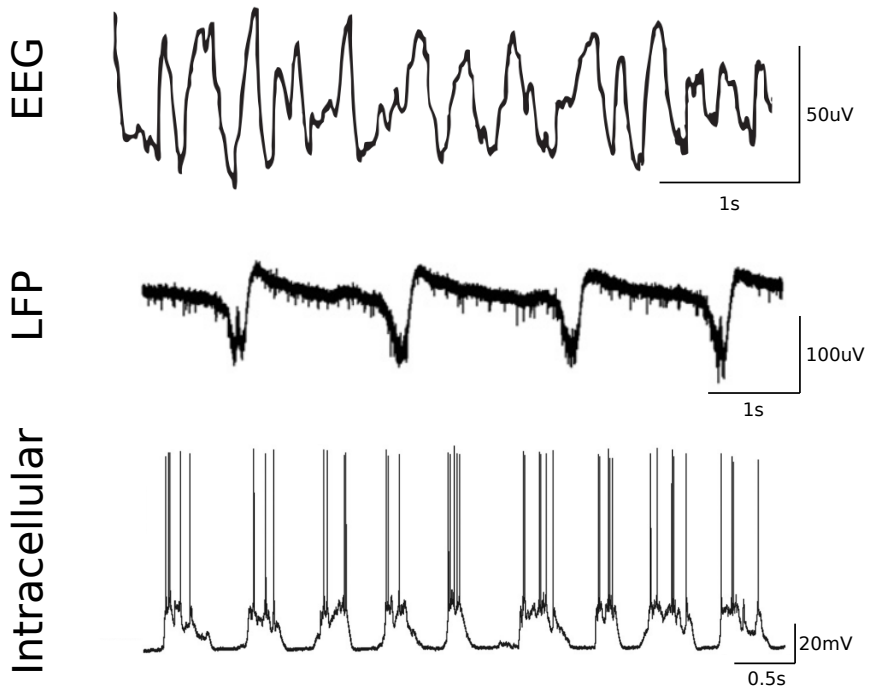

Figure 1 – Slow oscillations at different scales. Top: electroencephalogram (EEG) during NREM sleep (extracted from from [Brown et al., 2012]). Middle: spontaneous local field potentails (LFP) recorded in cortical slices (extracted from from [Barbero-Castillo et al., 2021]). Bottom: intracellular recordings of pyramidal cells on auditory cortex in anesthetized rat (extracted from from [Reig et al., 2015]).

1.1 Slow oscillations and their characterization

In 1993 Steriade and collaborators first described the slow wave activity in a series of three articles [Steriade et al., 1993a, Steriade et al., 1993b, Steriade et al., 1993c].

Slow oscillations (SO) are a hallmark of unconscious[§] brain states, such as deep sleep. SO are a synchronized network phenomenon characterized by periodic, or almost periodic, alternations between phases of neuronal depolarization (Up states) followed by phases of neuronal hyperpolarization (Down states, also called off-periods). This Up and Down alternation can be observed at different scales, micro (intracellular), meso (LFP), and macro (EEG) (Fig. 1). While the Up state is mediated by a balance between excitatory and inhibitory postsynaptic potentials [Sanchez-Vives and McCormick, 2000, Compte et al., 2009], the Down state is characterized by almost no synaptic activity and by the presence of afterhyperpolarization currents, such as activity-dependent slow K^+ current [Compte et al., 2003, Sanchez-Vives et al., 2010].

The Up state emerges from the cerebral cortex's recurrent connectivity [Lorente de No, 1938], which can induce reverberating neuronal firing in the circuit [Metherate and Ashe, 1993, Contreras et al., 1996, Sanchez-Vives and McCormick, 2000, Compte et al., 2003, McCormick and Yuste, 2006]. More specifically, the Up state has been reported to start in infragranular layer 5, which then propagates to deeper and more superficial layers [Sanchez-Vives and McCormick, 2000, Chauvette et al., 2010]. The persistent activity during the Up state is thought to depend mainly on recurrent excitatory synaptic activity, balanced by synaptic inhibition. Excitatory synaptic potentials (EPSPs) and inhibitory ones (IPSPs) are equally distributed during Up states [Compte et al., 2003, Compte et al., 2009]. Indeed, it has been demonstrated that an imbalance between excitation and inhibition has an impact on the Up state: while removal of fast inhibition ($GABA_A$) induces shorter Up states [Sanchez-Vives et al., 2010], removal of slow inhibition ($GABA_B$) induces larger Up states [Mann et al., 2009, Perez-Zabalza et al., 2020, Sanchez-Vives et al., 2021].

A disruption in the Up state occurs when the network cannot maintain self-sustained firing. Adaptation mechanisms are an essential mechanism for the recurrent network to generate slow oscillations (Fig. 2A) [Mattia and Sanchez-Vives, 2012]. Within the different potential adaptation mechanisms, slow potassium currents are thought to play a crucial role in generating negative feedback that will overcome the positive feedback inherent in local circuits, bringing the network to a period of almost no more firing, i.e., a Down state (Fig. 2B) [Sanchez-Vives and McCormick, 2000, Compte et al., 2003]. Steriade and collaborators [Steriade et al., 1993c], in the first characterization of cortical slow oscillations, have suggested the calcium-dependent potassium (KCa) channel as one of the mechanisms responsible for the termination of Up states, based upon the slow afterhyperpolarization (AHP) of the action potentials. In an experimental work, Sanchez-Vives and McCormick have suggested that the activation of sodium-

[§] We stay here with the following definition of conscious: "being conscious means that one is having an experience — the subjective, phenomenal 'what it is like' to see an image, hear a sound, think a thought or feel an emotion."[Koch et al., 2016]

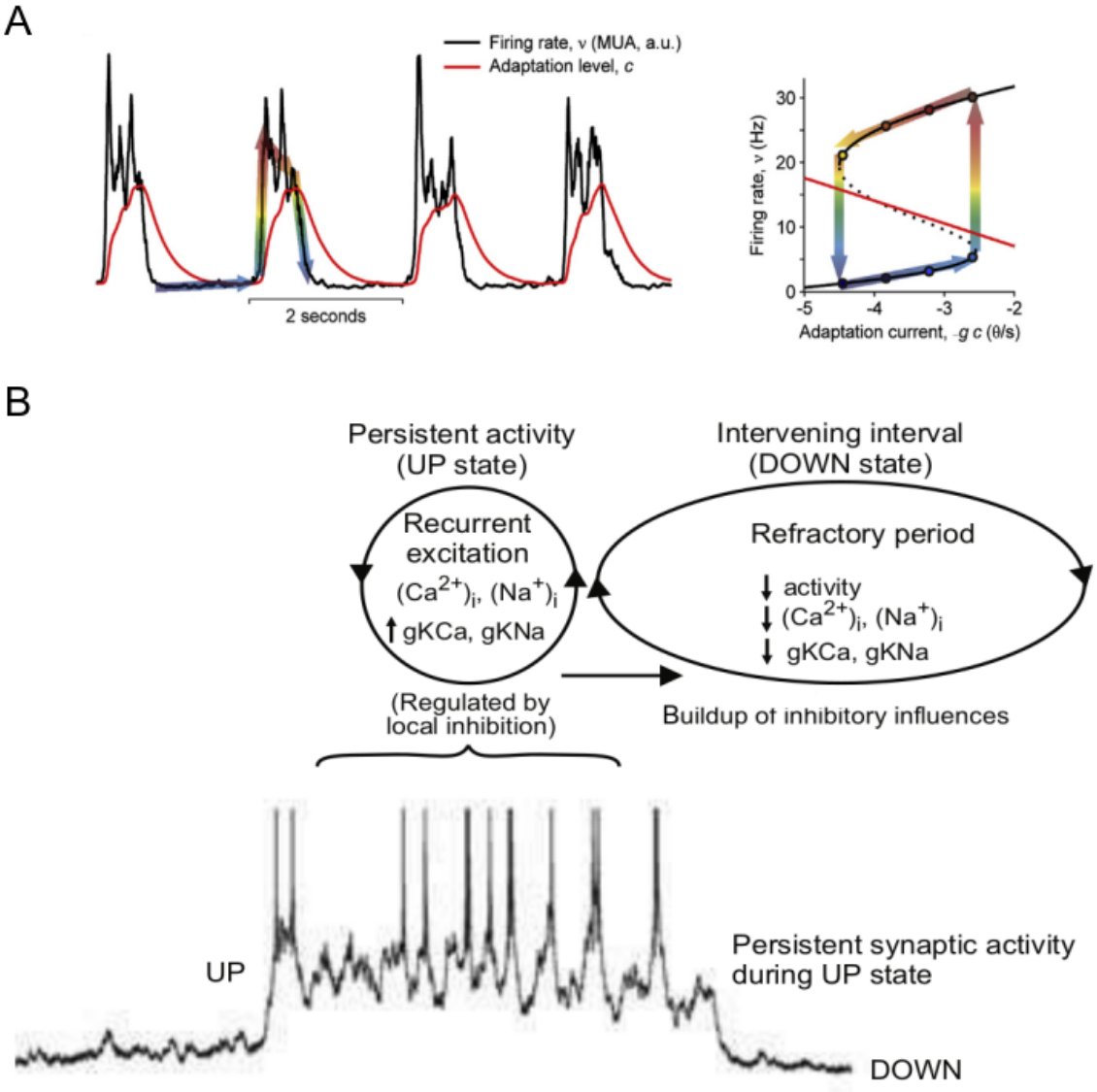

Figure 2 – Adaptation mediates Up and Down transitions. (A) Schematic representation of the cycle between Up and Down states where firing rate and adaptation current are responsible for the switches between states. Extracted from [Sanchez-Vives et al., 2017], originally adapted from [Mattia and Sanchez-Vives, 2012]. (B) A more detailed schematic representation of the cycle between Up and Down states. Slow potassium currents (I_{KCa} and I_{KNa}, see text) are suggested as the main mechanisms for the transition between Up to Down states. Extracted from [McCormick and Yuste, 2006].

dependent potassium (KNa), an AHP current, may also play a role on the termination of Up states [Sanchez-Vives and McCormick, 2000]. Indeed both channels, KCa and KNa, are inhibited by acetylcholine (ACh) [Schwindt et al., 1989, McCormick and Williamson, 1989]. ACh is one of the neurotransmitters responsible for wakefulness. There is a high concentration of ACh during wakefulness states while during NREM sleep a low concentration is observed [Jones, 2005]. Steriade and collaborators have showed that by

stimulation of brainstem nuclei, i.e., neurons that release ACh to the cortex, induced an state mimicking natural brain arousal through muscarinic receptors. In other words release of ACh disrupts the Up and Down dynamics characteristic of SO [Steriade et al., 1993a]. Another important channel that is also modulated by ACh and is known for regulating neuronal excitability is the voltage gated K^+ channel (K_{v7}) that generates the M-currents [Brown, 2010]. Despite the suggestions about the role of K^+ channels on the termination of Up states, the role of M-current remains to be explored [Neske, 2016].

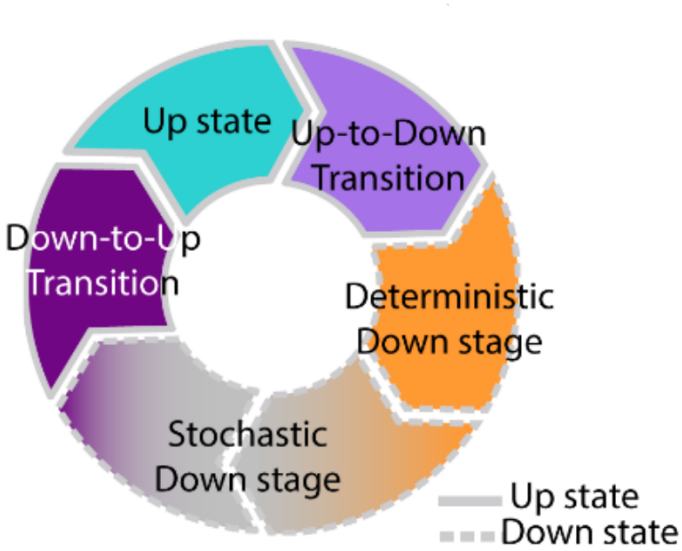

Figure 3 – Oscillatory cycle representation. Adapted from [Camassa et al., 2021a]. The Down state is proposed as been an metastable state composed of a deterministic and stochastic phase.

When the adaptation overcomes the activation, the network falls into a period of silence, i.e., into a Down state. As just discussed, a candidate mechanism for the initiation of Down states are the slow K^+ channels responsible for the afterhyperpolarization currents. Once the Down state is reached, neurons are in the refractory period, and the AHP currents slowly decrease in amplitude. The decay time of AHP currents is suggested to set the time scale for the reappearance of spontaneous firing that will be able to trigger a new Up state and so are thought to be responsible for the oscillatory cycle [Compte et al., 2003]. However, other mechanisms have been proposed to set the time scale of slow oscillations, such as synaptic depression [Holcman and Tsodyks, 2006, Benita et al., 2012], thalamic disfacilitation [Contreras et al., 1996], and $GABA_B$ activation [Mann et al., 2009, Perez-Zabalza et al., 2020, Sanchez-Vives et al., 2021]. Indeed, experimental observations have shown that, in the case of extreme long Down states, it could not be maintained only by AHP currents due to its intrinsic time scale [Sanchez-Vives et al., 2010]. Therefore, the duration of the Down state is not only set by the AHP's currents duration but also by the time it takes for the mechanisms that give rise to a new Up state

to build up, as, for example, the summation of randomly occurring miniature synaptic potentials, a mechanism proposed of Up state initiation in cortical slabs [Timofeev et al., 2000]. Another intrinsic mechanism, not dependent on K^+-channels, has also been proposed to regulate the duration of Down states. Hill and Tononi, in a thalamocortical model of sleep and wakefulness, have suggested that the removal of H-current is able to increase the Down state duration [Hill and Tononi, 2005]. H-current is a noninactivating hyperpolarization-activated cation current believed to be critical to the generation of slow rhythms in the thalamocortical system [Lüthi and McCormick, 1998b, Lüthi and McCormick, 1999]. Therefore, the Down state may be regulated by the participation of many mechanisms. Indeed, recently, Camassa and collaborators have proposed a view that summarizes this oscillatory frequency of slow oscillations [Camassa et al., 2021a]. They have proposed that the Down state is a metastable state composed of a deterministic and stochastic phase (Fig. 3). The deterministic phase is set by the intrinsic currents, while the stochastic phase is where random neuronal fluctuations would be critical to trigger a new Up state.

1.2 Brain complexity

Slow oscillations are a hallmark of physiological slow-wave sleep [Steriade, 2000, Massimini et al., 2004], but not exclusively, SO is also an emergent pattern during pathological conditions as coma, and drug induced states as deep anesthesia [Alkire et al., 2008, Dasilva et al., 2021a]. All these states have one thing in common, they are indicators of unconscious states. Thus, understanding the mechanisms behind SO may also help us to understand consciousness. One of the parameters that has been proposed as a signature of the level of consciousness is brain complexity, which relies on the balance between segregation and integration within a neural system [Tononi et al., 1994].

One of the existing approach to quantifying brain complexity is to induce a perturbation of the system to investigate the causal interactions that follow. The perturbational complexity index (PCI) [Casali et al., 2013, Comolatti et al., 2019], in which neural activity is exogenously perturbed by means of stimulation (transcranial magnetic stimulation or electrical stimulation) has been proposed as one such measure. This method has been validated for different instances such as physiological brain states [Casali et al., 2013], anesthesia levels [Sarasso et al., 2015, Dasilva et al., 2021b, Arena et al., 2021], and disorders of consciousness [Casarotto et al., 2016, Rosanova et al., 2018]. The PCI approach presents advantages with respect to an observational one (based on spontaneous activity[†]) because it is less affected by noise or isolated processes, and only

[†] A variety of such measures exist, including Lempel–Ziv compressibility [Szczepański et al., 2003, Hudetz et al., 2016], Shannon entropy [Zhao et al., 2010], entropy of wave propagation [Barbero-Castillo et al., 2019], and functional complexity [Zamora-López et al., 2016], among others

assesses information generated through deterministic interactions, which also gives advantages that are useful clinically [Casali et al., 2013].

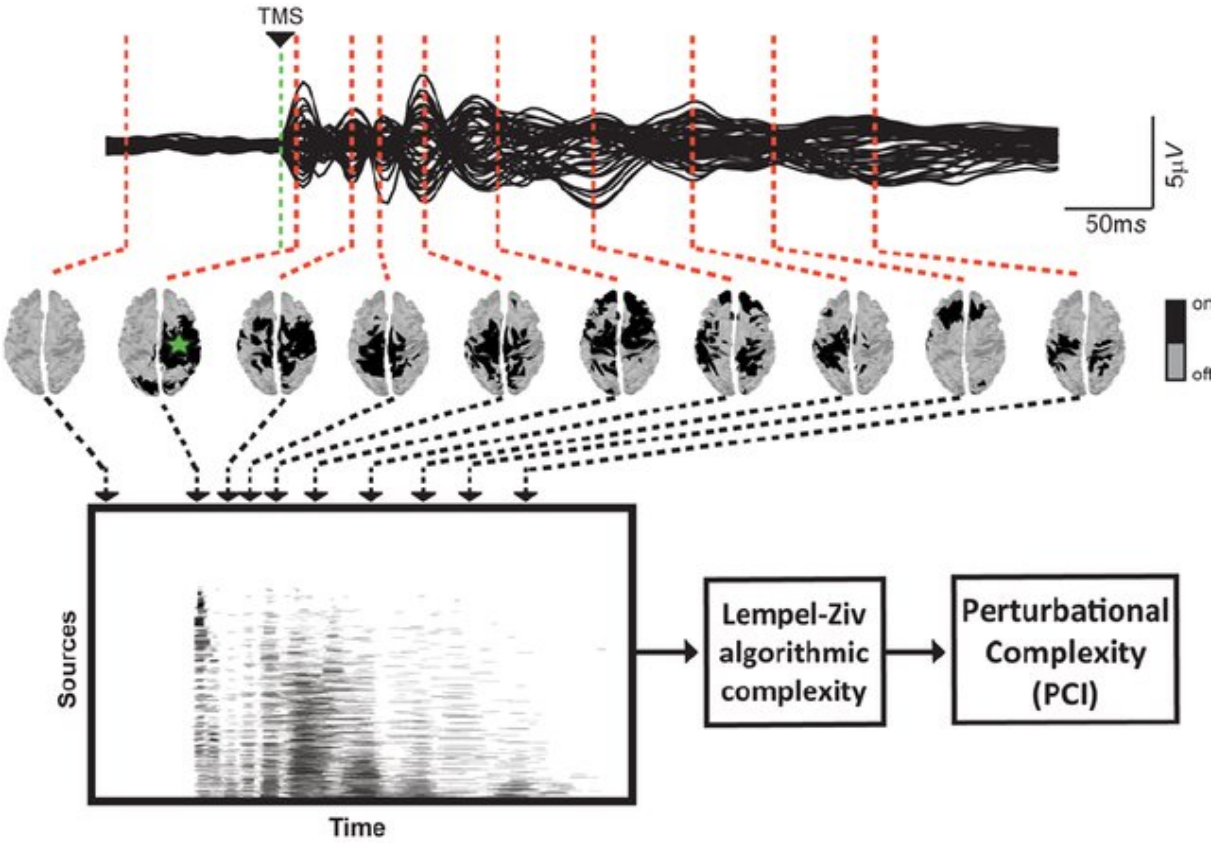

Figure 4 – Calculating the Perturbational Complexity Index (PCI). Extracted from [Sarasso et al., 2014], originally adapted from [Casali et al., 2013]. PCI is defined as the normalized Lempel-Ziv algorithmic complexity of the binary spatiotemporal matrix of significant cortical activation measured by EEG and triggered by exogenous stimulation (TMS). It is expected a low PCI value when there is a disruption in the segregation and integration balance, while it will by high when the balance is kept.

PCI consists of the estimation of the normalized Lempel-Ziv complexity [Ziv and Lempel, 1977, Ziv and Lempel, 1978] of the spatiotemporal matrix of cortical activation after perturbation (Fig. 4). Thus, PCI reflects cortical complexity in an index [Casali et al., 2013]. While conscious states present high values of PCI (high complexity), unconscious states present low values of PCI (low complexity). In these two cases, cortical responses are totally different: while during conscious the response if more heterogeneous and widespread, during unconscious states it is more homogeneous and local. In order to explore the underlying cellular and network mechanisms behind cortical complexity, D'Andola and collaborators adapted the PCI measure to *in vitro* slice experiments, known as slice PCI (sPCI) [D'Andola et al., 2018]. They showed that when the local network switched from a slow oscillatory state to a desynchronized state, the bistability of Up/Down states was reduced and there was an increase in sPCI. In this way, the isolated

cortical network *in vitro* was validated as a system which cannot only spontaneously generate slow oscillations [Sanchez-Vives and McCormick, 2000] and mimic other brain states [Mattia and Sanchez-Vives, 2012, Markram et al., 2015], but can also be used to investigate the cellular mechanisms of cortical complexity [D'Andola et al., 2018].

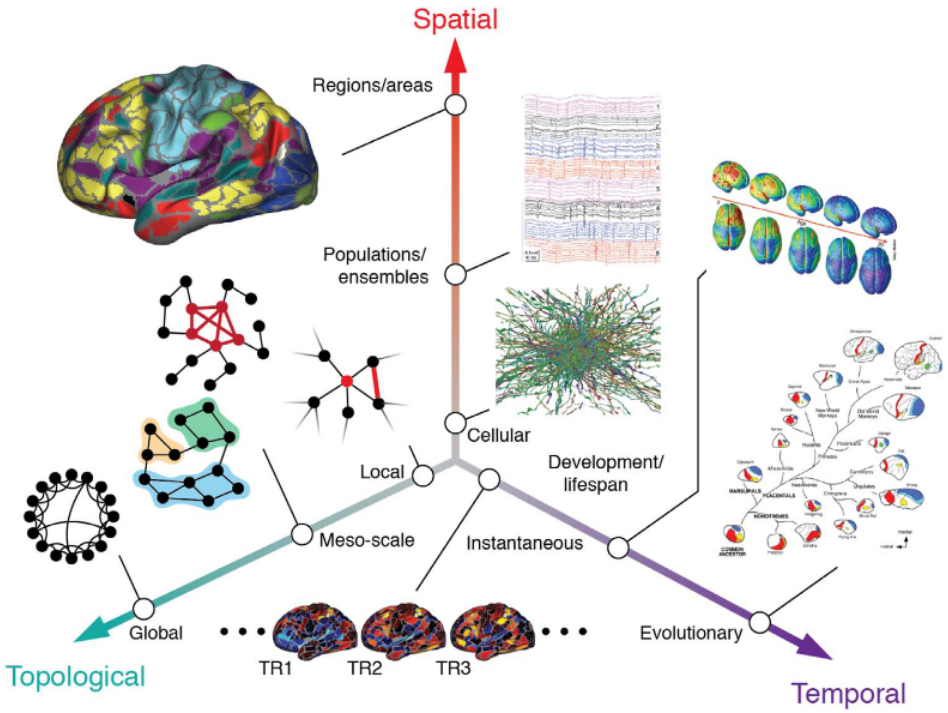

Figure 5 – Multiple spatiotemporal representations of the brain. Extracted from [Betzel and Bassett, 2017].

1.3 Computational modelling of brain components

Computational models are simplified versions of an experimental system and are ideally constrained by experimental data. However, in neuroscience, experimental data exists at many different spatial, temporal and topological scales and so do models (Fig. 5). Theoretical models are normally divided into two categories: biophysical and simplified. While the former takes into account the models of ionic channels and, for that, has a biophysical correspondence, the latter takes into account dynamical features to generate a spike and thus has a dynamical correspondence.

Biophysical modelling is rooted in the seminal work of A. Hodgkin and A. Huxley [Hodgkin and Huxley, 1952]. Studying the giant squid nerve fiber, they were the first to mathematically described how action potentials are initiated and propagated (Fig. 6). The HH (Hodgkin-Huxley) model is a four-dimensional dynamical system that

describe in details the generation of an action potential by activation and inactivation of sodium current (I_{Na}) and activation of potassium current (I_K). Its equation reads:

$$C_m \frac{dV}{dt} = -I_{Na} - I_K - I_L + I_{syn}, \tag{1.1}$$

with

$$I_j = g_j m^M h^N (V - V_j). \tag{1.2}$$

V is the membrane potential and C_m is the specific capacitance of the membrane. I_j describes the voltage-dependent currents ($j \in [Na, K]$), and I_L is the leakage current. The gating variables m and h are governed by the first-order kinetics equation $dx/dt = \phi[\alpha_x(V)(1-x) - \beta_x(V)x] = \phi[x_\infty(V) - x]/\tau_x(V)$. The original model is based only on two voltage-depended currents and thus cannot account for the wide diversity of intrinsic cellular properties, such as adaptation to long-lasting stimuli or the dependency of some conductances on various ionic concentrations. However, since the proposed HH model, plenty of ionic currents have been described and, even more, modeled using the same general framework proposed by Hodgkin and Huxley [Gerstner et al., 2014]. Thus, an HH model can be constructed with a variety of ion channels, each of them capable of a wide range of behaviors, from regular spiking to bursting, for example [Koch and Segev, 1998, Pospischil et al., 2008, Catterall et al., 2012]. Following the HH framework, other simplified biophysical model versions have been proposed [Gerstner et al., 2014]. One example is the Morris-Lecar model (see Sec. 3.2.2 for a mathematical description): a two-dimensional minimal model composed of I_K and calcium current (I_{Ca}) where the gate variables are modeled using hyperbolic functions. This model is useful when only qualitative or semi-quantitative characterizations of an action potential are required [Morris and Lecar, 1981, Rinzel and Ermentrout, 1998]. Variations of this model have also been employed in the literature [Estarellas et al., 2020].

In turn, the simplified modeling approach seeks to reproduce the dynamics of an action potential without necessarily having a biophysical correspondence. A simplified neuron model largely used is the integrate-and-fire model. Its equation reads:

$$\tau_m \frac{dV}{dt} = f(V) + I. \tag{1.3}$$

In this scenario, whenever V crosses a threshold V_{th}, one spike is emitted and, after a refractory period, the membrane potential (V) is reset to V_{res}. τ_m is the membrane time constant of the neuron and I is the current input. This is the general form of integrate-and-fire model. Variations of this model are made by choosing the function $f(V)$. For instance, if $f(V) = 0$ we have the perfect integrate-and-fire model. And, if $f(V) = -V + \Delta_T exp(\frac{V - V_{th}}{\Delta_T})$, we have the so called exponential integrate-and-fire. These models are very useful for analyzing the behavior of the neural system once the membrane potential is described only in terms of synaptic inputs and the injected current

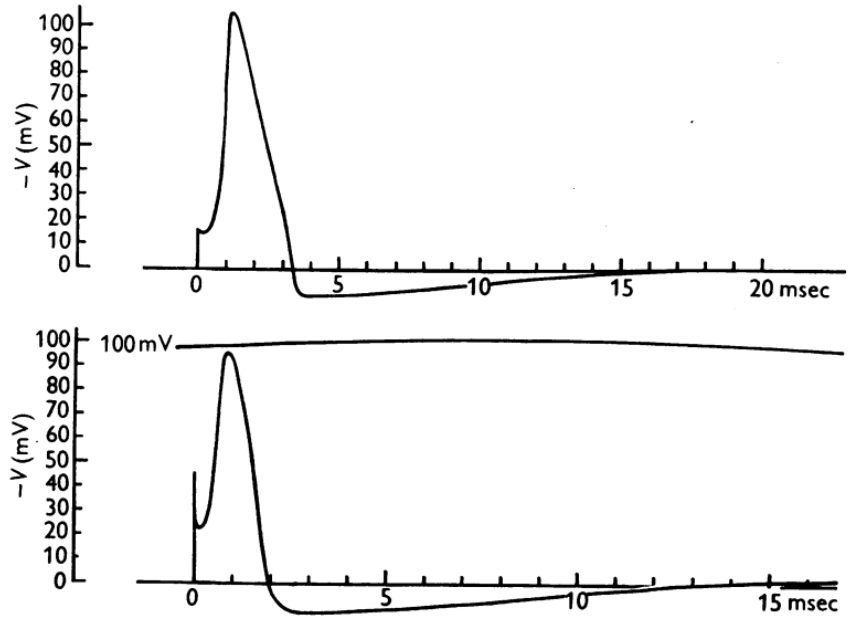

Figure 6 – First mathematical description of an action potential. Extracted from [Hodgkin and Huxley, 1952]. Top, Hodgkin-Huxley model simulations of an action potential. Bottom, experimental recording of an action potential.

(both are included in the I term). However, this kind of models lacks the description of an important feature of neurons: spike-frequency adaptation. To overcome this problem another variable is introduced into the system. Its equation reads:

$$\tau_m \frac{dV}{dt} = f(V) - w + I, \tag{1.4}$$

where,

$$\tau_w \frac{dw}{dt} = g(V, w). \tag{1.5}$$

If $f(V) = -V + \Delta_T exp(\frac{V - V_{th}}{\Delta_T})$ and $g(V, w) = aV - w + b\tau_w \sum \delta(t - t')$ we have the so called adaptive exponential integrate-and-fire (AdEx) model [Brette and Gerstner, 2005]. Now, for instance, if we choose $f(V) = \alpha V^2 + \beta V + \gamma$ and $g(V, w) = a(bV - w)$ we have the Izhikevich neuron model [Izhikevich, 2003]. Both of these models have been largely used in computational neuroscience due its simplicity and spiking patterns versatility through parameter tuning [Muller and Destexhe, 2012, Gollo et al., 2014, Górski et al., 2021, Dalla Porta et al., 2021] (see Fig. 2 in [Izhikevich, 2003] and Fig. 6.1 in [Gerstner et al., 2014]).

Another class of simplified modelling approach was introduced by Wilson and Cowan [Wilson and Cowan, 1972]. They described the dynamics of a population of neurons though a well-known differential equation where the input-output gain function is described by a sigmoid. These models are usually called "rate models" and permit a qualitative insight into the dynamics of a population of neurons [Wilson and Cowan,

1972, Hopfield, 1984, Sussillo and Abbott, 2009]). Moreover, a large effort has been made to derive population descriptions from the specificity of the network model under consideration. This bottom-up approach permits to obtain a dimensionally reduced mean-field description of the network population dynamics in different regimes [Amit and Brunel, 1997, van Vreeswijk and Sompolinsky, 1998, El Boustani and Destexhe, 2009, Capone et al., 2019b]. On one hand, these models permit a simpler, reduced picture of the dynamics of a population of neurons, thus allowing to unveil mechanisms determining specific observed phenomena [Reig et al., 2015, Jercog et al., 2017]. On the other hand, they enable a direct comparison with experimental studies where the spatial resolution implies that the recorded field represents the average over a large population of neurons (i.e., a mean field) [Capone et al., 2019b, Chemla et al., 2019]. We introduce the mean-filed formalism with more details in Sec. 3.2.3.

1.3.1 Network models for the slow oscillations

In the context of slow oscillations (SO), different models have been proposed, from simplified to biophysical detailed models. As an example of a simplified model of SO, Capone and collaborators reconstruct the SO dynamics observed in cortical slices through the use of large-scale network of spiking neurons (integrate-and-fire model) and mean-field models [Capone et al., 2019b]. By semi-quantitatively matching their model with the measured slow oscillations, they have explored how spontaneous activity in the form of slow oscillations is shaped by laminar structure. Their model suggests that excitability in layers 4 and 5 together with weakly stable Down state are ingredients for an optimal sensitivity and richness of the wave propagation. In turn, in light of SO biophysical mechanisms, at least three models have been proposed: two models of thalamocortical system [Bazhenov et al., 2002, Hill and Tononi, 2005], and one of the isolated cortical network [Compte et al., 2003]. The later has been able to predict many features of cortical slow oscillations and has been adapted, for instance, to study of cortico-hippocampal networks [Taxidis et al., 2013] and also for the study of endogenous electric fields [Fröhlich and McCormick, 2010].

The original model, by Compte and collaborators, was built based on experimental observations of the cortical slow oscillations *in vitro* slices [Sanchez-Vives and McCormick, 2000, Wang et al., 2003, Compte et al., 2003]. It consists of 1024 excitatory cells and 256 inhibitory cells modeled with detailed Hodgkin–Huxley-type channels and interconnected through realistic synaptic dynamics. Due to its recurrent connectivity and adaptation currents, mostly due to the sodium- and calcium-dependent potassium current (I_{KNa} and I_{KCa}, respectively), the model is able to switch back and forth between Up and Down states (Fig. 7). This model has been used in order to shed light on the mechanisms of different aspects of the SO. In experiments during

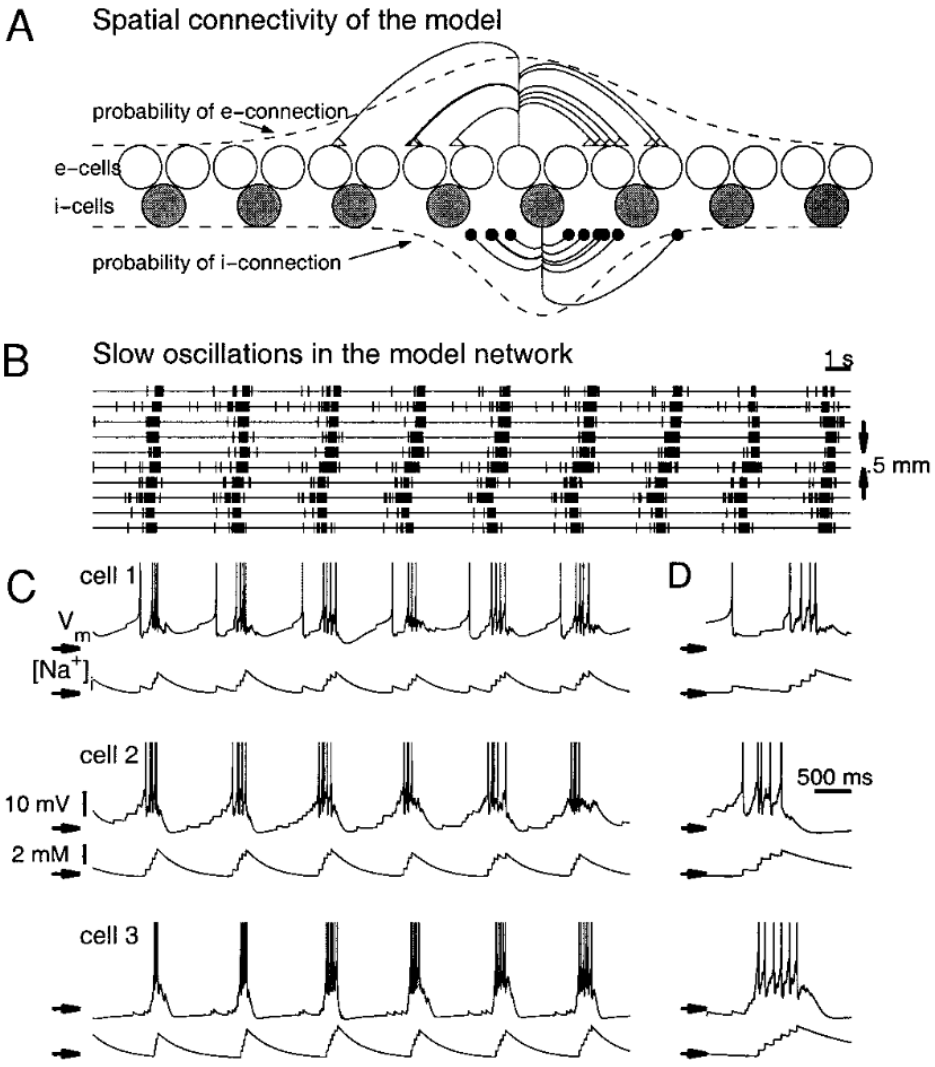

Figure 7 – Spontaneous slow oscillations in a cortical network model. Extracted from from [Compte et al., 2003]. (A) Schematic representation of the spatial connectivity in the network model. (B) Spontaneous network activity visualized as multi-unit recording (grouped neighboring cells). (C) intracellular somatic voltage and intracellular sodium concentration of 3 representative excitatory neurons. (D) Zoom in of an Up state of the cells depicted in (C). In this model, the only source of noise in the network comes from intrinsic parameters of the cells that are randomly distributed and from the random connectivity.

inhibitory modulation, through the blockage of $GABA_A$ receptors, the model suggests that strong recurrent feedback and activity-dependent potassium currents are sufficient to explain the typical modulations of network activity patterns [Sanchez-Vives et al., 2010]. During the exploration of high-frequency content during Up states, the model shows that a synaptic loop between excitatory and inhibitory neurons as well as manipulations in the intrinsic properties of the neurons (modulation of I_{KCa}) can explain the emergence of high-frequency oscillations [Compte et al., 2008]. Through manipulation of neuronal excitability (noise levels), by manipulations of extracellular

potassium, the model predicts a maximum collective coherence for intermediate noise levels [Sancristóbal et al., 2016]. The model also suggests that the precise relationship between excitatory and inhibitory inputs depends on the structural parameters defining the connectivity in the local cortical circuit [Compte et al., 2009]. Finally, the model is also able to explain the differences in emergent activity observed in different cortical areas through manipulations in the structural connectivity [Sanchez-Vives and Compte, 2005]. Thus, undoubtedly, this biologically realistic network model sets the right framework for the study of the biophysical mechanisms, ionic or synaptic, and network topology involved in the cortical slow oscillations. In Sec. 3.1 we describe this model in more detail.

Chapter 2

Objectives

The objective of this thesis is to investigate the emergence of activity generated by the cortical network, its mechanisms and properties, by combining experiments and a computational modelling approach. Specifically, the objectives are:

1. To implement the cortical network model of slow oscillations proposed by Compte and collaborators [Compte et al., 2003].
2. To investigate, *in vitro* and *in silico*, the impact of calcium-dependent potassium (KCa) channel on physiological network activity of the cerebral cortex.
3. To explore, *in silico*, how ionic properties of individual neurons become network properties through synaptic recurrency.
4. To investigate, *in vitro* and *in silico*, the impact of M-current on physiological network activity of the cerebral cortex.
5. To investigate, *in vitro* and *in silico*, the impact of H-current on physiological network activity of the cerebral cortex.
6. To develop an *in silico* model for the study of perturbational complexity and explore how synaptic mechanisms in the form of slow and fast inhibition contribute to network complexity.
7. To develop mean-field models of complexity different networks of spiking neurons.

Chapter 3

Models and Methods

In the following Sections we will present a detailed description of the cortical network models employed in this Thesis as well as the methods applied. In Sec. 3.1 we describe our implementation of the biophysically inspired cortical model of slow oscillations proposed by Compte et al. [Compte et al., 2003]. The model was adapted through implementation of new ionic channels, synaptic models and network topology, to address our scientific questions. In Sec. 3.2 we introduced the mean-field equations describing population dynamics, the template to estimate the transfer function, and the neuronal models under consideration. In Sec. 3.3 we described the experimental data analyzed, and finally in Sec. 3.4 the methods utilized throughout this Thesis.

3.1 Cortical network model of slow oscillations

3.1.1 One-dimensional cortical network model

3.1.1.1 Neuron model

There are currently many models of neuronal dynamics, each of them accounting for different levels of biological detail. For the purpose of this thesis, the biophysically detailed model of slow oscillations proposed by Compte and collaborators [Compte et al., 2003] was used. This model was introduced in 2002 in order to describe the cellular and network mechanisms of slow oscillations observed experimentally *in vitro* preparations. The original synapse model and one-dimensional network will be described in the next sections.

The ion channel kinetics are modelled following the Hodking-Huxley formalism [Hodgkin and Huxley, 1952]. In this formalism the gates have a probability of being activated, usually denoted by m or n, and a probability of being inactivated, denoted by h. Also, some channels do not inactivated (activated) resulting in a persistent (transient)

current. The timing-varying probabilities are given by:

$$\frac{dx}{dt} = \phi[\alpha_x(V)(1-x) - \beta_x(V)x] = \phi[x_\infty(V) - x]/\tau_x(V), \tag{3.1}$$

where $x \in \{m, n, h\}$ and ϕ is the temperature factor ($\phi = 1$ unless otherwise stated).

Excitatory neurons

In this model, excitatory neurons are modelled as containing a somatic and a dendritic compartment whose dynamical equations are modelled as:

$$C_m A_s \frac{dV_s}{dt} = -A_s(I_L + I_{Na} + I_K + I_A + I_{KS} + I_{KNa}) - I_{syn,s} - g_{sd}(V_s - V_d), \tag{3.2}$$

and

$$C_m A_d \frac{dV_d}{dt} = -A_d(I_L + I_{Ca} + I_{KCa} + I_{NaP} + I_{AR}) - I_{syn,d} - g_{sd}(V_d - V_s). \tag{3.3}$$

V_s and V_d stand for the somatic and dendritic voltage, respectively. $A_s = 0.015$ mm^2 is the soma area and $A_d = 0.035$ mm^2 the dendritic one. These two compartments are coupled electrically with a conductance $g_{sd} = 1 \pm 0.1$ μS [§] ensuring a high synchronization between them. Accordingly, $I_{syn,s}$ and $I_{syn,d}$ stand for the synaptic currents impinging on the soma and dendrites. In this model the somatic compartment receives the inhibitory synapses and the dendritic compartment the excitatory ones from the presynaptic neurons.

The sodium current $I_{Na} = g_{Na} m_\infty^3 h(V - V_{Na})$ has a maximal conductance of $g_{Na} = 50$ mS/cm^2 and a reversal potential of $V_{Na} = 55$ mV. The activation variable is replaced by its steady-state $m_\infty = \frac{\alpha_m}{\alpha_m + \beta_m}$ with $\alpha_m = \frac{0.1(V+33)}{1-\exp[-0.1(V+33)]}$ and $\beta_m = 4\exp[-\frac{1}{12}(V+53.7)]$. The inactivation variable is governed by $\alpha_h = 0.07\exp[-0.1(V+50)]$ and $\beta_h = \frac{1}{1+\exp[-0.04(V+44)]}$. The delayed rectifier current $I_K = g_K n^4(V - V_K)$ has a maximal conductance $g_K = 10.5$ mS/cm^2 and a reversal potential of $V_K = -100$ mV. The inactivation kinectis are set by $\alpha_n = \frac{0.01(V+34)}{1-\exp[-0.1(V+34)]}$ and $\beta_n = 0.125\exp(-0.04(V+44))$. For I_{Na} and I_K, $\phi = 4$. The passive leakage current, I_L, which is carried mostly by Cl^-, has a maximal conductance of $g_L = 0.0667 \pm 0.0067$ mS/cm^2 and a reversal potential of $V_L = -60.95 \pm 0.3$ mV.

The A-type potassium current $I_A = g_A m_\infty^3 h(V - V_K)$ has its activation variable modelled as $m_\infty = \frac{1}{1+\exp[-0.05(V+50)]}$ and the inactivation one as $h_\infty = \frac{1}{1+\exp[(V+80)/6]}$ and $\tau_h = 15$ ms. The non-inactivating K^+-channel $I_{KS} = g_{KS} m(V - V_K)$ has a maximal conductance of $g_{KS} = 0.576$ mS/cm^2 and its activation is controlled by $m_\infty = \frac{1}{1+\exp[-(V+34)/6.5]}$ and $\tau_m = \frac{8}{\exp[-(V+55)/30]+\exp[(V+55)/30]}$. The persistent sodium current $I_{NaP} = g_{NaP} m_\infty^3 (V - V_{Na})$

[§] In the model description the ± symbol is used to denote a variable that is Gaussian-distributed in the population, where mean ± SD are given.

has a maximal conductance $g_{NaP} = 0.0686$ mS/cm^2 and its activation given by $m_\infty = \frac{1}{1+\exp[-(V+55.7)/7.7]}$. The inwardly rectifying potassium current $I_{AR} = g_{AR} h_\infty (V - V_K)$ has a maximal conductance $g_{AR} = 0.0257$ mS/cm^2 and its activation is given by $h_\infty = \frac{1}{1+\exp[0.25(V+75)]}$. The calcium current $I_{Ca} = g_{Ca} m_\infty^2 (V - V_{Ca})$ has a maximal conductance $g_{Ca} = 0.43$ mS/cm^2 and activates following $m_\infty = \frac{1}{1+\exp[-(V+20)/9]}$.

Intracellular calcium concentration, $[Ca^{2+}]$, is modelled as:

$$\frac{d[Ca^{2+}]}{dt} = -\alpha_{Ca} A_d I_{Ca} - \frac{[Ca^{2+}]}{\tau_{Ca}}, \tag{3.4}$$

with $\alpha_{Ca} = 0.005$ μM(nA·ms)$^{-1}$ and $\tau_{Ca} = 150$ mS. The intracellular sodium concentration, $[Na^+]$, is modelled as:

$$\frac{d[Na^+]}{dt} = -\alpha_{Na}(A_s I_{Na} + A_d I_{NaP}) - R_{pump}\left\{\frac{[Na^+]^3}{([Na^+]^3 + 15^3)} - \frac{[Na^+]_{eq}^3}{[Na^+]_{eq}^3 + 15^3}\right\}, \tag{3.5}$$

with $\alpha_{Na} = 0.01$ mM(nA·ms)$^{-1}$, $R_{pump} = 0.018$ mMms^{-1}, and $[Na^+]_{eq} = 9.5$ mM.

The dynamic of the calcium-dependent (I_{KCa}) potassium current follows: $I_{KCa} = g_{KCa}\{[Ca^{2+}]/([Ca^{2+}] + K_D)\}(V - V_K)$, where $K_D = 30\mu$M and $g_{KCa} = 0.57$ ms/cm^2. The sodium-dependent (I_{KNa}) current is governed by: $I_{KNa} = g_{KNa} w_\infty([Na^+])(V - V_K)$, with $w_\infty([Na^+]) = 0.37/[1 + (38.7/[Na^+])^{3.5}]$ and $g_{KNa} = 1.33$ ms/cm^2.

For the two-dimensional network the leak potassium leakage ($I_{KL} = g_{KL}(V - V_K)$ with $g_{KL} = 1.86$ mS/cm^2) current was also included in the somatic compartment.

Inhibitory neurons

The inhibitory neurons are modeled only with the Hodgkin-Huxley spiking currents and with a somatic compartment. The dynamical equation governing its dynamics is given by:

$$C_m A_i \frac{dV}{dt} = -A_i(I_L + I_{Na} + I_K) - I_{syn,i}, \tag{3.6}$$

with the neuronal area being $A_i = 0.02$ mm^2. $I_{syn,i}$ stands for the sum of the synaptic currents from the presynaptic neurons. The ion channel kinetics follow the formalism described in Eq. 3.1. For the sodium current: $I_{Na} = g_{Na} m_\infty^3 h(V - V_{Na})$ where $m_\infty = \frac{\alpha_m}{\alpha_m + \beta_m}$ with $\alpha_m = \frac{0.5(V+35)}{1-\exp[-0.1(V+35)]}$, $\beta_m = 20\exp[-\frac{1}{18}(V+60)]$, $\alpha_h = 0.35\exp[-0.05(V+58)]$ and $\beta_h = \frac{5}{1+\exp[-0.1(V+28)]}$. Its maximal conductance is assumed to be $g_{Na} = 35$ mS/cm^2 and its reversal potential is $V_{Na} = 55$ mV. For the potassium current: $I_K = g_K n^4 (V - V_K)$ with $\alpha_n = \frac{0.05(V+34)}{1-\exp[-0.1(V+34)]}$ and $\beta_n = 0.625\exp(-0.0125(V+44))$. Its maximal conductance is assumed to be $g_K = 9$ mS/cm^2 and its reversal potential is $V_K = -90$ mV. Finally, for the leakage current, I_L has a maximal conductance of $g_L = 0.1025 \pm 0.0025$ mS/cm^2 and a reversal potential of $V_L = -63.8 \pm 0.15$ mV.

3.1.1.2 Synapses model

The original model proposed by [Compte et al., 2003] accounts for AMPA, NMDA and GABA-A synaptic model. Two types of excitatory synapses were considered, AMPA and NMDA mediated:

$$I_{\text{AMPA}} = g_{\text{AMPA}} s (V - E_{\text{AMPA}}), \tag{3.7}$$

and

$$I_{\text{NMDA}} = g_{\text{NMDA}} s (V - E_{\text{NMDA}}) \left(\frac{1}{1 + [\text{Mg}^{2+}] \exp(-0.062V/3.57)} \right), \tag{3.8}$$

where the reversal synaptic potential is $E_{AMPA} = E_{NMDA} = 0$ mV and the extracellular magnesium concentration $[\text{Mg}^{2+}] = 1.0$ mM. For AMPA-mediated synaptic transmission the gating variable $s(t)$ follows:

$$\frac{ds}{dt} = \alpha f(V_{\text{pre}}) - \frac{s}{\tau}, \tag{3.9}$$

with

$$f(V_{\text{pre}}) = \frac{1}{1 + \exp(-0.5(V_{\text{pre}} - 20))}, \tag{3.10}$$

where $\alpha = 3.48$ and $\tau = 2$ ms. For NMDAR-mediated synaptic transmission, the gating variable $s(t)$ follows:

$$\frac{ds}{dt} = \alpha(1 - s)x - \frac{s}{\tau}, \tag{3.11}$$

with

$$\frac{dx}{dt} = \alpha_x f(V_{\text{pre}}) - \frac{x}{\tau_x}, \tag{3.12}$$

where $f(V_{\text{pre}})$ is given by Eq. 3.10 and $\alpha = 0.5$, $\tau = 100$ ms, $\alpha_x = 3.48$, $\tau_x = 2$ ms.

For inhibitory synapses only GABA_A-mediated synaptic transmission was considered in the one-dimensional neuronal network, described by:

$$I_{\text{GABA}_\text{A}} = g_{\text{GABA}_\text{A}} s (V - E_{\text{GABA}_\text{A}}). \tag{3.13}$$

where s is given by Eq. 3.9, with $\alpha = 1$ and $\tau = 10$ ms and $E_{\text{GABA-A}} = -70$ mV.

For the two-dimensional network (described below), apart from the original synaptic dynamics considered by Compte et al.[Compte et al., 2003], we also implemented GABA_B-mediated synaptic transmission [Destexhe et al., 1996, Liu et al., 2019] being described by:

$$I_{\text{GABA}_\text{B}} = g_{\text{GABA}_\text{B}} \frac{s^4}{s^4 + K_g} (V - E_{\text{GABA}_\text{B}}), \tag{3.14}$$

$$\frac{dr}{dt} = 0.5T(1 - r) - 0.0012r, \tag{3.15}$$

with

$$\frac{ds}{dt} = 0.18r - 0.034s. \tag{3.16}$$

r and s represent the $GABA_B$ receptor and the synaptic gating variable, respectively. The transmitter concentration T is modeled as a square pulse of 0.5 mM lasting 3 ms. $K_g = 100\mu M^4$ is the dissociation constant of the binding of s on the K^+ channels [Destexhe et al., 1996].

3.1.1.3 One-dimensional network topology

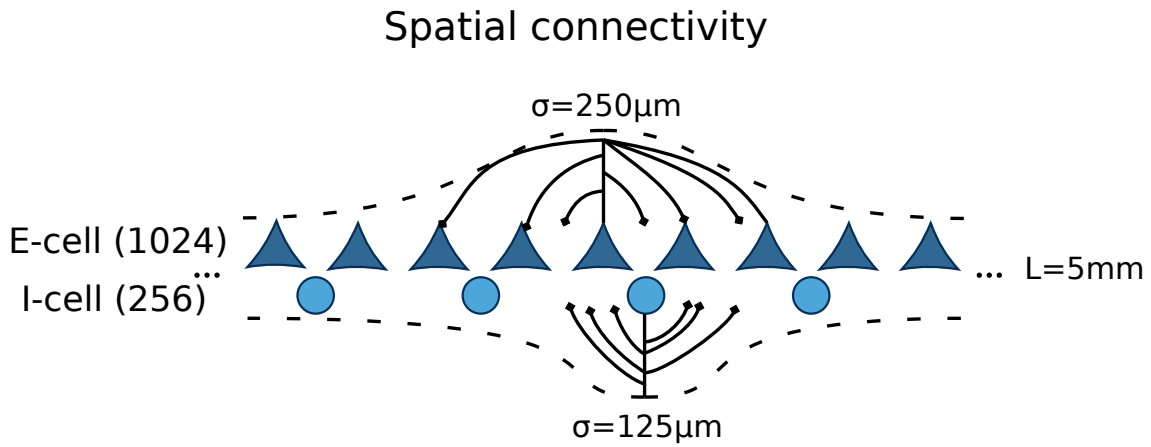

Figure 8 – One-dimensional cortical network. Schematic representation of the spatial connectivity. 1024 pyramidal neurons (E-cell) and 256 interneurons (I-cells) are synaptically connected through biologically plausible synaptic dynamics. Probability distribution of synaptic connections from one neuron at the center to the rest of the network is illustrated for pyramidal neuron (more globally connected) and interneuron (more locally connected). Autapses are not allowed although multiple connections to the same target are. The network is assumed to be 5 mm long.

The original model proposed by Compte et al. [Compte et al., 2003] introduced a one-dimensional network model. The network model consists of a population of 1024 excitatory neurons (pyramidal cells) and 256 inhibitory neurons (interneurons), keeping the 4 : 1 proportion as is the case reported for the mammals cerebral cortex [Hendry et al., 1987, Markram et al., 2004]. In this network, the neurons are sparsely connected to each other through a fixed number of connections. Excitatory and inhibitory neurons make 20 ± 5 connections to excitatory and to inhibitory neurons (autapses are not allowed although multiple contact onto the same target are). The probability that two neurons separated by a distance x are connected is decided by a Gaussian probability distribution centered at 0 with a defined standard deviation σ: $P(x) = \exp(-x^2/2\sigma^2)/\sqrt{2\pi\sigma^2}$. The

network is assumed to be 5 mm long and $\sigma_{exc} = 500\mu$m and $\sigma_{inh} = 125\mu$m (Fig. 8). The maximal synaptic conductance strengths are: excitatory to excitatory: $g^{EE}_{AMPA} = 5.4$ nS, $g^{EE}_{NMDA} = 0.9$ nS; excitatory to inhibitory: $g^{EI}_{AMPA} = 2.25$ nS, $g^{EI}_{NMDA} = 0.5$ nS; inhibitory to inhibitory: $g^{II}_{GABA_A} = 0.165$ nS; and inhibitory to excitatory: $g^{IE}_{GABA_A} = 4.15$ nS.

3.1.1.4 M and H currents

In order to study the effects of M and H current on the slow oscillations, we adapted the model described above to include these currents. For the M-current we implemented the model described in [McCormick et al., 1993]: $I_M = g_M m(V - V_K)$ with a maximal conductance of $g_M = 0.083$ mS/cm^2 and a reversal potential of $V_K = -100$ mV. The activation variable is controlled by $m_\infty = \frac{1}{1+\exp[-0.1(V+35)]}$ and $\tau_m = \frac{1000}{3.3\exp[(V+35)/20]+\exp[-(V+35)/20]}$. The M-current was included in the somatic compartment [Wang, 1999].

For the H-current we implement the model described in [Hill and Tononi, 2005]: $I_H = g_H m(V + 45)$ with a maximal conductance of $g_H = 0.0115$ mS/cm^2. The activation variable is controlled by $m_\infty = \frac{1}{1+\exp[(V+75)/5.5]}$ and $\tau_m = \frac{1}{\exp[-14.59-0.086V]+\exp[-1.87+0.0701V]}$. H-current was included in the dendritic compartment of 30% random selected pyramidal neurons [Robinson and Siegelbaum, 2003, Hill and Tononi, 2005].

To arrange the M and H currents on the model we have performed an adjustment at the channel maximal conductances for the remaining currents (only for pyramidal neurons) as follows: $g_{Na} = 50$ mS/cm^2, $g_K = 10.5$ mS/cm^2, $g_L = 0.0667 \pm 0.0067$ mS/cm^2, $g_{KL} = 1.86$ mS/cm^2, $g_A = 1$ mS/cm^2, $g_{Ks} = 0.576$ mS/cm^2, $g_{KNa} = 0.65835$ mS/cm^2, $g_{NaP} = 0.05145$ mS/cm^2, $g_{AR} = 0.0257$ mS/cm^2, $g_{Ca} = 0.43$ mS/cm^2 and $g_{KCa} = 0.5415$ mS/cm^2.

3.1.2 Two-dimensional neuronal network

The newly implemented network model in this Thesis work consists of a two-dimensional 50×50 squared network of pyramidal cells (80%) and interneurons (20%), randomly distributed and interconnected through biologically plausible synaptic dynamics. Each cell is sparsely and locally connected to its neighbors within a square of size $L \times L$ centered around it, where $L_{pyramidal} = 7$ and $L_{interneuron} = 5$ (Fig. 9). The fraction of synaptic connections (outgoing synapses) is set at 50% of the total number of neurons within the local range for pyramidal cells and 90% for interneurons, thus imposing local connections for interneurons and more sparse connections for pyramidal cells. The network structure is similar to that used in previous studies of cortical oscillatory neuronal networks [Bazhenov et al., 2008, Poil et al., 2012, DALLA PORTA and Copelli, 2019].

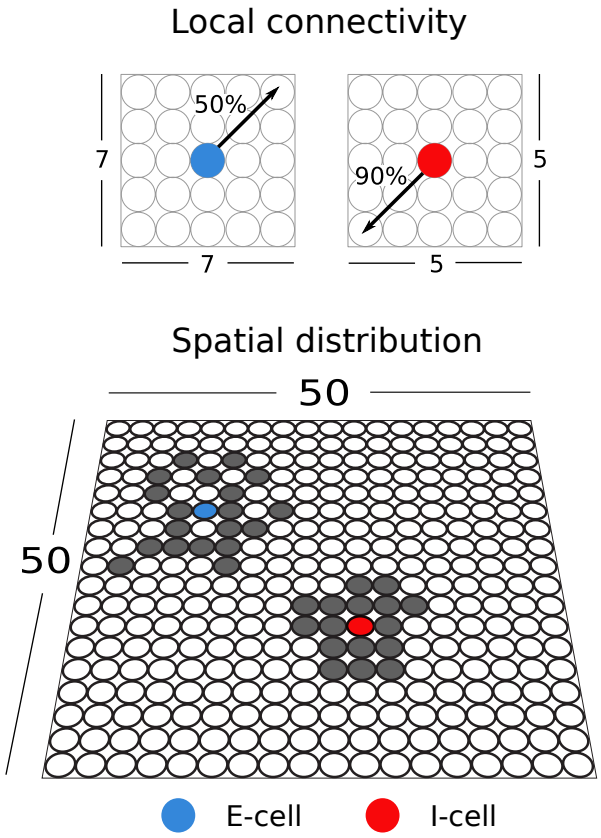

Figure 9 – Two-dimensional cortical network. Schematic representation of the local and spatial connectivity. The model consists of pyramidal neurons (blue) and interneurons (red) arranged in a 50×50 square lattice. The excitatory neurons may connect locally to a 50% fraction of its neighbors (gray circles) within a 7×7 square, while the inhibitory neurons to a 90% fraction within a 5×5 square, thus ensuring more sparse connections for pyramidal neurons and more local connections for interneurons. Autapses are not allowed although multiple connections to the same target are.

In order to arrange the neuron model in the two-dimensional network, we performed an adjustment at the synaptic maximal conductances and channel maximal conductances. The channel maximal conductances of pyramidal neurons were set to: $g_{Na} = 50\,\mathrm{mS/cm^2}$, $g_K = 10.5\,\mathrm{mS/cm^2}$, $g_L = 0.0667 \pm 0.0067\,\mathrm{mS/cm^2}$, $g_{KL} = 1.86\,\mathrm{mS/cm^2}$, $g_A = 1\,\mathrm{mS/cm^2}$, $g_{Ks} = 0.576\,\mathrm{mS/cm^2}$, $g_{KNa} = 0.65835\,\mathrm{mS/cm^2}$, $g_{NaP} = 0.05145\,\mathrm{mS/cm^2}$, $g_{AR} = 0.0257\,\mathrm{mS/cm^2}$, $g_{Ca} = 0.43\,\mathrm{mS/cm^2}$ and $g_{KCa} = 0.5415\,\mathrm{mS/cm^2}$. The synaptic maximal conductances were set to: $g^{II}_{GABA_A} = 1.96$ nS, $g^{IE}_{GABA_A} = 28.96$ nS, $g^{II}_{GABA_B} = 33.75$ nS, $g^{IE}_{GABA_B} = 39.2$ nS, $g^{EE}_{AMPA} = 6.2$ nS, $g^{EI}_{AMPA} = 0.6925$ nS, $g^{EE}_{NMDA} = 2.72$ nS, and $g^{EI}_{NMDA} = 0.595$ nS. Additionally, all neurons receive a heterogeneous Poisson train of excitatory, AMPA and NMDA, presynaptic potentials with a rate $R = 0.5$kHz [Dayan and Abbott, 2001]. The Poisson synaptic inputs are modeled as excitatory AMPA and

NMDA currents where the probability of a spike at one time step is given by: $1 - e^{-R\dot{dt}}$, where dt is the time step of simulation, and R the Poisson rate.

The simulated population membrane potential (sLFP) was computed as the sum of the absolute values of the excitatory and inhibitory synaptic currents acting on the excitatory neurons [Sancristóbal et al., 2016]. We virtually created 20 electrodes in the model, arranged as a 5×4 matrix. Each electrode covered an area of 49 neurons and were horizontally and vertically spaced by a distance of 10 neurons, thus ensuring no overlapping between electrodes. The neurons on the border were not considered. In order to simulate the experimental effects of $GABA_{A,B}$-Rs blockade, we progressively reduced the $GABA_{A,B}$ conductance (which, for simplicity, will be referred to as simple concentration) in inhibitory synapses to both neurons, pyramidal and interneurons, from 5% to 90% (disinhibited network). We proceeded in the same way to progressively increase the $GABA_A$ conductance, increasing it from 5% to 90% (inhibited network).

3.1.3 Numerical methods and simulations

For all the simulations regarding the one-dimensional and two-dimensional network described in Sec.3.1.1.3 and 3.1.2, simulations were performed using a fourth-order Runge-Kutta method with a time step of 0.06 ms implemented in a C code. Simulations were performed using the supercomputer MareNostrum from Barcelona Supercomputing Center (BSC, https://www.bsc.es/es).

3.2 Mean-field model

3.2.1 Network of spiking neurons

We considered a random directed network of $N = 10^4$ cells, where 80% are excitatory (E) regular-spiking (RS) and 20% inhibitory (I) fast-spiking (FS) neurons. The connectivity is set randomly between pairs of neurons with a fixed probability (P= 0.05). Unless otherwise stated, we used the same network and synaptic constants for all the neuronal models (Hodgkin-Huxley (HH), Adaptive Exponential Integrate-and-Fire (AdEx), and Morris-Lecar (ML)). The dynamics of each node k follows:

$$\frac{d\overline{x}_k}{dt} = F(\overline{x}_k) + I_{syn}, \tag{3.17}$$

where $\overline{x}$ and $F(\overline{x})$ stand for the neuronal state and dynamics. The later depending on the specific model (see the following sections). For simplicity of notation $\overline{x}_k$ is a $n-$dimensional vector, depending on the dimension of each neuron model. The synaptic

current (I_{syn}) impinging on the postsynaptic neuron k, is modeled as:

$$I_{syn} = (V_E - v_k)G^E_{syn} + (V_I - v_k)G^i_{syn}, \tag{3.18}$$

$$\tag{3.19}$$

where,

$$G^{E,I}_{syn}(t) = Q_{(E,I)} \sum_n \Theta\left[t - t_{sp}(n)\right] e^{\frac{t-t_{sp}(n)}{\tau}}. \tag{3.20}$$

$Q_E(Q_I)$ and V_E (V_I) are the excitatory (inhibitory) synaptic conductance and reversal potential, respectively. $\tau = 5$ ms is the decay timescale of excitatory and inhibitory synapses andΘ is the Heaviside step function and the summation runs over the overall presynaptic spiking times $t_{sp}(n)$. v_k stands for the membrane potential of neuron k. For HH and AdEx models we use $Q_E = 1.5$ nS and $Q_I = 5$ nS while for ML model $Q_E = 4$ nS and $Q_I = 10$ nS. Furthermore, all neurons are subject to an independent noisy spike train described by a Poisson distribution with a constant rate $v_{drive} = 4$ Hz, unless otherwise stated.

3.2.2 Single neuron models

We describe here the neuronal models: exponential Integrate-and-Fire, Morris–Lecar and Hodgkin–Huxley models.

Adaptive Exponential Integrate-and-Fire model

The dynamics of each of the adaptive exponential integrate-and-fire model (AdEx) neurons i is described by the following two-dimensional [here $\overline{x} = (v_i; w_i)$] differential equations [Brette and Gerstner, 2005]:

$$c_m \frac{dv_i}{dt} = g_L(V_L - v_i) + g_L \Delta e^{\frac{v_i - v_t}{\Delta}} - w_i + I_{syn}, \tag{3.21}$$

and

$$\frac{dw_i}{dt} = -\frac{w_i}{\tau_w} + b \sum_{t_{sp}(i)} \delta(t - t_{sp}(i)) + a(v_i - V_L). \tag{3.22}$$

$c_m = 150$ pF is the membrane capacitance, v_i is the voltage of neuron i, and, whenever $v_i > v_t = -50$ mV at time $t_{sp}(i)$, v_i is reset to the resting potential $v_{rest} = -65$ mV with a refractory time $T_r = 5$ ms. The leakage current has a maximal conductance $g_L = 10$ nS with a reversal potential $V_L = -65$ mV (unless otherwise states). The exponential term has a strength of $\Delta_E = 2$ mV and $\Delta_I = 0.5$ mV for excitatory and inhibitory neurons, respectively. w mimics the dynamics of spike frequency adaptation currents. Inhibitory neurons are modeled according to physiological insight as the fast-spiking (FS) with no adaptation while the excitatory are modeled as regular-spiking (RS) with adaptation. Here we consider $b = 60$ pA, $a = 4$ nS, and $\tau_w = 500$ ms, unless otherwise stated.

Hodking-Huxley model

The dynamics of Hodgkin-Huxley (HH) [Hodgkin and Huxley, 1952] is given by the following five-dimensional system of differential equations [Pospischil et al., 2008]:

$$\begin{aligned} c_m \frac{dv_i}{dt} &= g_L(V_L - v_i) + g_{Na} m_i^3 h_i (V_{Na} - v_i) + g_K n_i^4 (V_K - v_i) \\ &\quad + g_M p_i (V_K - v_i) + I_{syn}, \end{aligned} \tag{3.23}$$

$$\frac{dn_i}{dt} = \alpha_n(v_i)(1 - n_i) - \beta_n(v_i) n_i, \tag{3.24}$$

$$\frac{dm_i}{dt} = \alpha_m(v_i)(1 - m_i) - \beta_m(v_i) m_i, \tag{3.25}$$

$$\frac{dh_i}{dt} = \alpha_h(v_i)(1 - h_i) - \beta_h(v_i) h_i, \tag{3.26}$$

$$\frac{dp_i}{dt} = \frac{p_\infty(v_i) - p_i}{\tau_p(v_i)}, \tag{3.27}$$

with the gating functions,

$$\begin{aligned} \alpha_n(v) &= \frac{-0.032(v - V_t - 15)}{e^{\frac{V_t + 15 - v}{5}} - 1}, \\ \beta_n(v) &= 0.5 e^{\frac{V_t + 10 - v}{10}}, \\ \alpha_m(v) &= \frac{-0.032(v - V_t - 13)}{e^{\frac{V_t + 13 - v}{4}} - 1}, \\ \beta_m(v) &= \frac{0.28(v - V_t - 40)}{e^{\frac{v - V_t - 40}{5}} - 1}, \\ \alpha_h(v) &= 0.128 e^{\frac{V_t + 17 - v}{18}}, \\ \beta_h(v) &= \frac{4}{e^{\frac{V_t + 40 - v}{5}} + 1}, \\ p_\infty(v) &= \frac{1}{e^{\frac{35 - v}{10}} + 1}, \\ \tau_p(v) &= \frac{\tau_{max}}{3.3 e^{\frac{v + 35}{20}} + e^{\frac{-v - 35}{20}}}. \end{aligned} \tag{3.28}$$

v_i is the voltage and (n_i, m_i, h_i, p_i) are the corresponding gating variables of the ith neuron. The spike emission t_{sp} is set for this model to time steps in which the membrane potential v exceeded a voltage threshold of 10 mV. The membrane capacitance is set to $c_m = 200$ pF/cm^2. The maximal conductance for the leakage current (L), sodium current (Na), potassium current (K) and the slow non-inactivating potassium current (M) were set to $g_L = 10$ mS/cm^2, $g_{Na} = 20$ mS/cm^2, $g_K = 6$ mS/cm^2 and $g_M = 0.03$ mS/cm^2 ($g_M = 0$ mS/cm^2 for inhibitory neurons), with corresponding reversal potential $V_L = -65$ mV, $V_{Na} = 50$ mV, $V_K = -90$ mV, and $V_M = V_K$, respectively. The spiking threshold is set to $V_T = -53.5$ mV and $\tau_{max} = 0.4$ s.

Morris-Lecar model

The dynamics of the Morris-Lecar model is described by the system of differential equations [Morris and Lecar, 1981]:

$$c_m \frac{dv_i}{dt} = g_L(V_L - v_i) + g_{Ca} M_{ss}(v_i)(V_{Ca} - v_i) + g_K N_i (V_K - v_i) + I_{syn} + I_0, \tag{3.29}$$

$$\frac{dN_i}{dt} = \frac{N_{ss}(v_i) - N_i}{\tau_N(v_i)}, \tag{3.30}$$

with the membrane capacitance $c_m = 2\mu\text{F/cm}^2$, v_i is the membrane potential in mV, and N_i and M_{ss} are the fraction of open potassium and calcium channels, respectively. $I_0 = 0.2$ nA/cm^2 is a reference DC external current. Spiking thresholds set to $V_T = -53.5$ mV, as in the HH model. The maximal conductances for the leakage current (L), calcium current (Ca), and potassium current (K) were set to $g_L = 20$ mS/cm^2, $g_{Ca} = 80$ mS/cm^2, and $g_K = 160$ mS/cm^2, with corresponding reversal potential $V_L = -50$ mV ($V_L = -70$ mV for inhibitory neurons), $V_{Ca} = 120$ mV, and $V_K = -84$ mV. The quantities M_{ss} and N_{ss} are modeled as:

$$M_{ss}(v) = \frac{1}{2}\left[1 + tanh\left(\frac{v - V_1}{V_2}\right)\right], \tag{3.31}$$

$$N_{ss}(v) = \frac{1}{2}\left[1 + tanh\left(\frac{v - V_3}{V_4}\right)\right], \tag{3.32}$$

with

$$\tau_N(v) = \frac{1}{2}\left[\phi cosh\left(\frac{v - V_3}{V_4}\right)\right], \tag{3.33}$$

where $V_1 = -1.2$ mV, $V_2 = 18$ mV, $V_3 = 2$ mV and $V_4 = 30$ mV are tuning parameters that determine the half activating voltage and slope of the activation curves for calcium and potassium conductances. Such choice of parameters was made in order the ML neuron is te in a type II class of excitability, i.e., its response to a DC current is discontinuous and the neuron firing increases very slowly with the injected current.

3.2.3 Mean-field formalism

Mean-field theory scales the analysis of interacting pointwise neurons to their macroscopic, collective, dynamics based on the moment-statistics of the system, requiring a self-averaging hypothesis for physical quantities. We make here an additional hypothesis that the biological neural network is set to asynchronous dynamical regime. The latter is chosen for its biological plausibility [Destexhe et al., 2003] as observed in awake cortical states of adult mammalian brains. The master equation formalism is borrowed from Ref. [El Boustani and Destexhe, 2009]. Such formalism provides us

a system of ordinary differential equations that describe the evolution of the mean and variance of the neuronal firing rate of excitatory and inhibitory neurons. The main argument of this formalism is to consider the network dynamics as Markovian on an infinitesimal (a time resolution T, typically $\sim$ 20 ms) scale [Ohira and Cowan, 1993, Ginzburg and Sompolinsky, 1994, Buice et al., 2010]. Furthermore, this a theory is based on the assumption that neurons emit maximum one spike over the Markovian step T, i.e., assuming a low firing rate of neurons, lower than 1/T$\sim$ 50 Hz [El Boustani and Destexhe, 2009], as is the case of asynchronous regimes here investigated. It is described by the system of differential equations:

$$T\frac{dv_\mu}{dt} = (F_\mu - v_\mu) + \frac{1}{2}c_{\lambda\eta}\frac{d^2F_\mu}{dv_\lambda dv_\eta}, \tag{3.34}$$

$$\begin{aligned} T\frac{dc_{\lambda\eta}}{dt} = \delta_{\lambda\eta}\frac{F_\lambda(T^{-1} - F_\eta)}{N_\lambda} + (F_\lambda - v_\lambda)(F_\eta - v_\eta) + \frac{dF_\lambda}{dv_\mu}c_{\eta u} \\ + \frac{dF_\eta}{dV_\mu}c_{\lambda\mu} - 2c_{\lambda\eta}, \end{aligned} \tag{3.35}$$

where $\mu = E, I$ is the population index (excitatory or inhibitory, respectively), v_μ the population firing rate, and $c_{\lambda\eta}$ the covariance between populations λ and η. The transfer function $F_\mu = F_\mu(v_E, v_I)$ describes the firing rate of population μ as a function of excitatory and inhibitory inputs (with rates v_E and v_I). In a first order approximation the model reduces to the well known Wilson-Cowan model, with the specificity that the function F needs to be obtained according to the specific single neuron model under consideration. We introduce this procedure in the next subsection.

3.2.4 Transfer function estimation

The transfer function (TF) relates the firing rate of a postsynaptic neuron to a presynaptic excitatory and inhibitory firing rates. The particular form of the TF is related to the dynamics describing neuronal activity. Deriving an analytical expression for the transfer function is a nontrivial endeavor due to the nonlinear character of the dynamics, e.g., through conductance based interactions. Therefore, we use here a semi-analytic approach to fit a family of plausible transfer functions to the data obtained by means of numerical simulations with the desired neuron model. The method was first developed by Zerlaut et al. [Zerlaut et al., 2016] where it was applied on experimental data from mouse layer V pyramidal neurons. It is based on the assumption that the transfer function depends only on the statistics of the subthreshold membrane voltage dynamics, which is assumed to be normally distributed. These statistics are the average membrane voltage, μ_v, its standard deviation σ_v, and autocorrelation time τ_V. Under

these assumptions the neuronal output firing rate, F_v, is given by the following function:

$$F_v = \frac{1}{2}\tau_v erfc\left(\frac{V_{thr}^{eff} - \mu_V}{\sqrt{2\sigma_V}}\right), \tag{3.36}$$

where $erfc$ stands for the Gauss error function and V_{thr}^{eff} is an effective or phenomenological threshold accounting for nonlinearities in the single-neuron dynamics. Note that when dealing with extremely high spiking frequencies, e.g., in the case of Hodgkin–Huxley model close to depolarization block, a multiplicative factor α can be added in front of right-hand side of Eq. 3.36 allowing then the fitting procedure to deal with such high frequencies. In the asynchronous dynamical regime, neurons have relatively low firing rate (smaller than 30 Hz). Accordingly, we did not use this extension.

From input rates to subthreshold voltage moments

We start by calculating the averages (μ_{G_E},μ_{G_I}) and standard deviations (σ_{G_E},σ_{G_I}) of the conductances given by Eq. 3.20 under the assumption that the input spike trains follow the Poisson statistics (asynchronous regime). Thus, we obtain [Zerlaut et al., 2018]:

$$\begin{aligned}
\mu_{G_E}(v_E, v_I) &= v_E K_E \tau_E Q_E, \\
\tau_{G_E}(v_E, v_I) &= \sqrt{\frac{v_E K_E \tau_E}{2}} Q_E, \\
\mu_{G_I}(v_E, v_I) &= v_I K_I \tau_I Q_I, \\
\tau_{G_I}(v_E, v_I) &= \sqrt{\frac{v_I K_I \tau_I}{2}} Q_I,
\end{aligned} \tag{3.37}$$

where $K_{E,I}$ is the average input connectivity received from the excitatory or inhibitory population (in our cases typically $K_E = 400$ nad $K_I = 100$) and in our model $\tau_E = \tau_I = \tau$ (see Eq. 3.20).

The mean conductances will control the total input of the neuron μ_G and therefore its effective membrane time constant τ_m^{eff}:

$$\mu_{G_E}(v_E, v_I) = \mu_{G_E} + \mu_{G_I} + g_L, \tag{3.38}$$

$$\tau_m^{eff}(v_E, v_I) = \frac{c_m}{\mu_G}. \tag{3.39}$$

Here we make the assumption that the subthreshold moments (μ_V, σ_V, τ_V) are not affected by the dynamics of the currents coming into play at the spiking time (e.g., sodium channel dynamics or the exponential term of the AdEx model). We thus consider, for all neurons, only the leakage term and the synaptic input to estimate subthreshold moments. Accordingly, we can write the equation for the mean subthreshold voltage as:

$$\mu_V(v_E, v_I) = \frac{\mu_{G_E} E_E + \mu_{G_I} E_I + g_L E_L}{\mu_G}. \tag{3.40}$$

The final equation for σ_V and τ_V follow from calculations introduces in Ref. [Zerlaut et al., 2018], they read:

$$\sigma_V(\nu_E, V_I) = \sqrt{\sum_s K_s \nu_s \frac{(U_s \cdot \tau_s)^2}{2(\tau_m^{eff} + \tau_s)}}, \tag{3.41}$$

$$\tau_V(\nu_E, V_I) = \left\{ \frac{\sum_s \left[K_s \nu_s (U_s \cdot \tau_s)^2 \right]}{\sum_s K_s \nu_s (U_s \cdot \tau_s)^2 (\tau_m^{eff} + \tau_s)^{-1}} \right\}, \tag{3.42}$$

where we defined $U_s = Q_s(E_s - \mu_s)\mu_G^{-1}$ and s =(E,I). Notice that neglecting all the currents for the generation of action potentials (e.g., sodium current) becomes a poorer assumption as the neuron activity increases. Although, as we show in the following subsection, the fitting procedure will account for discrepancies in the actual evaluation of voltage moments by permitting an accurate prediction of neuron output firing rate

From subthreshold voltage moments to the output firing rate

The quantities μ_V, σ_V, and τ_V, obtained in the previous subsection, can now be plugged into Eq. 3.37 when an additional relation is taken into account. This relation follows from theoretical and experimental considerations [Zerlaut et al., 2016] showing that the voltage effective threshold V_{thr}^{eff} can be expressed as a function of $(\mu_V, \sigma_V, \tau_V)$. In Zerlaut et al. [Zerlaut et al., 2016], the phenomenological threshold was taken as a second order polynomial in the following form:

$$\begin{aligned} V_{thr}^{eff}(\mu_V, \sigma_V, \tau_V^N) = P_0 + \sum_{x \in \{\mu_V, \sigma_V, \tau_V^N\}} P_x \cdot \left(\frac{x - x^0}{\delta x^0} \right) + \\ \sum_{x,y \in \{\mu_V, \sigma_V, \tau_V^N\}^2} P_{xy} \cdot \left(\frac{x - x^0}{\delta x^0} \right) \left(\frac{y - y^0}{\delta y^0} \right), \end{aligned} \tag{3.43}$$

where we introduced the quantity $\tau_V^N = \tau_V G_l / c_m$. We evaluated $\{P\}$ through a fit according to simulations on single neurons activity setting first $\mu_V^0 = -60$ mV, $\sigma_V^0 = 0.004$ mV, $(\tau_V^N)^0 = 0.5$, $\delta\mu_V^0 = 0.001$ mV, $\delta\sigma_V^0 = 0.006$ mV, and $\delta(\sigma_V^N)^0 = 1$. By the fitting procedure we find the values of the P parameters for the three neuronal model considered here (taking into account two neuronal types: excitatory regular-spiking (RS) and inhibitory fast-spiking (FS)). We report the results in the Tables 1 , 2 and 3.

3.3 Experimental methods *in vitro*

Cortical slices were prepared as previously described [Sanchez-Vives and McCormick, 2000]. Briefly: adult ferrets ($3 - 7$ months old, either sex) were anesthetized with sodium pentobarbital (40 mg/kg) and decapitated. The entire forebrain was rapidly

Table 1 – Fit parameters AdEx neurons

Cell type	P_0	P_{μ_V}	P_{σ_V}	P_{τ_V}	$P_{\mu_V^2}$	$P_{\sigma_V^2}$	$P_{\tau_V^2}$	$P_{\mu_V\sigma_V}$	$P_{\mu_V\tau_V}$	$P_{\sigma_V\tau_V}$
RS	-49.8	5.06	-23.4	2.3	-0.41	10.5	-36.6	7.4	1.2	-40.7
FS	-49.8	5.06	-23.4	2.3	-0.41	10.5	-36.6	7.4	1.2	-40.7

Values are in mV. AdEx, adaptive exponential integrate-and-fire model; FS, fast-spiking; RS, regular-spiking. See Eq. 3.43 for parameter definitions.

Table 2 – Fit parameters Hodgkin-Huxley neurons

Cell type	P_0	P_{μ_V}	P_{σ_V}	P_{τ_V}	$P_{\mu_V^2}$	$P_{\sigma_V^2}$	$P_{\tau_V^2}$	$P_{\mu_V\sigma_V}$	$P_{\mu_V\tau_V}$	$P_{\sigma_V\tau_V}$
RS	-48.1	3.2	10.9	-0.32	0.98	1.1	-1.2e-3	-1.4	3.9	-0.11
FS	-51.2	1.8	-6.1	-0.86	1.6	-0.70	-11	-0.18	1.2	-1.2

Values are in mV. FS, fast-spiking; RS, regular-spiking.

Table 3 – Fit parameters Hodgkin-Huxley neurons

Cell type	P_0	P_{μ_V}	P_{σ_V}	P_{τ_V}	$P_{\mu_V^2}$	$P_{\sigma_V^2}$	$P_{\tau_V^2}$	$P_{\mu_V\sigma_V}$	$P_{\mu_V\tau_V}$	$P_{\sigma_V\tau_V}$
RS	-48.1	3.2	10.9	-0.32	0.98	1.1	-1.2e-3	-1.4	3.9	-0.11
FS	-0.615	-2.56	-17.6	-164	0.83	-55	108	-7.4	24.6	288

Values are in mV. FS, fast-spiking; RS, regular-spiking.

removed to oxygenated cold (4 – 10° C) bathing medium and cut in 400μm thick coronal slices from the occipital cortex containing primary and secondary visual cortical areas (areas 17, 18, and 19). Then, slices were placed in an interface style recording chamber (Scientific Systems Design, Inc.), and bathed for 30 minutes in an equal mixture of the sucrose-substituted solution and ACSF (Artificial Cerebro- Spinal Fluid). Afterwards slices were maintained 2 hours in ACSF for recovery. Finally, an *in vivo* like ACSF solution was applied throughout the rest of the experiment. Electrophysiological recordings started after allowing at least 1 hour of recovery.

Extracellular local field potential (LFP) was recorded using 16-channel multi-electrode arrays or with 2 – 4ΩM tungsten electrodes. Signals were amplified using a PGA16 Multichannel System at a sampling rate of 5 or 10kHz. All experiments were carried out in accordance with protocols approved by the Animal Ethics Committee of the University of Barcelona, which comply with the European Union Guidelines on Protection of Vertebrates used for Experimentation (Directive 2010/63/EU of the European Parliament and the Council of 22 September 2010).

For the sake of clarity, none of the experimental recordings used in this thesis were acquired by the author, who has been involved only in the *post hoc* analysis. All

the experimental procedures and data acquisition were performed by qualified and authorized members of the Sanchez-Vives lab.

3.4 Data analysis

3.4.1 Relative firing rate (LogMUA)

A good estimate of the population firing rate is given by the normalized multiunit activity (MUA) spectrum, once the normalized Fourier components at high frequencies have densities proportional to the spiking activity of the involved neurons [Mattia and Del Giudice, 2002]. We followed the implementation described in [Reig et al., 2010]. Briefly, the MUA is estimated as the power change in the Fourier components of the recorded local field potential (LFP) at high frequencies. The time-dependent MUA is computed from the power spectrum in 50 ms windows, each frequency normalized by the corresponding amplitude of the power spectrum computed over the whole time series, and averaged within the $0.2 - 1.5$ kHz band. MUAs were logarithmically scaled to balance the large fluctuations of the nearby spikes and further smoothed by a moving average with a sliding window of 80 ms. After this preprocessing with have the so called LogMUA.

3.4.2 Experimental Up and Down states detection

Up and Down states were singled out by setting a threshold in the LogMUA (see 3.4.1) time series. The threshold was set to 60% (adjusted when needed) of the interval between the peaks in the bimodal distributions (typical from slow oscillations, SO) of LogMUA corresponding to Up and Down states [Reig et al., 2010, Sanchez-Vives et al., 2010]. From the detection of Up and Down states we estimate many parameters reported in this thesis. We calculated the following: i) Up and Down state durations; ii) cycle frequency (Up + Down events; UD-cycle); iii) as a measure of SO variability the coefficients of variation (CV=SD/mean) of Up state duration, Down state duration and UD duration; iv) the relative firing rate during Up and Down states as well UD-cycle, defined as the mean LogMUA across time; and v) the upward (Down to Up) and downward (Up to Down) transition slopes were the gradients of the linear fits of the average LogMUA in the time intervals $(-10, 25$ ms) and $(-25, 10$ ms), respectively. For the scatter plots of Up *versus* Down state durations, Kernel density estimation (KDE) was used to obtain and construct univariate (1D histogram) and bivariate (2D histogram) [Waskom, 2021]. For the dataset recorded with multielectrode array, only the channels located at the infragranular region were considered.

3.4.3 Up and Down durations in the cortical network model

Up state durations in the model were evaluated in two forms: i) locally, based on the mean neuronal burst duration (also called mean network burst duration), and ii) globally, based on the total activity of the network (a quantity similar to experimental LogMUA). For i) we computed the spike-train autocorrelation functions (ACF) for each neuron in the network and estimated the width of the central peak of ACF by fitting a Gaussian function. Then, the Up state duration was defined as two standard deviations of the Gaussian distribution (see 17). For ii) we chose arbitrarily a threshold to define the initiation and termination of Up and Down states.

3.4.4 Spectral analysis and network synchronization

From the simulated network model we obtained from the spike-trains the power spectrum. For each neuron in the network the spike-train power spectrum was computed with a multi-tapper estimator (5 slepian tapers with bandwidth 0.1 Hz). Power spectra were then averaged to obtain the network's activity spectrum, which was then normalized by the average firing rate to compare across simulations with different parameter conditions. Furthermore, power spectra were smoothed by a Gaussian kernel with prescribed standard deviation $\sigma = 0.25$ Hz. The software Chronux (`http://chronux.org/`) was used for such analysis.

The Kuramoto order parameter (R) was estimated as:

$$R(t) = \frac{1}{N}\left|\sum_{k=1}^{N} e^{i\phi_k(t)}\right|, \tag{3.44}$$

where $\phi(t)$ is the phase vector overt time. The phase of neuron k is obtained by:

$$\phi_k(t) = 2\pi\frac{t - t_{k,m}}{t_{k,m+1} - t_{k,m}}, \tag{3.45}$$

where $t_{k,m}$ corresponds to the time of the m$-th$ spike of neuron k ($t_{k,m} < t < t_{k,m+1}$). $R(t)$ varies between 0 and 1, where $R = 1$ stands for a fully synchronized network while $R = 0$ to a fully desynchronized one [Pikovsky et al., 2002, Di Santo et al., 2018].

The synchrony measure χ quantifies the normalized average voltage fluctuation. χ is defined as:

$$\chi^2 = \frac{\sigma_V^2}{\frac{1}{N}\sum_{i=1}^{N}\sigma_{V_i}^2}, \tag{3.46}$$

where $\sigma_V^2 =< [V(t)]^2 > -[< V(t) >]^2$ is the mean variance over time of the population average voltage:

$$V(t) = \frac{1}{N} \sum_{k=1}^{N} V_K(t). \tag{3.47}$$

$\sigma_{V_i}^2 =< [V_i(t)]^2 > -[< V_i(t) >]^2$ is the mean variance over time of the single-cell membrane potential. χ varies between 0 (asynchronous state, i.e., fully desynchronized) and 1 (fully synchronized state) [Hansel and Sompolinsky, 1992, Golomb and Rinzel, 1993, Golomb et al., 2006, Golomb, 2007].

Pairwise spiking cross-correlation was computed as:

$$CC = \left\langle \frac{Cov(S_i, S_j)}{\sigma_i \sigma_j} \right\rangle, \tag{3.48}$$

where $Cov(S_i, S_j)$ is the covariance between two spikes trains S_i and S_j. $\sigma(S_{i,j})$ is the standard deviation of each spike train and <> stands for average over all the possible neuron pairs. CC is between -1 and 1. and takes high values only for synchronous states [Destexhe, 2009, Renart et al., 2010, Fontenele et al., 2019]

The autocorrelation firing rate function (ACF) was computed as [Harris et al., 2020]:

$$ACF(\tau) = \frac{\sum_{i=0}^{N-1}(x_i - < x >)(x_{i+\tau} - < x >)}{\sum_{i=0}^{N-1}(x_i - < x >)^2}, \tag{3.49}$$

where τ is the time lag, x is the network firing rate and <> stands for the mean over time. The global firing rate was defined as the sum of all network spikes in time bins.

3.4.5 Perturbational complexity index (sPCI)

In order to estimate perturbational complexity in brain slices and in the model, we used an adaptation of the PCI used in humans [Casali et al., 2013], named sPCI [D'Andola et al., 2018]. The stimulation electrode was placed in infragranular layers. Pulses had a duration of 0.1 ms, an intensity of $150 - 200$ mA, and were applied every 10 s, with a random jitter from $0.5 - 1.5$ s to avoid activity entrainment to the specific frequency of stimulation. A binary spatiotemporal distribution of significant activity was calculated in the multiunit activity (MUA) signal: we assessed the statistical differences between the network activity baseline and its response to the electrical stimulation using a bootstrap procedure as in [D'Andola et al., 2018]. The significance threshold was estimated as the one tail $(1 - \alpha)$ 99th percentile of the bootstrap distribution. Also, we first low-pass filtered (< 10 Hz) the trial average computed on the MUA signal, and considered significant only the periods in which the activity of each channel lay above

the significance threshold for > 50 ms. The sPCI was then defined as the normalized Lempel-Ziv complexity of the binary matrix of significant evoked MUA spatiotemporal patterns [D'Andola et al., 2018]. It is worthy of note that members of the Sanchez-Vives lab developed this algorithm, and it is not a result of the present thesis.

For the stimulation procedure performed in the model, described in Sec. 3.1.2, we depolarized all the neurons by a brief (40 ms) external stimulation current of 0.5 nA with an interval of stimulation of 5 ± 1 s (mean ± SD given). The sPCI was obtained exactly as described above for brain slices.

Chapter 4

Results

This thesis thoroughly investigates the mechanisms and dynamics of slow oscillations (SO), an emergent pattern of activity generated by the cerebral cortex, from a combined experimental and computational approach. SO is characterized by the rhythmic alternations between periods of neuronal depolarization and discharge (Up states) followed by periods of neuronal hyperpolarization and thus, silence (Down states, also called off-periods). This pattern of activity is characteristic of slow wave sleep and deep anesthesia but also spontaneously emerges in isolated cortical networks. Here, we have used *in vitro* experimental data to shed light on the mechanisms by which SO are maintained and thus also understand the mechanisms mediating brain transitions. Also, we have implemented, modified and thoroughly investigated a network model of slow oscillations. The development of these computational models is one of the central part of this thesis, which allowed us to a directly comparison with experimental data and a more detailed exploration of the parameter space. In the following, I will specifically describe the results obtained in this thesis.

4.1 Role of SK calcium-activated potassium channels on cortical slow oscillations

We first recorded from cerebral cortex slices (n=8) that generated spontaneous slow oscillations (SO), consisting of interspersed Up (active) and Down (silent) states. To investigate the role of SK calcium-activated potassium channels (KCa) [Sah and Faber, 2002] on this network activity, we next applied apamin, a bee toxin that specifically blocks this ionic current (I_{KCa}) [Castle et al., 1989], and studied the changes in the emergent pattern. Next, since there are experimental limitations to the understanding of the mechanisms bridging from neuronal membrane properties to networks, we studied the role of KCa channel in a biologically-plausible Hodgkin-Huxley model of the cerebral cortex network.

4.1.1 Effects of KCa channel blockade on the Up/Down state cycles

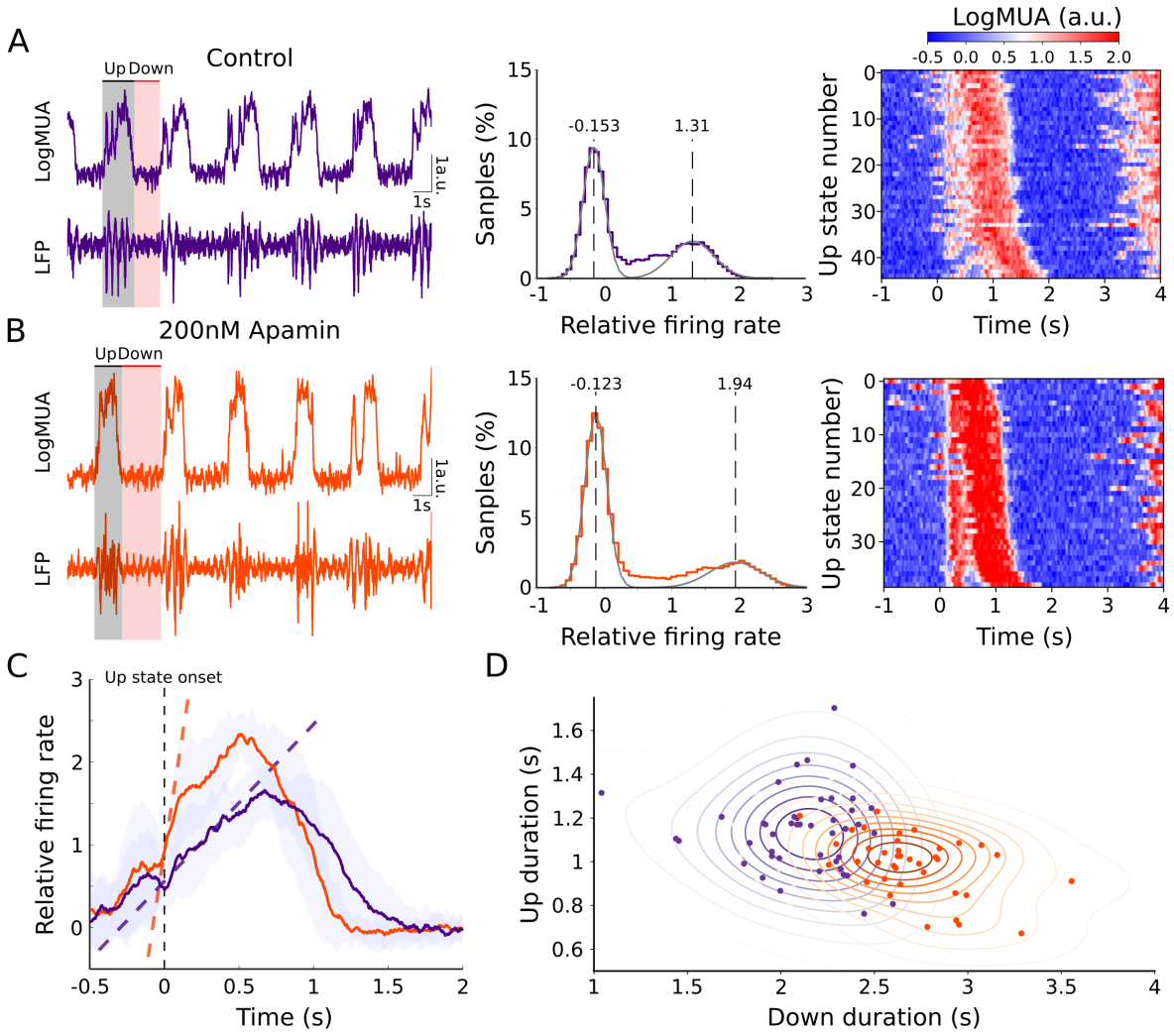

Figure 10 – Effect of KCa channel blockage on slow oscillations of a single recording. (A), left: Local field potential (LFP; bandpass filtering), recorded with a tungsten electrode, and relative firing rate (LogMUA) of the spontaneous slow oscillations (SO). Up states were detected from the LogMUA (see Methods Sec.3.4). Middle: histogram of the relative firing rate values illustrating the bimodality of SO. Right: raster plot of the relative firing rate. (B), Same as in (A) for blockade of KCa channel by bath application of apamin (200 nM). (C), Average firing rate for Up states during the control (orange) and apamin (purple). Dashed line illustrating the increase of the firing rate slope of Down to Up state transition. (D), Scatter plot of Up and Down duration. Irregular ellipses stand for the bivariate (2D) kernel density estimate (KDE; see Methods Sec.3.4 for details).

The baseline frequency of the slow oscillations (SO) in our experimental sample was 0.40 Hz (mean 0.40 ± 0.14 Hz, n= 8), with a duration of Up/Down states of 0.82 ± 0.33 s and 2.27 ± 1.53 s respectively. KCa channel antagonist, apamin 200 nM, after applied to the bath resulted in several changes in the Up states of the cortical slices

(see Fig. 10 for a representative slice). The two main changes that were observed were an increase in the population firing rate during the Up state and a shortening of this period following the blockade of KCa channel (Fig. 10A, B, C and D). In the distribution of Up and Down states in the case illustrated in Fig. 10B and D, there is also a visible elongation of the Down states, albeit this was not significant at the population level.

Regarding the firing rate during Up states, the raster plots displayed in Fig. 10A and B suggest a more synchronized, higher firing rate, with a change in the firing pattern that appears less dispersed in the presence of apamin (compare Fig. 10A right column with 10B right column). This relevant aspect of the Up state's firing pattern and how it is shaped by potassium adaptation (KCa channel) was later explored in detail in the computational model.

We investigated different properties of slow oscillations at the population level (Fig. 11). We found both the shortening of Up states (Control: 0.82 ± 0.33 s; Apamin: 0.55 ± 0.23 s, p= 0.0234, n=8) and an increase in the firing rate (Control: 1.05 ± 0.18 a.u.; Apamin: 1.43 ± 0.37 a.u., p= 0.0156, n= 8) to be significant at the population level. Both properties are indeed mechanistically related, since it has been proposed that the termination mechanism of the Up state is the recruitment of adaptation, being dependent on the firing rate during the Up states [Compte et al., 2003]. Indeed, the slope of Up state initiation was also significantly steeper in apamin (Control: 3.53 ± 2.85 s^{-1}; Apamin: 9.75 ± 4.26 s^{-1}; p= 0.0312, n=8), suggesting a link between these three features of the oscillation that we subsequently explored in the cerebral cortex model.

Other properties (Table 4), such as the Down states duration, the frequency of the full oscillatory cycle, or the regularity (coefficient of variation) of the Up and Down states and oscillatory cycle, did not significantly vary when blocking KCa channel (Fig. 11). This is highly suggestive that the impact of the KCa channel is largely on the Up states' firing pattern and initiation mechanisms, but less noticeable for the rest of the cycle, even when in individual cases, the effect on the Down states is significant (Fig. 10D).

4.1.2 Impact of KCa channel on the cortical network model

To carry out a detailed, mechanistic, and quantitative exploration of the role of KCa channel in the cortical network, we implemented a biophysically detailed computational model of the cortical network (see Methods Sec. 3.1). The model can reproduce many features of slow oscillations observed in *in vitro* [Compte et al., 2003, Compte et al., 2008, **?**]. It consists of pyramidal and inhibitory conductance-based neurons equidistantly distributed on a line and interconnected through biologically plausible synaptic dynamics. In the network, neurons are sparsely connected with a probability that decays with the distance between them. This together with some randomly distributed intrinsic parameters are the only source of noise in the model, i.e.,

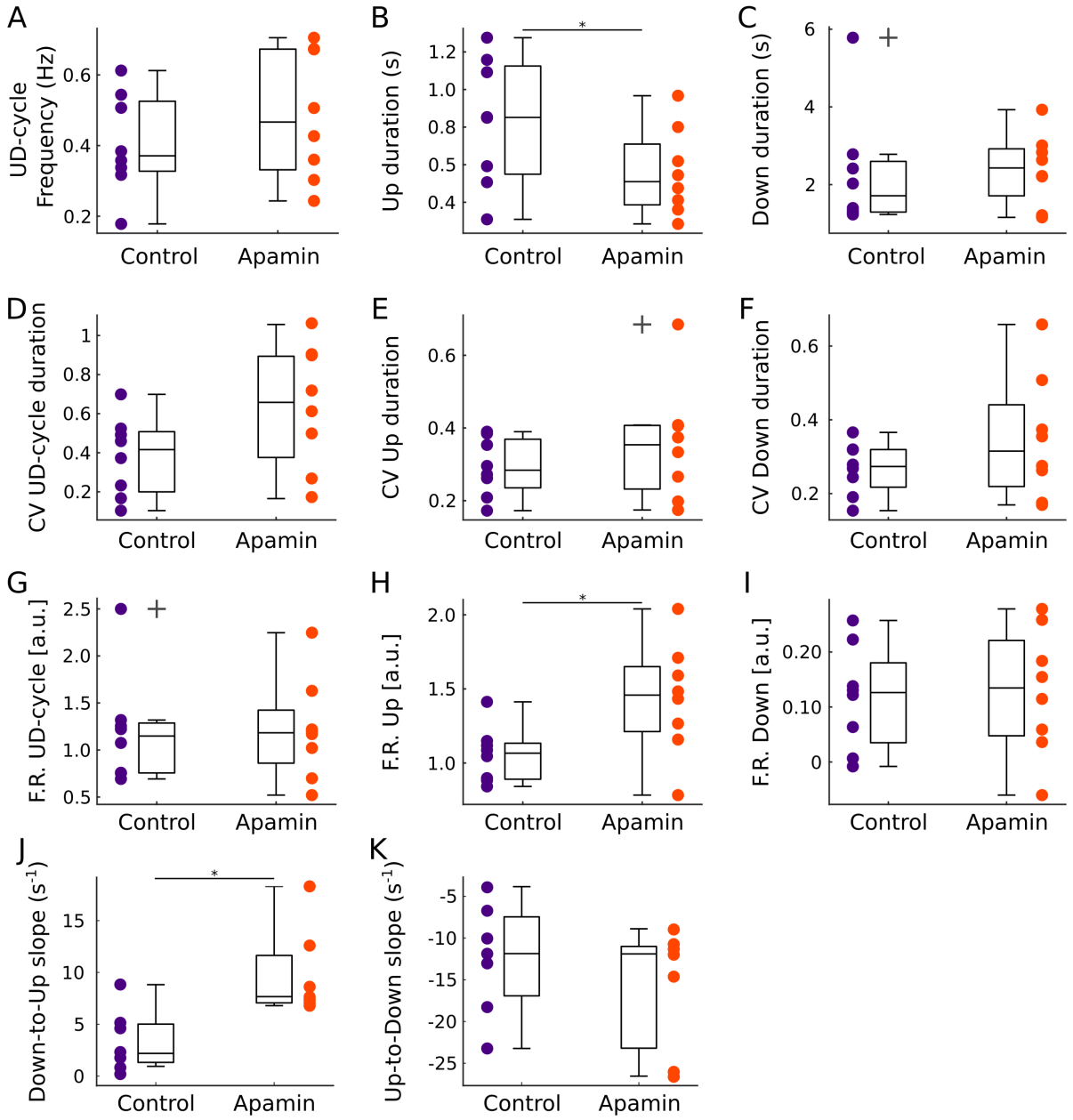

Figure 11 – Relative changes of Up and Down state properties during the blockage of KCa channel. (A), Frequency of the Up and Down cycle (UD-cycle). (B), Up state duration. (C), Down state duration. (D), Coefficient of variation (CV) of UD-cycle duration. (E), CV of Up state duration. (F), CV of Down state duration. (G), Relative firing rate of UD-cycle. (H), Relative firing during Up states. (I), Relative firing rate during down states. (J), Transition slope of Down to Up states . (K), Transition slope of Up to Down states. Relative firing rate is defined as the mean LogMUA across time (see Methods Sec.3.4 for details). * stands for a p-value $p<0.05$ (two-sided Wilcoxon signed rank test).

neurons do not receive any external input (see Methods Sec. 3.1).

Our computational model generated spontaneous activity in the form of Up

Table 4 – Relative changes of Up and Down state properties during the blockage of KCa channel. P-value of a two-sided Wilcoxon signed rank test

Parameter	**Control (mean±sd)**	**Apamim (mean±sd)**	**p-value**
Frequency (Hz)	0.40 ± 0.14	0.48 ± 0.18	0.19
Up state duration (s)	0.82 ± 0.33	0.55 ± 0.23	0.02
Down state duration (s)	2.27 ± 1.53	2.40 ± 0.92	0.38
CV Up-Down state cycle duration	0.38 ± 0.20	0.63 ± 0.31	0.05
CV Up state duration	0.29 ± 0.07	0.35 ± 0.16	0.25
CV Down state duration	0.26 ± 0.07	0.34 ± 0.16	0.31
Up-Down cycle relative firing rate	1.19 ± 0.58	1.21 ± 0.53	1
Up state relative firing rate	1.05 ± 0.18	1.43 ± 0.37	0.01
Down state relative firing rate	0.1 ± 0.09	0.12 ± 0.11	0.64
Down to Up transition slope (s^{-1})	3.53 ± 2.85	9.75 ± 4.26	0.03
Up to Down transition slope (s^{-1})	−12.40 ± 6.63	−15.74 ± 7.40	0.21

(periods of persistent activity) and Down (periods of quiescence) states and the cortical activity under blockade of KCa channels (Fig. 12A). In the model, the blockage was performed by parametrically decreasing the maximal conductance (g_{KCa}) from 100% to 10% of KCa current (I_{KCa}) in the pyramidal neurons. Representative dynamics of pyramidal cells, their intracellular calcium concentration and interneurons, under control, and KCa channel blockade are illustrated in Fig. 12B. Even when this is the membrane potential of individual cells, the network dynamics are determined by the recurrent connectivity between the cells and the intrinsic excitability, in absence of any external input. The firing rate for individual excitatory neurons displays a typical pattern, as the one that has been reported from intracellular recordings both in *in vitro* [Sanchez-Vives and McCormick, 2000, Mann et al., 2009, Sanchez-Vives, 2012] and in *in vivo* [Steriade et al., 1993c, Timofeev et al., 2000, Compte et al., 2009]. During an Up state, with each action potential, there is calcium entering the cell and increasing intracellular calcium in the submembrane compartment, which activates KCa channel (Fig. 12B). Fast spiking neurons (interneurons) also express slow oscillations, however, in our mode, they do not have KCa channel (Fig. 12B, bottom). When KCa channel is decreased in the model through the blockage of KCa current (I_{KCa}), simulating experimental blockade with apamin, firing rate increased during Up states (Fig. 12A) and the network activity became more regular (Fig. 12C), as a consequence of blocking the SK-mediated adaptation. Interestingly, not only the pyramidal cells that have the expression of KCa channel have an increment in its firing rate (Control: 1.05 ± 0.41 Hz, 90% KCa blockade: 2.41 ± 0.73 Hz) as fast spiking neurons too (Control: 17.28 ± 4.44 Hz, 90% KCa blockade: 26.69 ± 7.78 Hz) (Fig. 13A and B). This was concurrent with a more regular spiking pattern, revealed by the absence of intermediate ISI (interspike intervals;

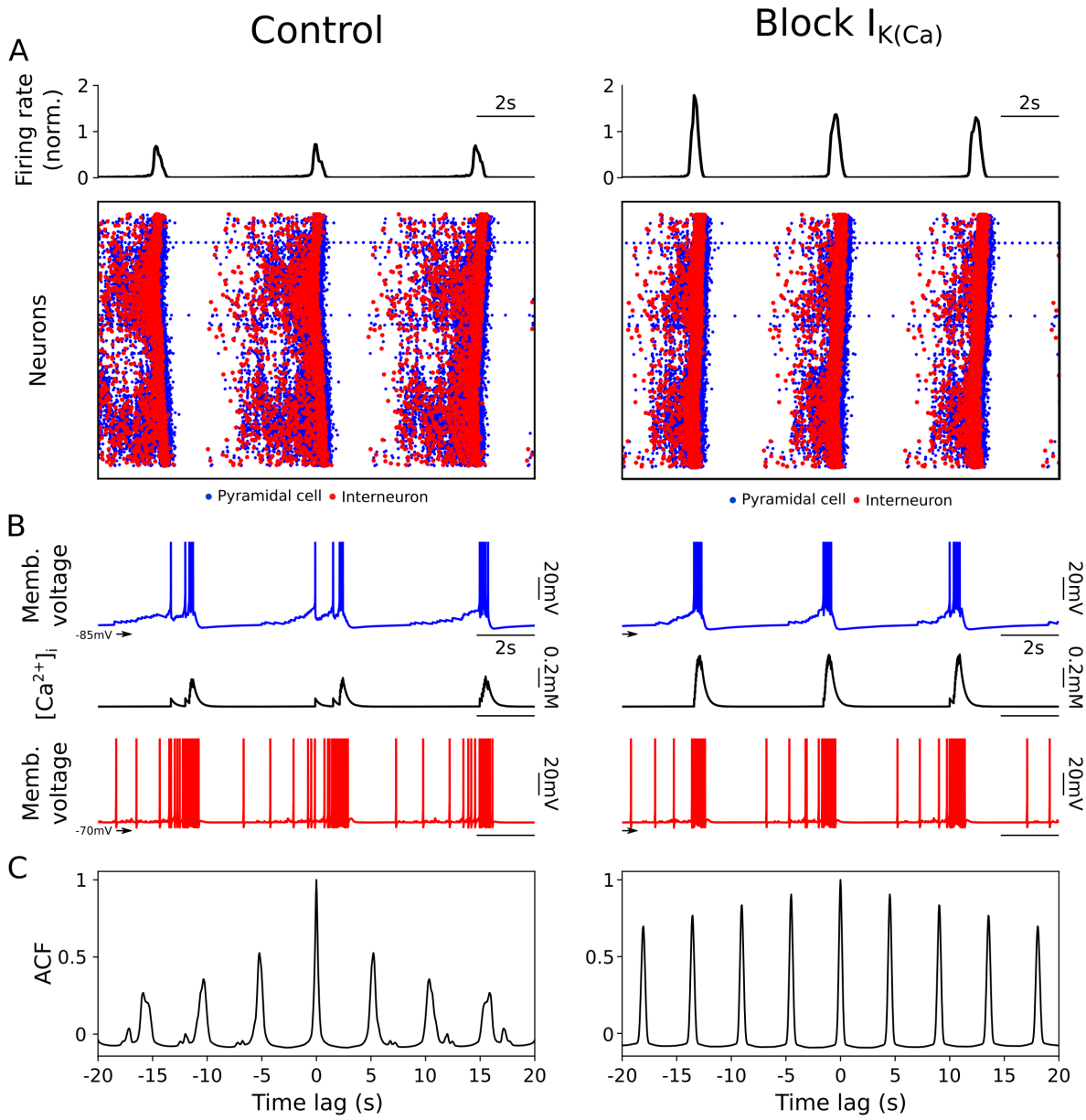

Figure 12 – Impact of KCa channel on the cortical network model. (A), Slow oscillatory activity in the form of Up and Down states in a control network (slow oscillations, SO). (B), Effect of KCa channel blockade (90%) on the slow oscillatory activity. (B), Representative membrane potential of pyramidal cell (blue) and interneuron (red) as well as the intracellular calcium concentration of pyramidal neurons, during SO (left) and blockage of KCa channel (right). (C), Autocorrelation function of the network firing rate depicted in (A), for control and blockage of KCa channel, respectively.

Fig. 12B and Fig. 13C).

To better understand the relationship between the firing rate and duration of Up states we carried out a parametric variation of the KCa channel expression (Fig. 13). We found that there was an inverse relationship with the firing rate, such

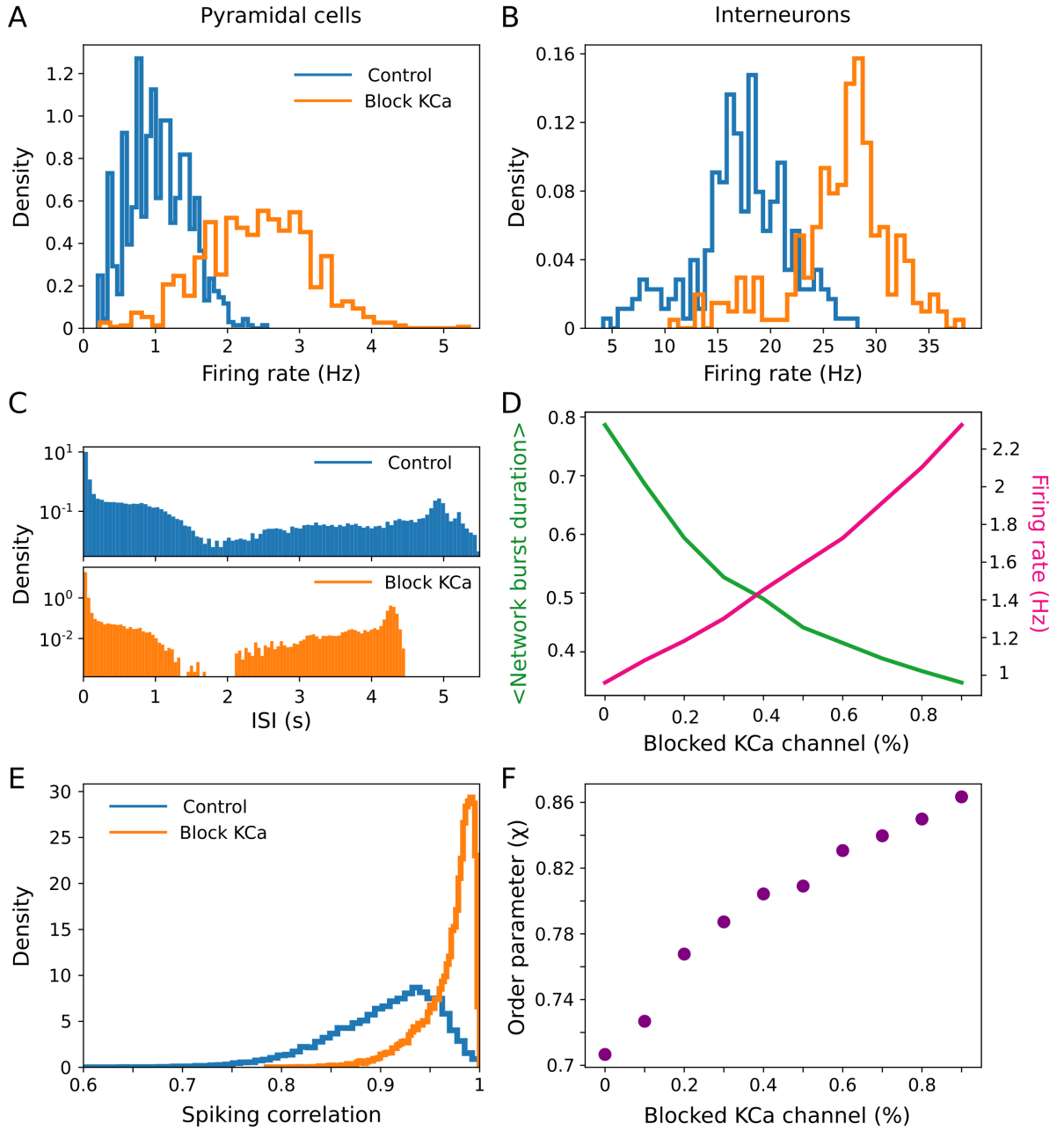

Figure 13 – Impact of KCa channel on the cortical network model. (A) and (B), Mean neuronal firing rate during control (slow oscillations, SO) and blockade of KCa channel for pyramidal cells and interneurons, respectively. (C), Pyramidal cells mean interspike interval during control (slow oscillations, SO) and blockage of KCa channel. (D), Up state duration and neuronal firing rate *versus* blockade of KCa. The Up state duration was estimated as the mean network burst duration, see Methods Sec. 3.4.3). (E), Pairwise spiking correlation histogram, where mean and standard deviations are 0.89 ± 0.06 and 0.97 ± 0.02 for control and a blockage of 90% of KCa channel, respectively. (F) the normalized average voltage fluctuations (χ) order parameter as a function of KCa channel blockage.

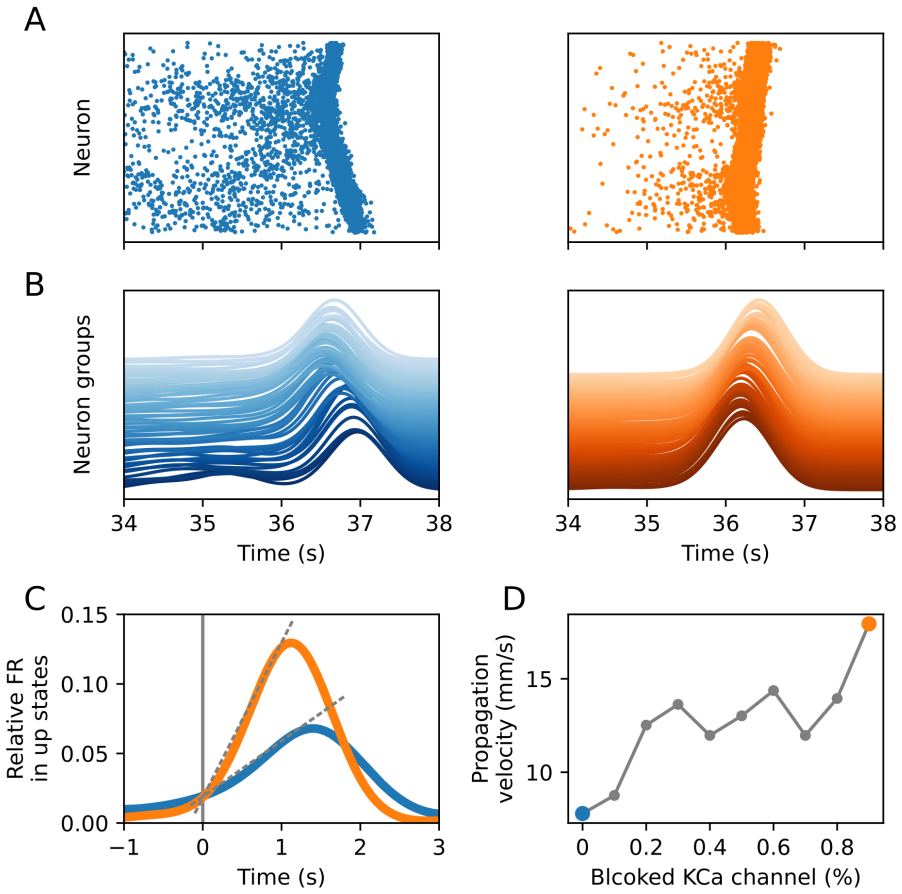

Figure 14 – Intrinsic neuronal properties shape emergent cortical activity. (A), Raster plot of a control network (slow oscillations, SO; left) and during the blockade of KCa channel (right). (B) Firing rate of subpopulation of neurons (15 neurons per group) during an Up state for control (left) and during blockade of KCa channel (right). (C), Average firing rate for Up states during the control (orange) and blockage of KCa channel (purple). Dashed line illustrating the increase of the firing rate slope of Down to Up state transition. (D), Wave velocity propagation dependence on the KCa channel concentration. Blue dot represents the full presence of KCa channel and orange dot the blockage of 90% of KCa channel. Colors in (A), (B) and (C) stand for the concentration of KCa channel depicted in (D).

that the lower the expression, the higher the firing rate and the shorter the duration of Up states (here estimated as the mean pyramidal burst duration over the network (Fig. 13D; see Methods Sec. 3.4.3). This effect suggests that, together with the regularity expressed by the firing rate autocorrelogram (ACF; Fig. 12C) and the ISI distribution (Fig. 13C), the network activity is more synchronized during the absence of KCa channel expression. Through the analysis of spiking correlations, we found that the pairwise spiking correlation structure under KCa channel blockage is different from that observed in a control situation (Fig. 13E). The mean of pairwise spiking correlation increased (Control: 0.89, KCa blockage: 0.97) together with a decrease in the standard

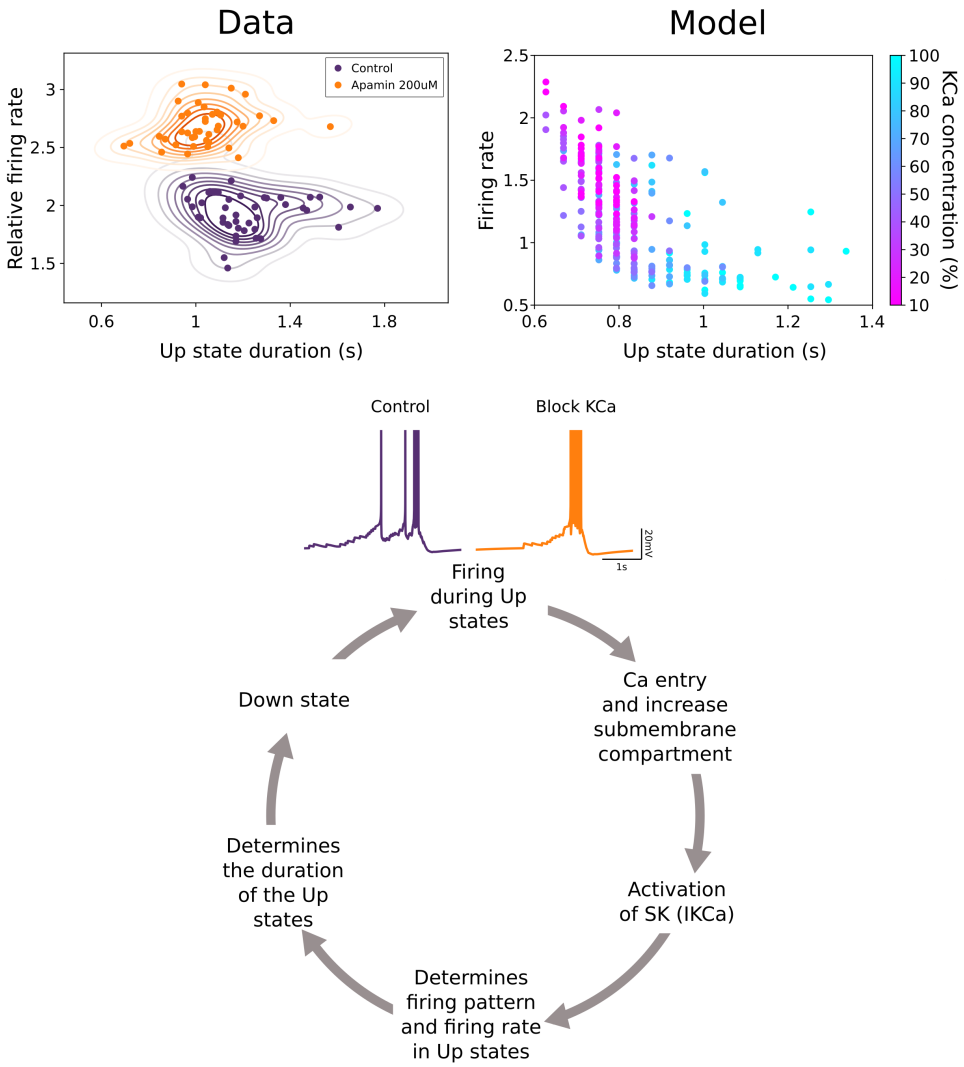

Figure 15 – Effect of KCa channel on the cortical network dynamics and the slow oscillatory cycle mechanisms. Top: firing rate versus Up state duration for slice data (top left) and the cortical network model (top right) show the critical role of KCa channel on the firing pattern and Up state duration. Bottom: schematic representation of the periods composing an oscillatory cycle and the KCa channels role.

deviation (Control: 0.06, KCa blockage: 0.02), indicating a more synchronous regime. Also, the absence of intermediate interspike intervals during blockage of KCa channel suggests, that the cellular membrane fluctuations may also reflect a synchronous regime. In order to test that we implemented an order parameter (χ) proposed in [Golomb et al., 2006] which quantifies the normalized average cellular membrane fluctuations. By parametrically changing the KCa concentration, we found that, concurrent with the network autocorrelogram (Fig. 12C), ISI distribution (Fig. 13C), and pairwise spiking correlation (Fig. 13E), the absence of KCa introduce more regularity in the membrane potential, i.e., a more synchronized state. Therefore, KCa has an important

role decorrelating neuronal firing, as previously described in [Wang et al., 2003].

Also, in the model, we could detect a slight influence of KCa channel on the Down states. However, given the time constant of the channel (150 ms; see Methods Sec. 3.1.1.1), based on experimental data [Markram et al., 1995, Helmchen et al., 1996, Svoboda et al., 1997, Wang, 1998] and the spikes per Up state, results on a weak influence on the Down state which has an average duration of ~ 5 seconds. However, this does not imply that in other situations, for example, the response of a stimulus, or a pre-epileptic discharge [Sanchez-Vives et al., 2010] it may have a different role.

Furthermore, the increment in the network synchronization (Fig. 13E and F) caused by the blockage of KCa channel suggests that intrinsic properties of the neurons become network properties. To examine it, we next evaluated a population phenomenon (group of neurons) and a network property (interaction between group of neurons), namely the slope of Down-to-Up transition (which had a significant difference for the experimental data, Fig. 11J), and the velocity of propagation. As discussed above a more regular activity is achieved when KCa channel is blocked, which becomes visible in the raster plot (Fig. 14). By grouping nearby neurons in a population (15 neurons per group) we were able to evaluate two aspects of the network: i) the slope of the transition between Down to Up states (Fig. 14C) which was visually steeper for blockage of KCa channel, following the experimental data (Fig. 11J); and ii) the wave propagation velocity that is faster with the absence of KCa channel (Fig. 14D).

Together, all the above described metrics suggest that calcium dependent potassium channel has a critical role in the firing pattern during Up states and in the membrane fluctuations. We proceed then to analyze the experimental and model data relation between each detected Up state and its firing rate. A relationship between both is observed in the two cases (Fig. 15), i.e., the presence of KCa regulates the firing rate of Up states and its duration. Within this picture, we proposed a cycle between Up and Down states based on the intrinsic properties of the cells. Specifically, increasing the intracellular calcium concentration activates the KCa channels which in turn determines the firing pattern and firing rate in Up states as well as its duration, however having no significant effects on the down state duration.

4.2 Impact of KCa and KNa channels on the dynamics of the cortical network

Our model reproduced the slow alternation between periods of active states, (Up states) and periods of almost no firing (Down states) observed experimentally in *in vitro* preparations [Sanchez-Vives and McCormick, 2000, Compte et al., 2003]. Neurons are sparsely connected forming a recurrent network and were modeled by a

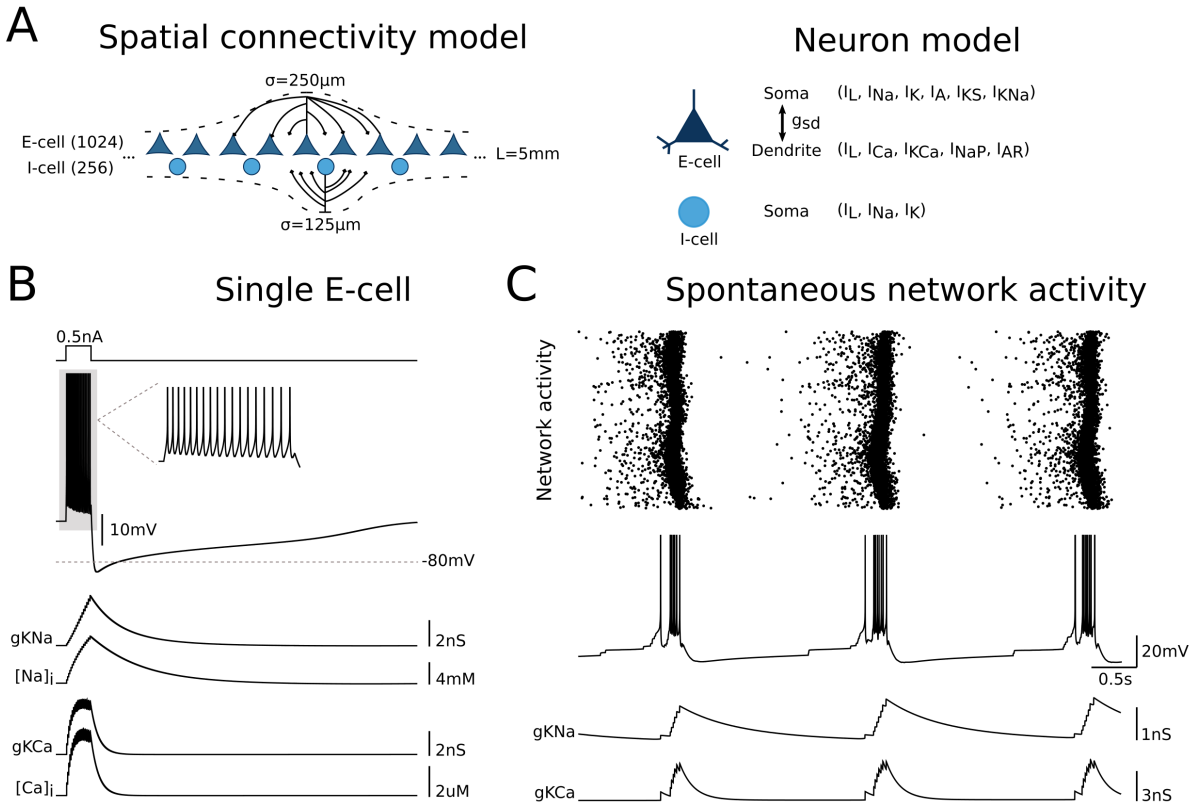

Figure 16 – Network model. (A), Schematic representation of the spatial connectivity and the neuron model. Our network is assumed to be 5 mm long and is composed by pyramidal cells (E-cells) and interneurons (I-cells). The probability of connection between neurons are given by Gaussian probability distribution with distance decay, centered at each neuron, and with a prescribed standard deviation σ (Methods Sec. 3.1.1.3). (B) Response of a single pyramidal neuron when depolarized by a current of 0.5 nA for 0.5 s. The average firing is $\sim$ 36 Hz. Below intrinsic conductances for sodium dependent potassium (g_{KNa}) and calcium dependent potassium (g_{KCa}) channels, and the intracellular concentration for sodium ($[Na]^i$) and calcium ($[Ca]^i$). (C) Rastergram of spontaneous network activity. Below a representative pyramidal neuron intracellular somatic voltage and the intrinsic conductance dynamics for g_{KNa} and g_{KCa}. For the simulations in (B-C) g_{KNa}= 1.0 mS/cm^2 and g_{KCa}= 0.9 mS/cm^2.

variety of ionic channels (Fig. 16A; see Methods Sec. 3.1.1.1 for details). Disconnected pyramidal neurons, when depolarized by a current of 0.5 nA during 0.5 s, fired at an average of $\sim$ 36 Hz followed by spike-frequency adaptation, modeled here as sodium and calcium dependent potassium currents, KNa and KCa, which are dependent on the intracellular concentration of sodium and calcium, respectively (Fig. 16B). When synaptically connected, neurons fired in bursting followed by long-lasting periods of silence, $\sim$ 2s (Fig. 16C). These spontaneous Up and Down dynamics are guided by recurrent excitation and slow afterhyperpolarization currents. When an adjacent group

of neurons is together activated they trigger a cascade of recurrent excitation that brings the network into the active state (firing regime). During this active state, slow activity-dependent K^+ start to accumulate reducing the neuronal excitability and eventually bringing the network to a down state. After a slow recovery, guided by the decay time of KNa and KCa currents, the neuronal excitability is recovered and the neurons are able to engage again in an active state (Fig. 16C). Notice that the contribution of KNa and KCa currents follow different intrinsic dynamics, where the latter accumulates faster but also decay faster when compared to the former (Fig. 16C).

We call the attention here to the fact that the main features of the model can be qualitatively reproduced even by changing intrinsic neuronal properties [Sancristóbal et al., 2016]. However, some intrinsic parameters can directly affect the collective network dynamics. In the next sections we explored potassium slow afterhyperpolarization currents, namely I_{KCa} and I_{KNa}, that have been suggested to be critically implicated in the stability of Up and Down dynamic [Steriade et al., 1993a, Sanchez-Vives and McCormick, 2000, Bhattacharjee and Kaczmarek, 2005] (for a review see [Neske, 2016]).

4.2.1 Effect of modulating Ca^{2+}-dependent K^+ channel on network stability

To explore how the presence of KCa channel modulates the emergent pattern of cortical slow oscillations, we departed from an expression in all cells and parametrically blocked the activation of this channel on pyramidal neurons (randomly from 0% to 90%). For each concentration of blockade, we also tested the dependence on the KCa maximal conductance (g_{KCa}, from 0.4 to 1.2 mS/cm^2).

We first observed that blockade of KCa channel induced a more regular firing pattern in the spontaneous network activity (Fig. 17A and B). For instance, in a control network (with no KCa blockage), there is some spiking prior to the onset of an Up state (Fig. 17A and B, left column), which indeed is part of the mechanism mediating the initiation of a new Up state [Compte et al., 2003]. Conversely, when KCa channel is blocked, fewer cells show spiking during the Down states followed by more firing rate during Up states (Fig. 17A and B, middle and right column).

For a detailed quantification of the KCa impact on the spontaneous slow oscillations, we analyzed the Up state duration by estimating the average width of the peak of spike-train autocorrelation function (ACF) for each neuron in the network (Fig. 17C). As observed in the single membrane potential of the embedded neurons in the network (Fig. 17B), when blocking the activation of KCa channel, the width of ACF becomes narrow and high, indicating a shortening in the Up state and an increment in the neuronal firing rate (Fig. 17C). Indeed, when we parametrically altered the blockade of KCa, we observed that the Up state duration became shorter, reaching stable values for a blockade greater than 50% (Fig. 18A). We also noticed that the Up state's duration

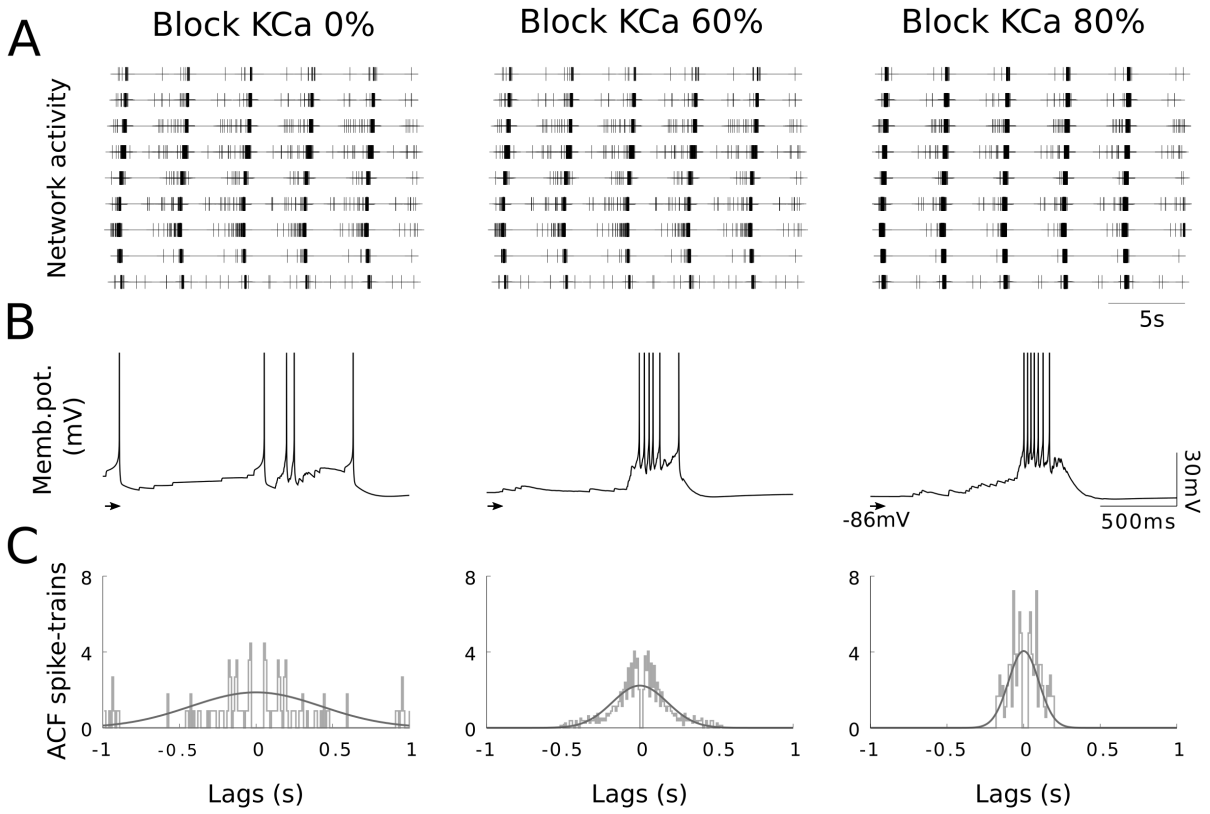

Figure 17 – Network activity under Ca^{2+}-dependent K^+ channel modulation. (A), Impact of Ca^{2+}-dependent K^+ (KCa) modulation on spontaneous network slow oscillations (visualized as multi-unit recordings, 15 neighboring cells per site). (B), Representative network neurons membrane potential (V_m). Arrow point at −86 mV for voltage traces. (C), Spike-train autocorrelation (ACF): solid lines represent the Gaussian fit to the autocorrelation's central peak, from which the Up state duration is estimated. KCa blockage in (A-C): control 0% (left column), 40% (middle column) and 80% (right column), respectively. Simulations in (A-C) were run with g_{KCa}= 1.1 mS/cm^2.

for low blockage of KCa is larger for higher values of KCa maximal conductance (g_{KCa}, Fig. 18A). Furthermore, we notice how the standard variation of the Up state duration reached low values for large values of KCa blockage, suggesting though a more regular dynamics (Fig. 18A inset).

We next evaluated the evolution of the mean neuronal firing rate (FR). We observed an almost linear increment on the FR while progressively blocking the activation of KCa, independent of the KCa maximal conductance (Fig. 18B). Also, the autocorrelogram peaks of the global network FR indicate an even more synchronized network when KCa activation was blocked (Fig. 18C, ACF peak values are: 0.79, 0.82 and 0.85 for a blockage of 10%, 70% and 90%, respectively). ACF also indicates that the down duration becomes longer for larger blockage of KCa current (compare the time lag for different concentrations in Fig. 18C). To further quantify the synchronization in these

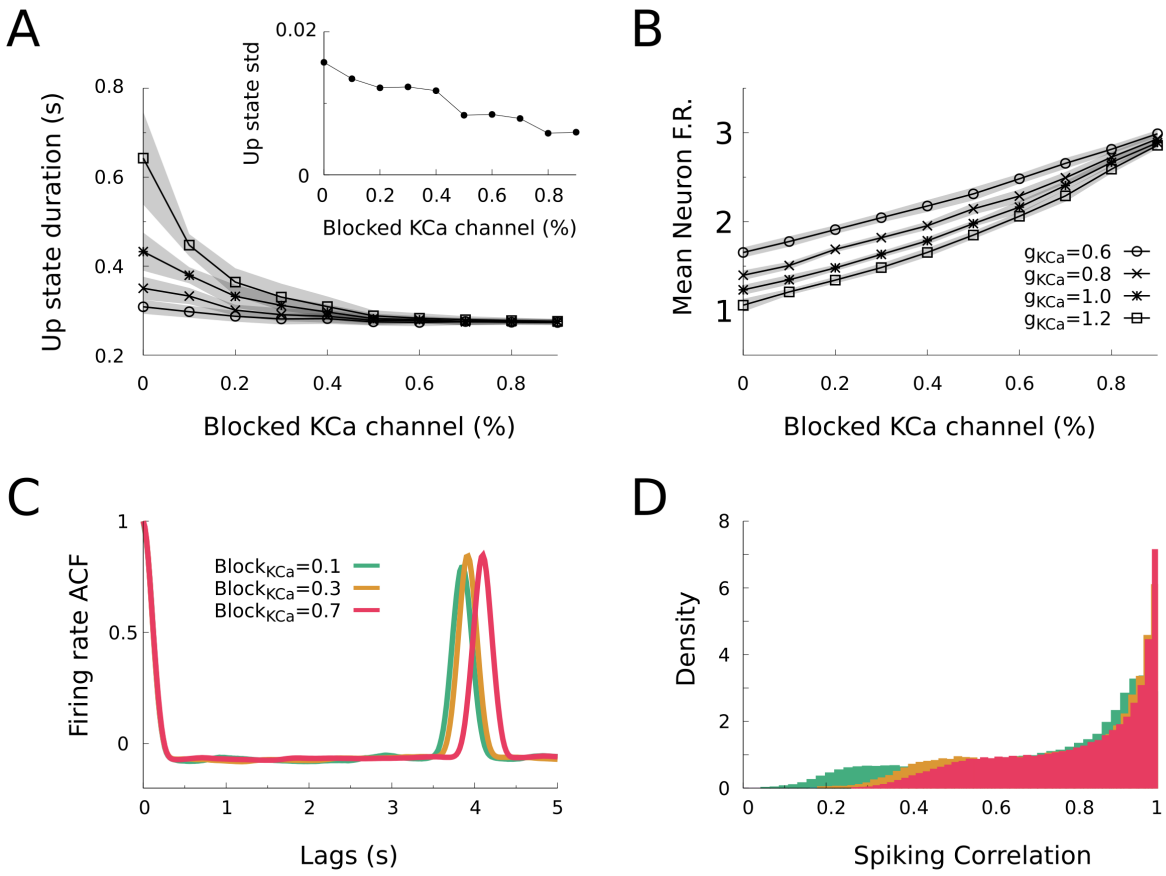

Figure 18 – Effects of progressive Ca^{2+}-dependent K^+ channel modulation on slow oscillations. (A), Duration of Up states, estimated as the spike-train autocorrelation width averaged over all neurons as a function of Ca^{2+}-dependent K^+ (KCa) channel modulation. Inset: standard deviation of Up state durations for g_{KCa}= 0.6 nS. (B), Mean neuronal firing rate (F.R.) as a function of KCa modulation. (C), Global network F.R. autocorrelation function. (D), Pairwise spiking correlation histogram, where mean and standard deviation are 0.70 ± 0.24, 0.77 ± 0.20 and 0.81 ± 0.18 for a blockage of 10%, 70% and 90% of KCa channel, respectively. Shadow areas in (A-B) represent the standard deviation over 10 different simulations; markers stand for different values of KCa maximal conductance (g_{KCa}), described in (B). The color code in (C-D) represents different values of KCa blockage, as described in (C). Simulations in (C-D) were run with g_{KCa}= 1.1 mS/cm^2.

networks, we computed the pairwise spiking correlations. In those networks where KCa channel was more active a slightly wider histogram was observed (mean correlation: 0.70 ± 0.24, for 10% of KCa blockage), than those with less KCa activation (mean correlation: 0.81 ± 0.18, for 90% of KCa blockage), indicating than a less synchronized state (Fig. 18D).

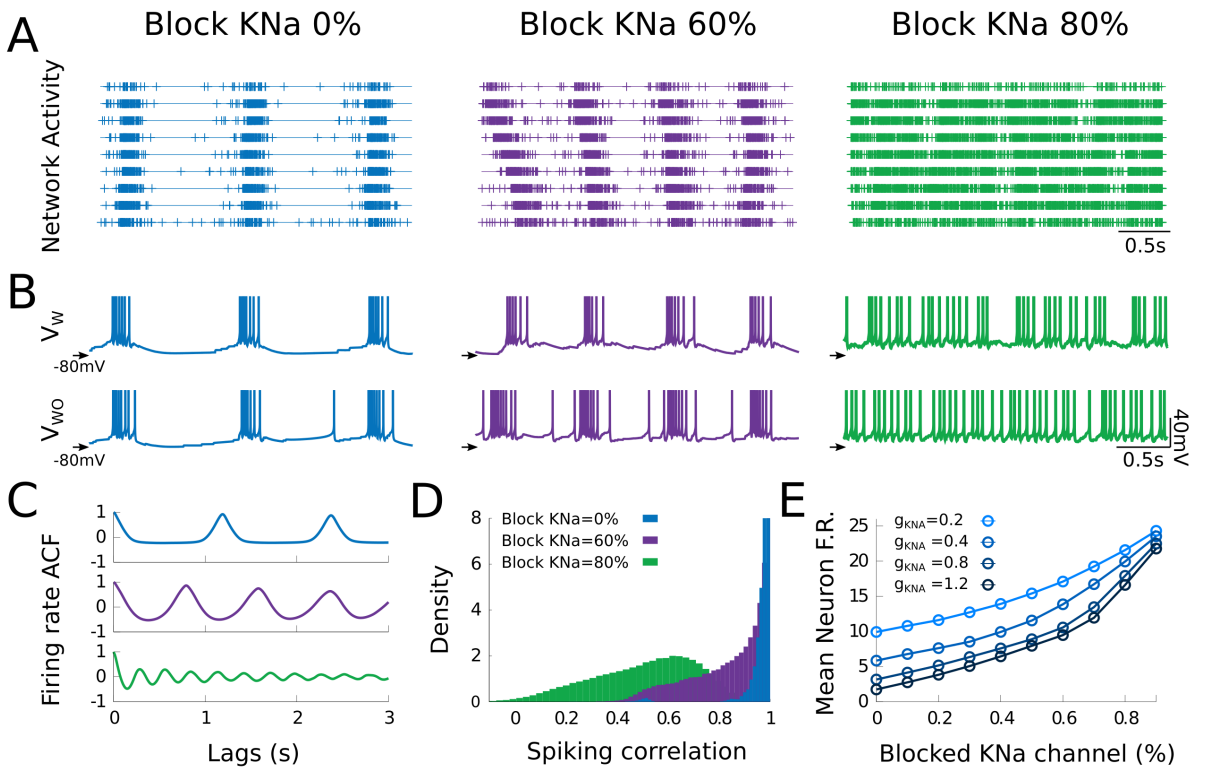

Figure 19 – Modulation of Na^+-dependent K^+ channel breaks-off Up and Down network dynamics. (A), Impact of Na^+-dependent K^+ (KNa) channel modulation on spontaneous network slow oscillations (visualized as multi-unit recordings, 15 neighboring cells per site). (B), Representative network neuron membrane potential, where V_w stands for neurons with the presence of KNa channel and V_{wo} stands for those without KNa channel. Arrows point at −80 mV for voltage traces. (C), Global network firing rate (F.R.) autocorrelation function (ACF) for the three cases depicted in (A). (D), Pairwise spiking correlation histogram, where mean and standard deviation are 0.96 ± 0.05, 0.82 ± 0.15 and 0.48 ± 0.20 for a blockage of 0%, 60% and 80% of KNa channel, respectively. (E) Mean neuronal firing rate (F.R.) as a function of KNa modulation. Simulations in (A-D) were run with g_{KNa}= 0.4 mS/cm^2.

4.2.2 Effect of modulating Na^+-dependent K^+ channel on network stability

We next explored whether the alone manipulation of the sodium-dependent potassium channel (KNa) might modulate the regime of slow oscillations (SO). KNa activation blockage had a strong effect on the modulation of the spontaneous Up and Down network dynamics (Fig. 19A). For an increment on the KNa blockage the network departs from Up and Down dynamics to a more asynchronous irregular activity state, which is reflected by the multi-unit activity (Fig. 19A), the neuronal membrane potential (Fig. 19B), the global network firing rate autocorrelation function (Fig. 19C) and by the pair-wise spike correlation (Fig. 19D). Indeed, looking at the membrane potential of those neurons embedded in such networks, we noticed the transition from bursting

firing to a persistent firing (tonic-firing) which is characteristic of states of vigilance or awake-like states (Fig. 19B). Such transition was also followed by an increment in the mean neuronal firing rate, independently of the KNa maximal conductance (Fig. 19D). Interestingly, independent of the network state, those neurons which had (V_w) and did not have (V_{wo}) the presence of KNa channel, displayed similar dynamics (Fig. 19B, compare V_w with V_{wo}. We will return to this point in the next section).

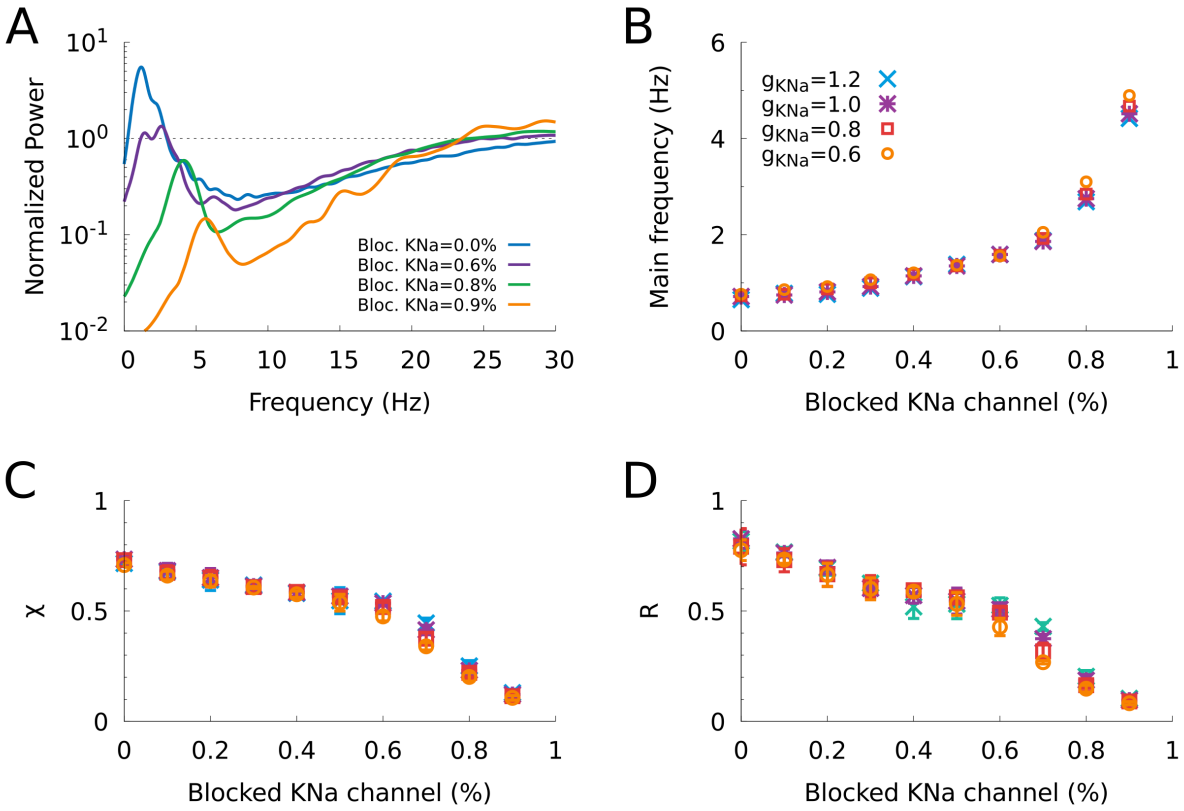

Figure 20 – Network synchronization dependence on Na^+-dependent K^+ channel. (A), Spike-train power spectrum, estimated with a multi-taper estimator, for different Na^+-dependent K^+ (KNa) channel modulation. (B), Main oscillatory frequency as a function of the KNa channel's modulation. Network synchrony measures: (C) the normalized average voltage fluctuations (χ), and (D) complex phase order parameter (R). The same color code and markers apply to (B-D).

We next looked at the frequency content modulation by KNa activation blockage evaluating the normalized spike-train power spectrum. We observed a departure from low frequencies (~ 1 Hz) with high power, to higher frequencies (~ 5 Hz) with low power (Fig. 20A). The main network frequency was modulated by the presence of KNa channel in an exponential-like way, being independent of the KNa maximal conductance (g_{KNa}) (Fig. 20B). To further characterize the network transition, from synchronous to asynchronous states, we used two different metrics, one based on the neuronal membrane potential fluctuations (χ) and the other based on the spiking phase of the

neurons (R) (see Methods Sec. 3.4). Both metrics (χ and R) exhibited the same panorama: a transition from synchronous (χ and R values close to one) to desynchronized (χ and R values close to zero) states (Fig. 20C and D), independently of g_{KNa}. Furthermore, χ and R metrics showed a slow decay of synchronization for blockage less than 60%, and a steeper decay for values above 60%.

4.2.3 Single neurons dynamics within a network

The spontaneous neuronal activity dynamics of each neuron, when embedded in a network, are almost indistinguishable, even though the neurons have different intrinsic properties, i.e., the presence or not of KNa channel (Fig. 19B). This is a critical finding of this study, since it evidences that intrinsic, ionic channels-dependent properties, are seamlessly transmitted to the recurrent network, such that the emergent patterns are virtually identical in cells with and without the ionic channels. To better understand if this effect is exclusively due to KNa or due to the heterogeneity of the network (e.g., maximal conductance of K+ leak channel, see Methods), we proceeded to analyze two isolated identical neurons (i.e. with the same set of parameters, except for the presence or not of KNa) subject to a plausible network input (Fig. 21A). In Fig. 21B we show the membrane potential traces for two isolated neurons when submitted to the same network input (Fig. 21B EPSP and IPSP) where the incidence was 90%, 70% and 10% of KNa channel. A more excitable membrane potential for the neuron without KNa (V_{wo}) can be observed when compared to the one with KNa (V_w) channel (Fig. 21B). To quantify these differences we measured the mean firing rate (Fig. 21C), the mean inter-spike-interval (Fig. 21D) and the minimum membrane potential (Fig. 21E) of these two neurons. As illustrated by the membrane potential traces (Fig. 21B), the neurons without KNa show a higher firing rate (Fig. 21C) followed by a shorter inter-spike-interval (Fig. 21D) when compared to the neuron with KNa. The minimal membrane potential also indicates a more depolarized membrane potential for the neurons without KNa (Fig. 21E).

4.2.4 Dependence of slow afterhyperpolarization currents on off-periods

We next simulated the evoked network activity to shed light on the activity-dependent K^+ afterhyperpolarization channels role on the off-periods [Pigorini et al., 2015, Rosanova et al., 2018]. Our approach consisted in, during a regime of slow oscillations, stimulating by a depolarizing current a group of neurons to evoke a network response. Once the network activity starts to fell down to an off-period we then block KCa, KNa, or both together (AHP) to better understand the contribution of each current on the break of causality (off-period). First, we characterized the network response without any channel activation blockage (Fig. 22 left column). The stimulation procedure evoked an active state followed by the occurrence of an off-period, characterized by almost no

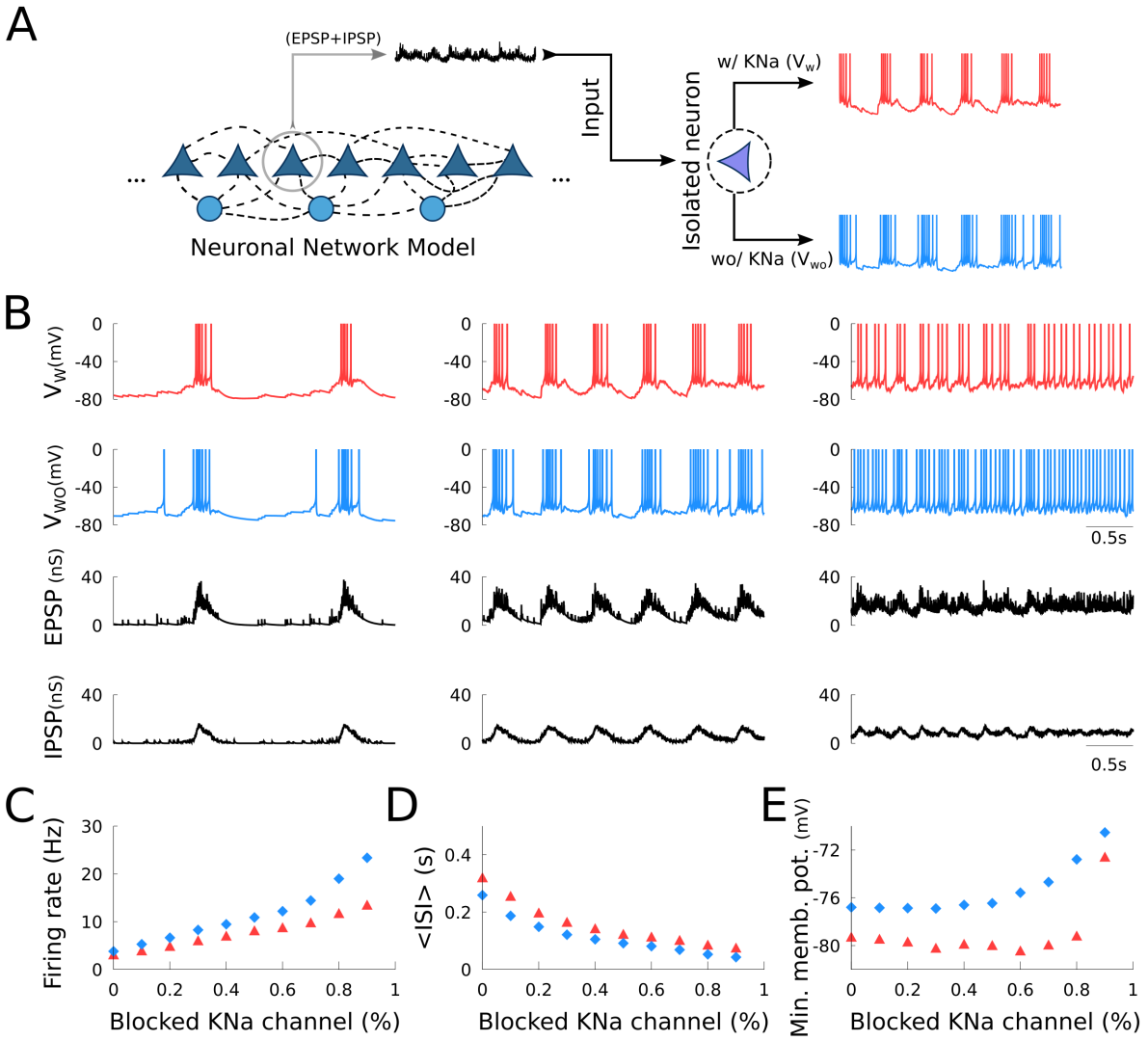

Figure 21 – Contribution of Na^+-dependent K^+ channel to spontaneous neuronal activity. (A), Schematic representation of the excitatory postsynaptic potential (EPSP) and inhibitory postsynaptic potential (IPSP) extraction from a neuron embedded in a network and converting it to an input to an isolated neuron with (red, V_w) and without (blue, V_{wo}) the presence of Na^+-dependent K^+ (KNa) channel. (B), Neuronal membrane potential for neurons with (V_w) and without (V_{wo}) KNa channel, under three different network inputs (EPSP+IPSP), representing the distinct dynamical states. Below, excitatory (EPSP) and inhibitory (IPSP) postsynaptic potential served as external input: network input with 90% (left column), 70% (middle column) and 10% (right column) of KNa concentration. (C-E), Comparison of the KNa channel activation impact on single neuron properties: (C) firing rate, (D) mean inter-spike-interval and (E) minimum membrane potential. The same color code from (A) applies to (C-E).

spiking activity (Fig. 22A left column) and consequently without excitatory or inhibitory post-synaptic potentials (EPSP and IPSP; Fig. 22B left column). Also, the simulated local

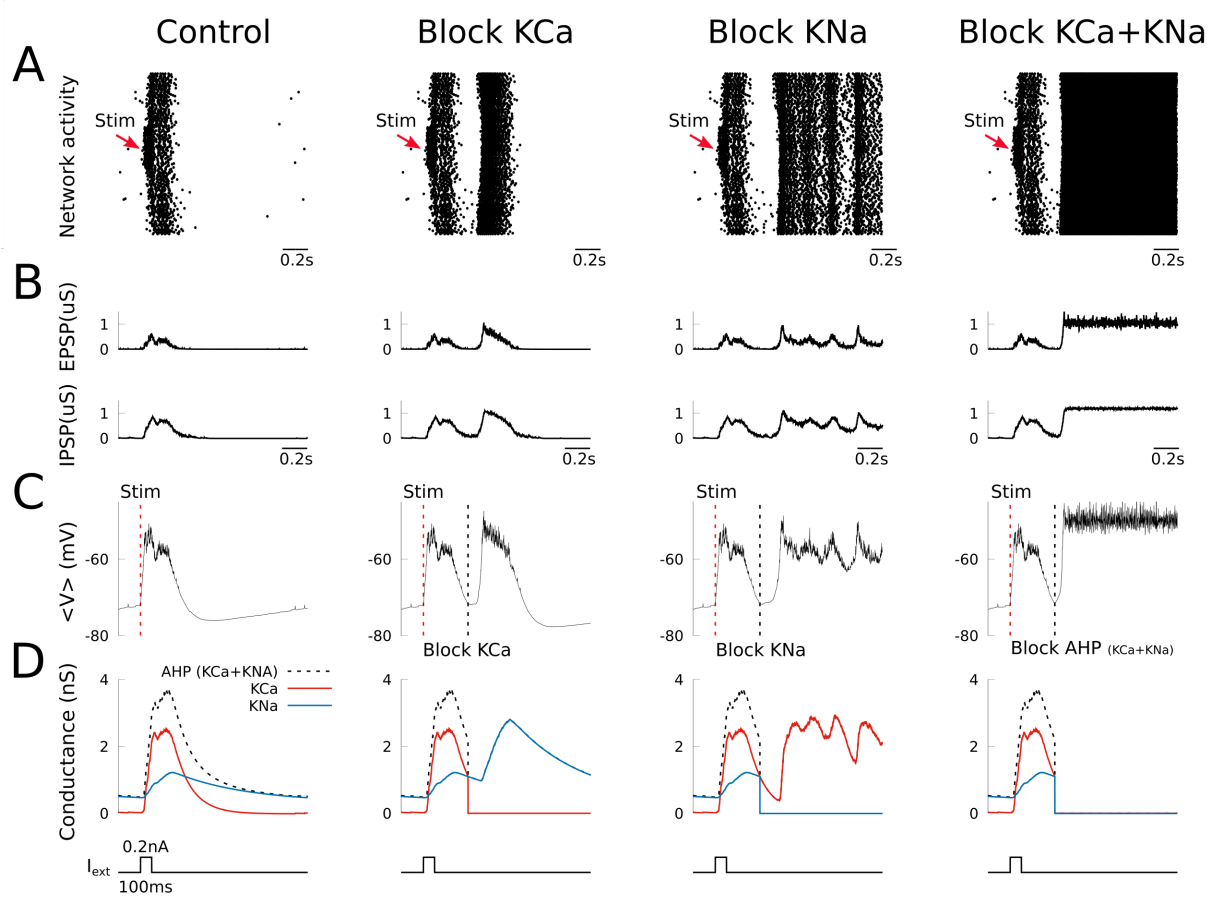

Figure 22 – Impact of slow potassium dependent currents on evoked network activity. (A), Network response (200 neurons depicted) to a brief stimulation: control condition (no blockage, left column), blockage of Ca^{2+}-dependent K^+ (KCa) channel (middle-left column), blockage of Na^+-dependent K^+ (KNa) channel (middle-right column) and blockage of afeterhyperpolarization (AHP, KCa+KNa) channels (right column). Stimulation was applied to a group of 52 neurons and channel activation blockage occurred 400 ms after stimulation. (B), Mean excitatory and inhibitory postsynaptic potentials (EPSP and IPSP, respectively). (C), Network local field potential (mean neuronal membrane potential). (D), Mean network conductance dynamics for KCa, KNa and AHP (KCa+KNa). Below, representation of network stimulation: neurons are depolarized by a 0.5 nA current during 100 ms. Simulations were run for networks with 90% KNa concentration, 100% KCa concentration, g_{KNa}= 0.8 mS/cm^2 and g_{KCa}= 0.9 mS/cm^2.

field potential (Fig. 22C left column) showed a clear network response after stimulation followed then by an off-period. We also observed that Ca^{2+}-dependent K^+ (KCa) channel accumulated faster than Na^+-dependent K_+ (KNa) channel during the active stated, although KCa decayed faster than KNa, suggesting though a different participation of KCa and KNa in the off-period (Fig. 22D left column). We next evaluated the individual contribution of each K^+-dependent channel on the off-period. The blockage of KCa channel allowed the network activity to re-enter in an active state again and only after that

reached a period of silence (Fig. 22 middle-left column), which was probably caused by the high activation of KNa channel (Fig. 22D middle-left). Conversely, when we blocked the activation of KNa channel, the network also re-entered the active state, although not falling back into a Down state. Instead, the after stimulation state was characterized by a reverberating-like activity (similar to the effect of cholinergic and noradrenergic neuromodulation [Barbero-Castillo et al., 2021]; Fig. 22 middle-right column). Finally, when we blocked the activation of both activity-dependent K^+ afterhyperpolarization channels, the network entered in a fully active state where the spontaneous activity was characterized by an asynchronous-like dynamics (Fig. 22 right column).

4.3 Role of voltage gated K^+ channel (M-current) on cortical slow oscillations

The voltage-gated K^+ channel 7 (K_{V7}) generates the M-current (I_M) and is suppressed by the activation of muscarinic acetylcholine receptors, which in turn leads to a transient increase in excitability and underlies some forms of cholinergic excitation [Brown, 2010, Radnikow and Feldmeyer, 2018]. Here, we first recorded from cerebral cortex slices (n= 7) that generated spontaneous slow oscillations (SO), consisting of interspersed active (Up states) and almost silent (Down states) periods. In order to investigate the role of voltage-gated K^+ channel (I_M current) on this network activity, we next bath applied 100μM of XE991, which specifically blocks the M-current, and studied the changes in the emergent pattern (Fig. 23A). Finally, since there are experimental limitations to the understanding of the mechanisms bridging from neuronal membrane properties to networks, we implemented and studied the role of M-current in a biologically-plausible Hodgkin-Huxley network model of the cerebral cortex.

4.3.1 Effects of M-current blockade on the Up/Down state cycles

The baseline frequency of the slow oscillations (SO) in our experimental sample was 0.42 Hz (mean 0.42 ± 0.13 Hz, n= 7), with a duration of Up/Down states of 0.50 ± 0.08 s and 2.58 ± 0.99 s respectively (Fig. 23B). M-current blocker, XE991 100μM, applied to the bath resulted in changes in the Up states of the cortical slices (Fig. 23C). The main changes that were observed were an increase in the population firing rate during the Up and Down states (Fig. 24) and elongation of Up states following the blockade of M-current (Fig. 24A and B). In the distribution of Up and Down states in the case illustrated in Fig. 24B, there is also a visible elongation of the Down states, albeit this was not significant at the population level.

In Table 5, we summarized the effects of M-current blockage described in Fig. 25. Notice that, as shown in the raster and density plot of Fig. 24, the Up duration and firing

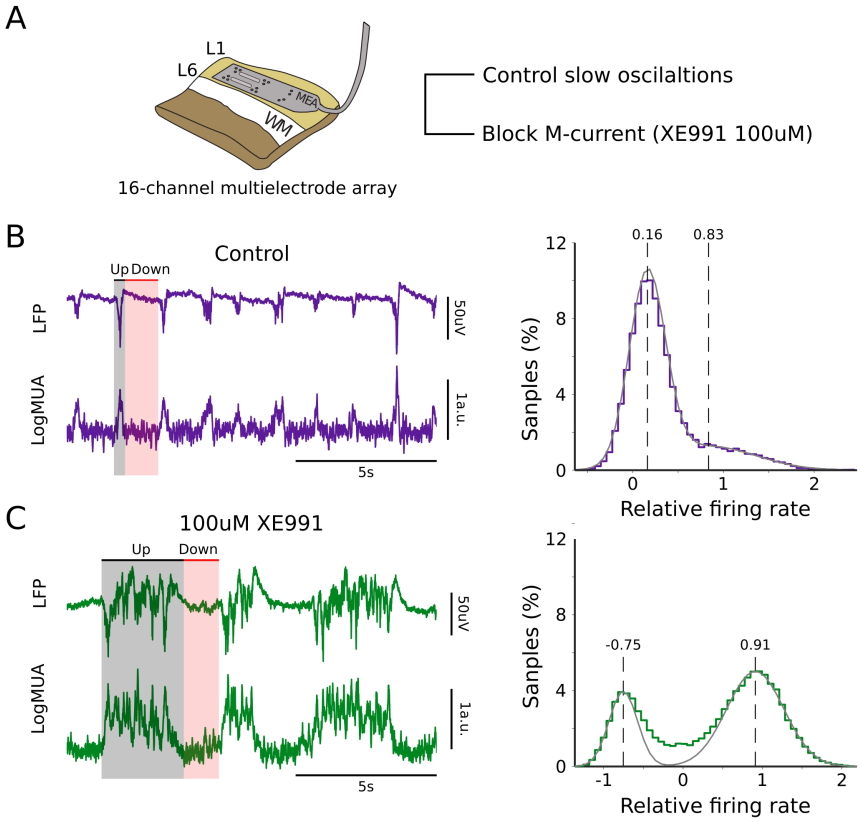

Figure 23 – Effect of M-current blockage on slow oscillations of a single recording. (A), Schematic representation of multielectrode array (16-channels) recording during control (slow oscillations, SO) and after the blockage of M-current through bath application of 100μM of XE991. (B), Representative recording during control slow oscillations (purple; left), and its firing rate distribution (right). (C), Representative recording after bath application of XE991, the M-current blocker (green; left) and its firing rate distribution (right). Grey and red shadowed area represent the Up and Down state detection, respectively.

rate were widely distributed compared to the control condition , i.e., more dispersed than control (see standard deviation in Table 5). Next, we explored these features in detail in the computational model.

Table 5 – Relative changes of Up and Down state properties during the blocakge of M-current. P-value of a two-sided Wilcoxon signed rank test

Parameter	**Control (mean±sd)**	**XE991 (mean±sd)**	**p-value**
Frequency (Hz)	0.42 ± 0.13	0.31 ± 0.11	0.10
Up state duration (s)	0.50 ± 0.08	1.59 ± 0.93	0.01
Down state duration (s)	2.58 ± 0.99	2.56 ± 1.48	0.81
Up state relative firing rate	0.61 ± 0.30	1.35 ± 0.59	0.01
Down state relative firing rate	0.05 ± 0.04	0.18 ± 0.12	0.01
Relative firing rate per second	34.42 ± 22.04	116.19 ± 69.49	0.01

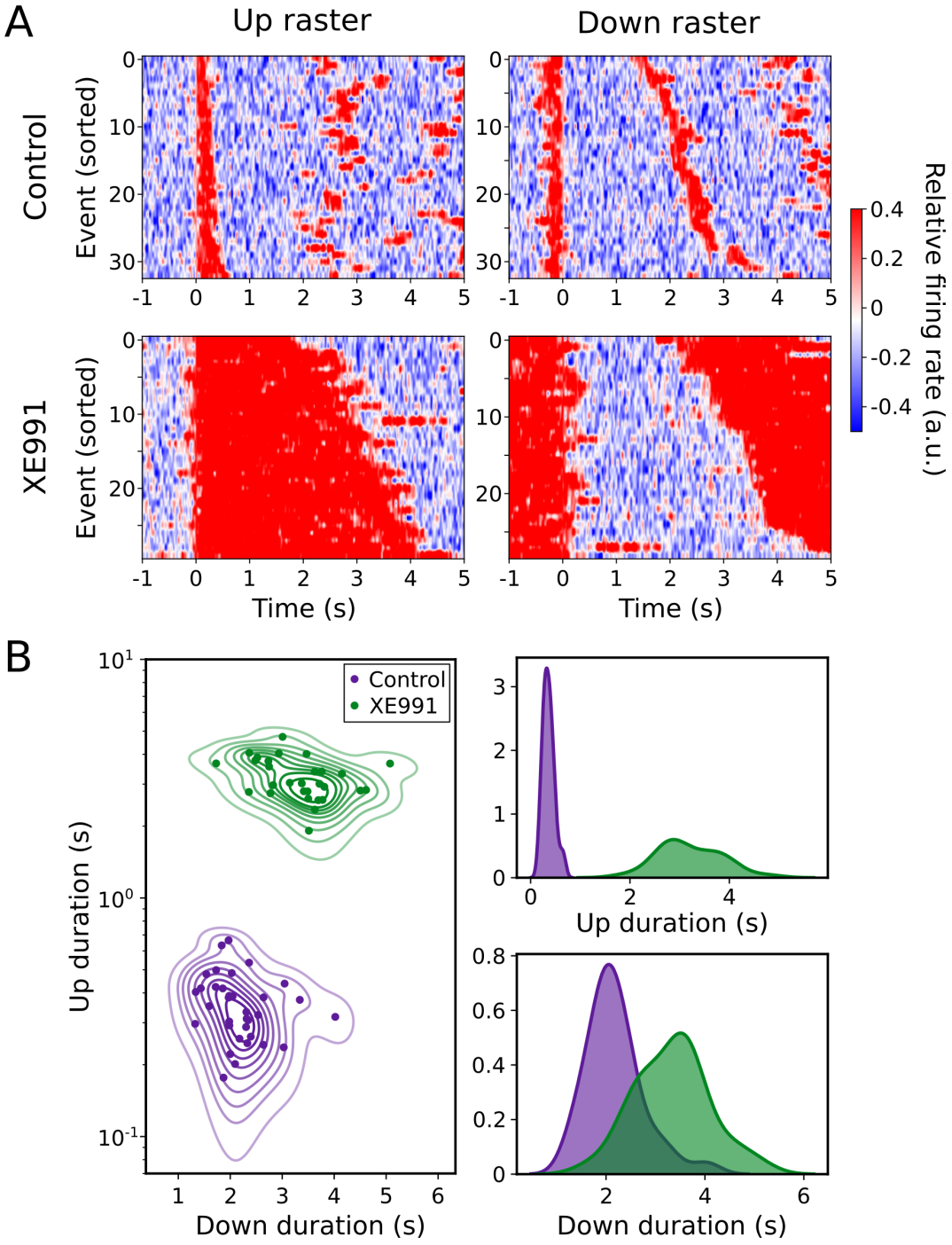

Figure 24 – Modulation of Up and Down states through the blockage of M-current. (A) Raster plots of relative firing rate (LogMUA) of all Up and Down states detected in control (top row) and blockage of M-current (bottom row). (B), Scatter plot of Up and Down durations. Irregular ellipses stand for the bivariate (2D) kernel density estimated (KDE). For details see Methods Sec. 3.4

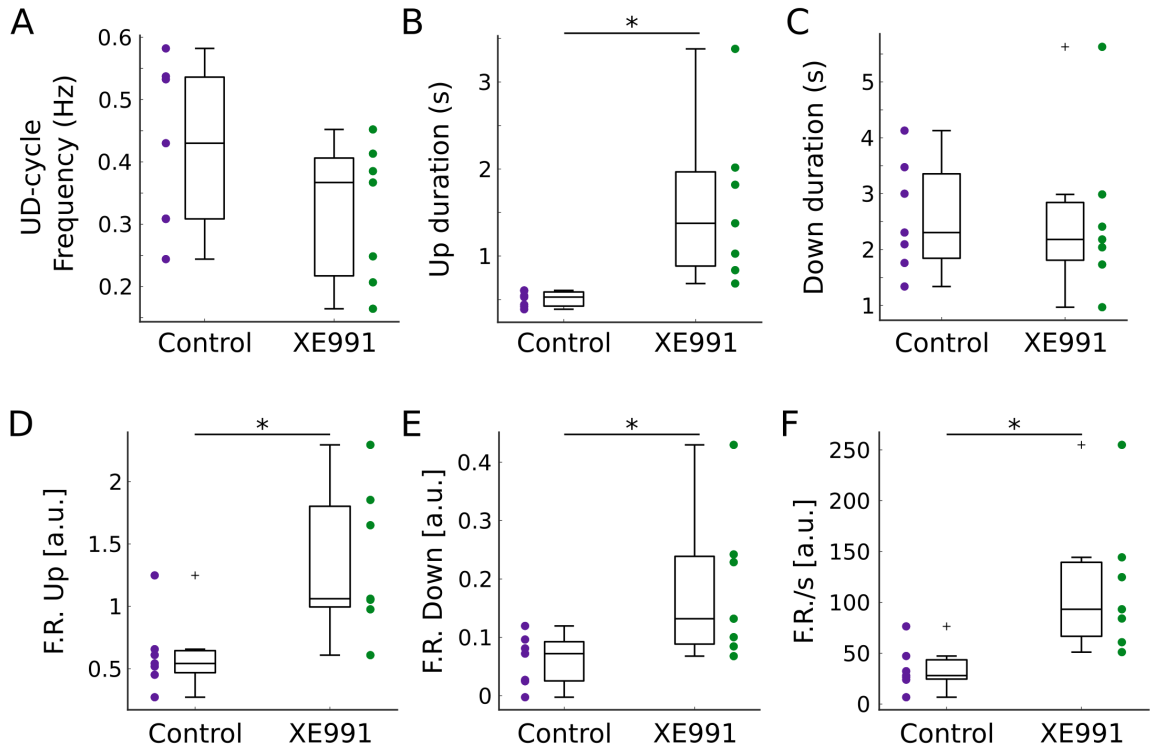

Figure 25 – Relative changes of Up and Down state properties during the M-current blockage. (A), Frequency of the Up and Down cycle (UD-cycle). (B), Up state duration. (C), Down state duration. (D), Relative firing during Up states. (E), Relative firing rate per second. Relative firing rate is defined as the mean LogMUA across time (see Methods Sec. 3.4). * stands for a p-value p<0.05 (two-sided Wilcoxon signed-rank test).

4.3.2 Impact of M-current on the cortical network model

In order to explore the role of M-current in the cortical network, we implemented a cortical network model of slow oscillations (SO) proposed by Compte et al. [Compte et al., 2003]. Although this model has been able to reproduce many features of SO observed in *in vitro* [Compte et al., 2003, Compte et al., 2008, Sanchez-Vives et al., 2010] it does not account for the M-current. With the aim of exploring the effects of M-current on the cortical network model, we slightly modified the original model including the M-current model described in [McCormick et al., 1993] (see Methods 3.1.1.4 for details).

Our model was able to reproduce the Up (active state) and Down (silent state) dynamics observed during the slow oscillations as well as the activity under blockage of M-current (Fig. 26). To explore the M-current effect on the model we parametrically decreased its maximal channel conductance (g_M) from 100% to 10% in the pyramidal neurons. The periodic alternation between Up and Down states during control slow oscillations (Fig. 26A) became more irregular after the blockage of the M-current

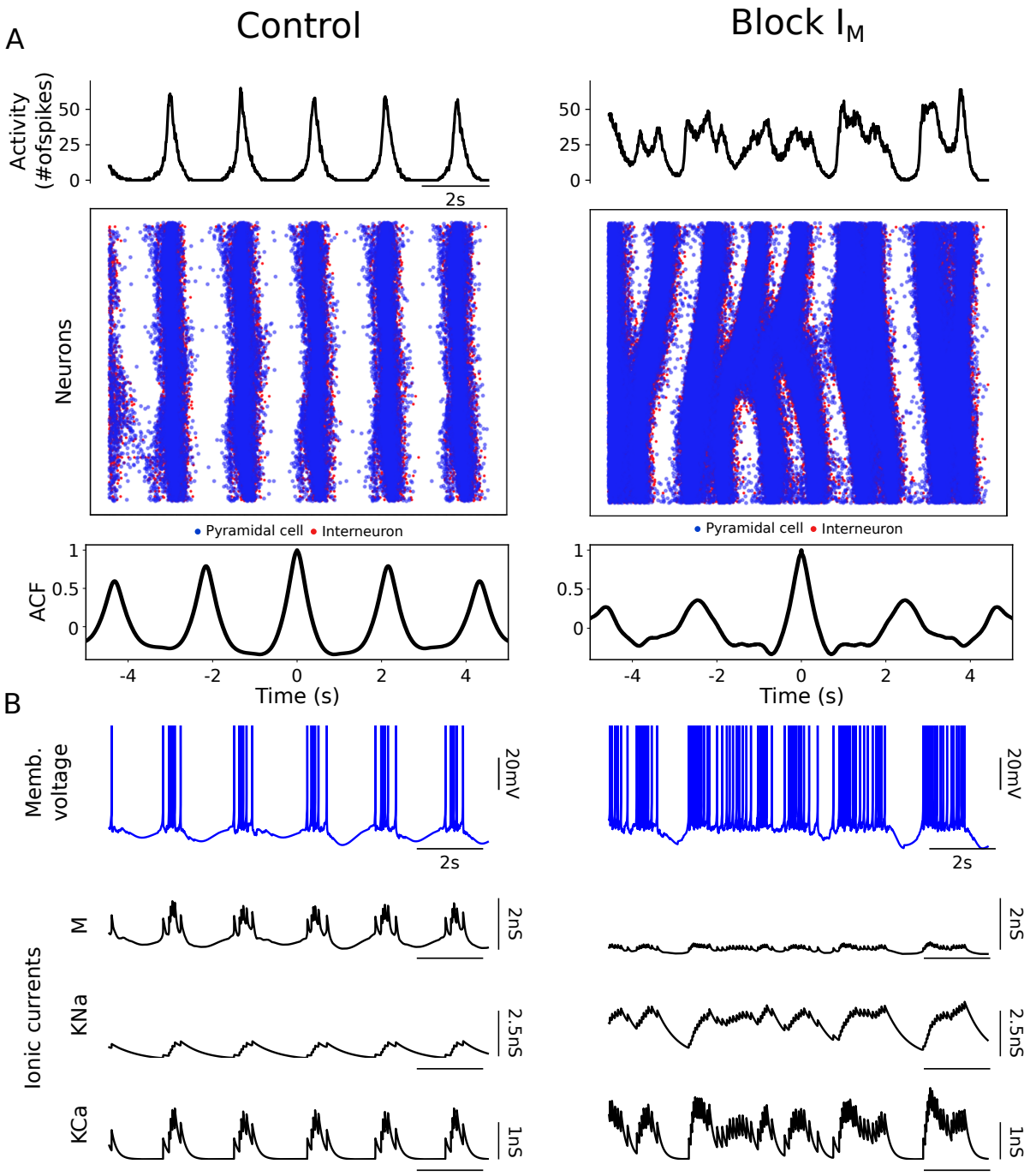

Figure 26 – Impact of M-current on the cortical network model. (A) left, Slow oscillatory activity in the form of Up and Down states in a control network (slow oscillations, SO) visualized as the sum of network activity (top) and raster plot (bottom). (A) right, Effect of M-current blockage (80%) on the slow oscillatory activity. (B), Representative membrane potential of the pyramidal cell as well the intrinsic channel conductances for M, sodium (KNa) and calcium (KCa) dependent potassium currents for control (left column) and under partial blockage of M-current (right). Blue and red dots in (A) stand for pyramidal cells and interneurons, respectively.

(compare autocorrelation function, ACF, in Fig. 26A, left and right). Also, irregular waves emerged in the system after M-current blockage (see raster plot in Fig. 26A, right). The dynamics of single neurons during control display typical dynamics of pyramidal cells during SO [Sanchez-Vives and McCormick, 2000, Steriade et al., 1993b]. Following each action potential, there was an increase in the main afterhyperpolarization currents of the model: M-current, sodium-dependent potassium current (I_{KNa}) and calcium-dependent potassium current (I_{KCa}). When the network was no more excitable enough to sustain the periods of high activity (Up states) it entered in a silent state (Down state). After the decay of M, KNa, and KCa currents the network, through its recurrent excitation, was able to trigger a new Up state. After the blockage of M-current, the single neuron activity reverted to activity with less periodicity and longer Up states showing periods of longer tonic firing, a pattern reminiscent of the awake-like states (see data in [Timofeev et al., 2001] for comparison).

Seeking to better understand the relationship between the firing rate and duration of Up states we carried out a parametric variation of the M-current (Fig. 27). As visible by the membrane potential of single neurons in Fig. 26B, the neuronal firing rate increase, when the M-current is decreased, not only for pyramidal neurons (Control: 3.02 ± 0.99 Hz, 80% M blockage: 6.81 ± 1.94 Hz), but also for inhibitory neurons (Control: 7.04 ± 1.74 Hz, 80% M blockage: 16.29 ± 3.39 Hz), that does not contain the M-current (Fig. 27A and B). The interspike interval distribution, for the control situation, shows a clear decrease in density for intermediate time values, which are typical of slow oscillations where it represents the Down state. Conversely, when M-current is decreased a more uniform distribution of ISI is observed, i.e., a less clear time separation - resembling the tonic firing (Fig. 27C). We also found that there was a correlated relationship between the duration of Up states with the firing rate, such that the lower the expression, the higher the duration of Up states and the firing rate (Fig. 27D). We next, looked at the synchronization within neurons. The mean of pairwise spiking correlation decreased (Control: 0.90, 80% M blockage: 0.72) together with an increase in the standard deviation (Control: 0.06, 80% M blockage: 0.20), indicating a less synchronous regime after the blockage of M-current. Also, the absence of intermediate ISIs during blockage of M-current suggests a less synchronous regime, due to the lack of quiescent periods. In order to test that we implemented an order parameter (χ) proposed in [Golomb et al., 2006] which quantifies the normalized average cellular membrane fluctuations. By parametrically changing the M-current concentration, we found that, concurrent with the network autocorrelogram (ACF in Fig. 26A), ISI distribution (Fig. 27C), and pairwise spiking correlation (Fig. 27E), the low expression of M-current introduce, in a nonlinear shape, more fluctuations in the membrane potential, i.e., a more desynchronized state (Fig. 27F).

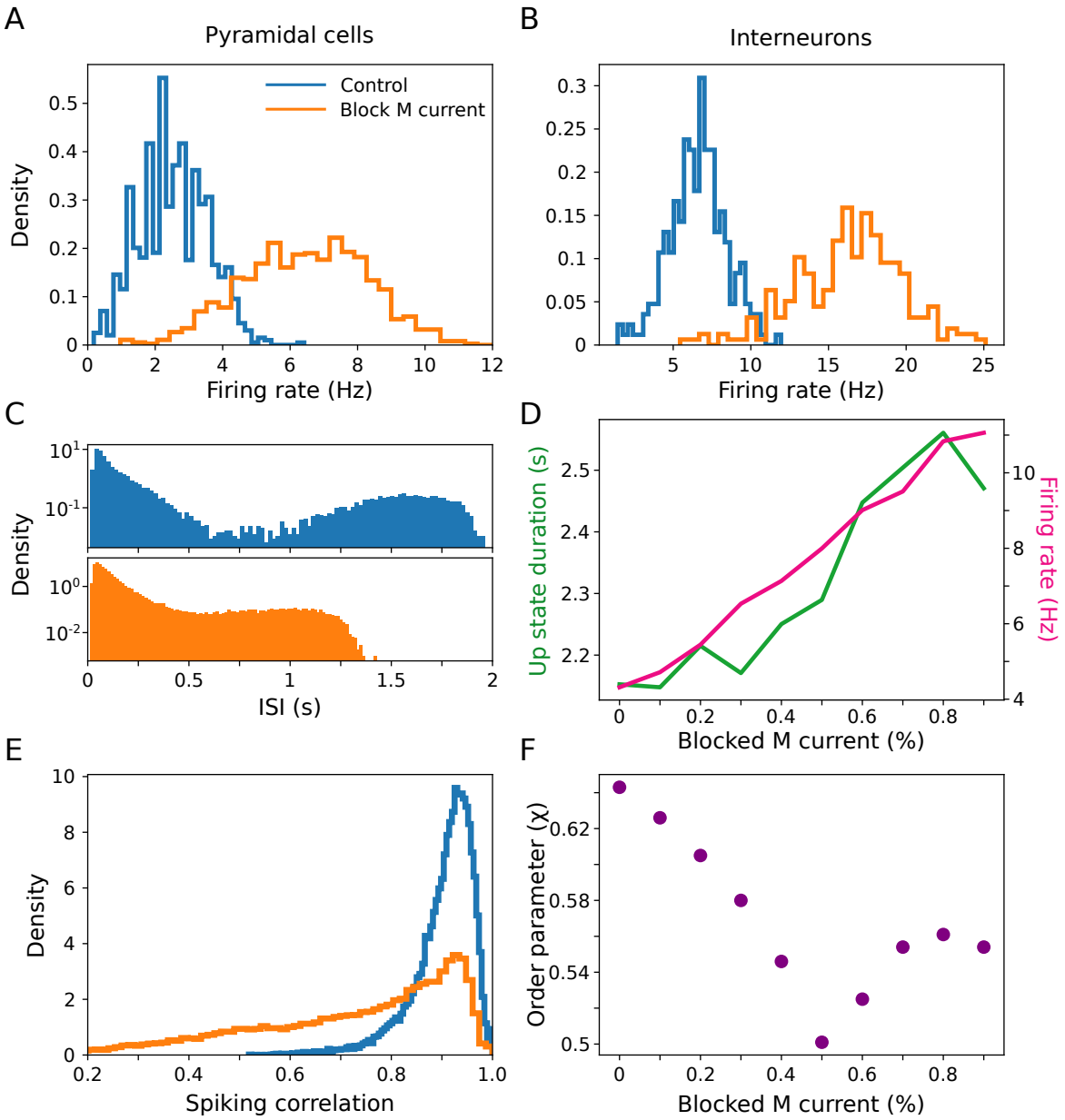

Figure 27 – Network features under M-current blockage in the cortical model. (A) and (B), Neuronal firing rate distribution during control (slow oscillations, SO) and blockage (80%) of M-current for pyramidal cells and interneurons, respectively. (C), Interspike interval distribution (ISI) for pyramidal cells during SO and M-current blockage. (D), Pairwise spiking correlation distribution as a function of M-current expression. Inset: normalized average voltage fluctuations (χ) order parameter. (E) and (F), Up and Down state duration and neuronal firing as a function of M-current expression, respectively. Up and Down state were detected arbitrarily thresholding the network activity.

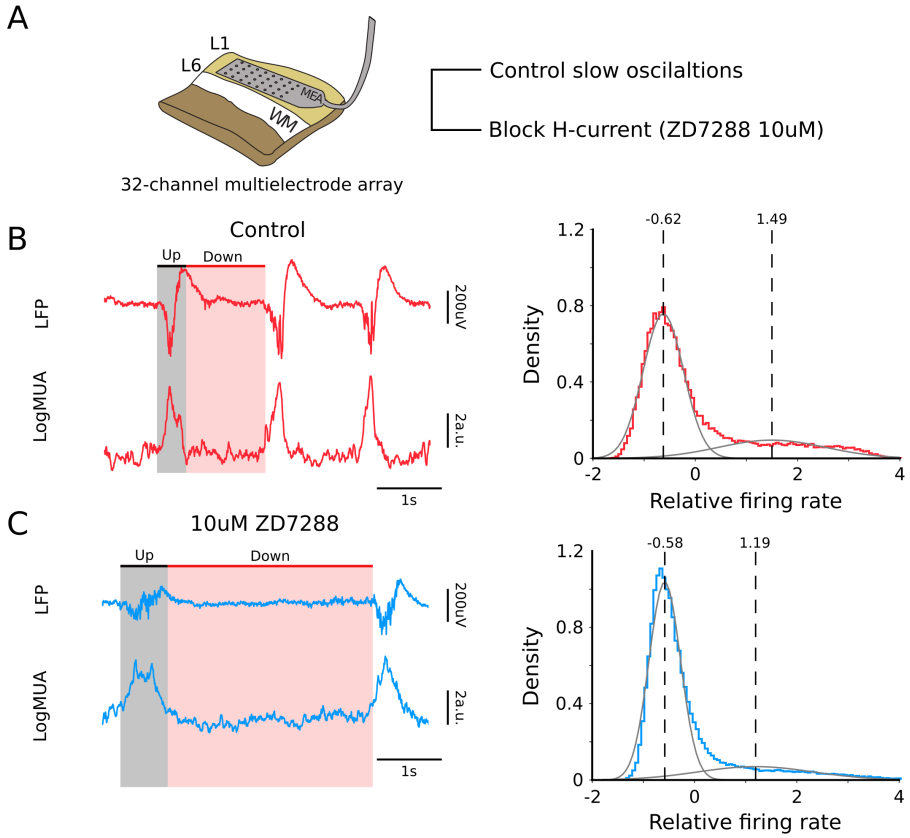

Figure 28 – Effect of H-current blockage on slow oscillations of a single recording. (A), Schematic representation of multielectrode array (32-channels) recording during control (slow oscillations) and after the blockage of H-current through bath application of 10μM of ZD7288. (B), Representative recording during control slow oscillations (red; left) and its firing rate distribution (right). (C), Representative recording after bath application of ZD7288, the H-current blocker (blue; left) and its firing rate distribution (right). Grey and red shadowed area represent the Up and Down state detection, respectively.

4.4 Role of hyperpolarization-activated cation channel (H-current) cortical slow oscillations

The hyperpolarization-activated cation current (H-current, I_H) is believed to be critical to the generation of slow periodic rhythms in the thalamocortical system [Lüthi and McCormick, 1998b, Lüthi and McCormick, 1999]. Studies of thalamocortical relay neurons have shown that H-current inactivation results in hyperpolarization of the cells slowing the frequency of spindle oscillations [Lüthi and McCormick, 1998b, McCormick and Pape, 1990, McCormick and Huguenard, 1992]. Although, H-current has been proposed to have a substantial role in the slow periodicity of thalamocortical rhythms during sleep (such as spindle waves) [Williams et al., 1997, Hughes et al., 1999, Lüthi and McCormick, 1999] it is still not clear the H-current impact the slow rhythmic oscillations

in an isolated cortical model (see [Lüthi and McCormick, 1998a, Neske, 2016] for a review).

4.4.1 Effects of H-current blockade on the Up/Down state cycles

Here, we first recorded from the isolated cerebral cortex slices (n= 7) that generated spontaneous slow oscillations (SO), consisting of interspersed active (Up states) and almost silent (Down states) periods. To investigate the role of the hyperpolarization-activated cation current (I_H) on this network activity, we next bath applied 10μM of ZD7288, a blocker of I_H, and studied the changes in the emergent pattern (Fig. 28A). Finally, since there are experimental limitations to the understanding of the mechanisms bridging from neuronal membrane properties to networks, we implemented and studied the role of H-current in a biologically-plausible Hodgkin-Huxley model of the cerebral cortex network. The baseline frequency of the slow oscillations in our experimental sample was 0.44 Hz (mean 0.44 ± 0.2 Hz, n= 7), with a duration of Up/Down states of 0.28 ± 0.04 s and 3.59 ± 1.92 s respectively (Fig. 28B and Fig. 29A, top row; Table 6). H-current blocker, ZD991 10μM, applied to the bath resulting in changes in the Up and Down of the cortical slices (Fig. 28C and Fig. 29A, bottom row). The main changes that were observed were an elongation of Up and Down states duration following the blockade of H-current (Fig. 29), and no significant differences in the Up and Down cycle frequency. Also, regarding the firing rate, no significant changes were observed at the population level (Fig. 30). In Table 6, we summarized the effects of H-current blockage.

Table 6 – Relative changes of Up and Down state properties during the blockage of H-current. P-value of a two-sided Wilcoxon signed rank test

Parameter	**Control (mean±sd)**	**ZD7288 (mean±sd)**	**p-value**
Frequency (Hz)	0.44 ± 0.20	0.32 ± 0.11	0.40
Up state duration (s)	0.28 ± 0.04	0.57 ± 0.22	0.03
Down state duration (s)	3.59 ± 1.92	8.14 ± 5.94	0.03
Up state relative firing rate	1.75 ± 0.32	1.64 ± 0.55	0.68
Down state relative firing rate	0.22 ± 0.06	0.24 ± 0.05	0.62
Relative firing rate per second	75.62 ± 13.10	73.79 ± 9.04	0.43

4.4.2 Impact of H-current on the cortical network model

To further explore the role of H-current on the slow oscillations we implemented a modified version of a cortical network model of SO proposed by Compte et al. [Compte et al., 2003]. It consists of pyramidal and inhibitory conductance-based neurons interconnected through biologically plausible synaptic dynamics. Such model

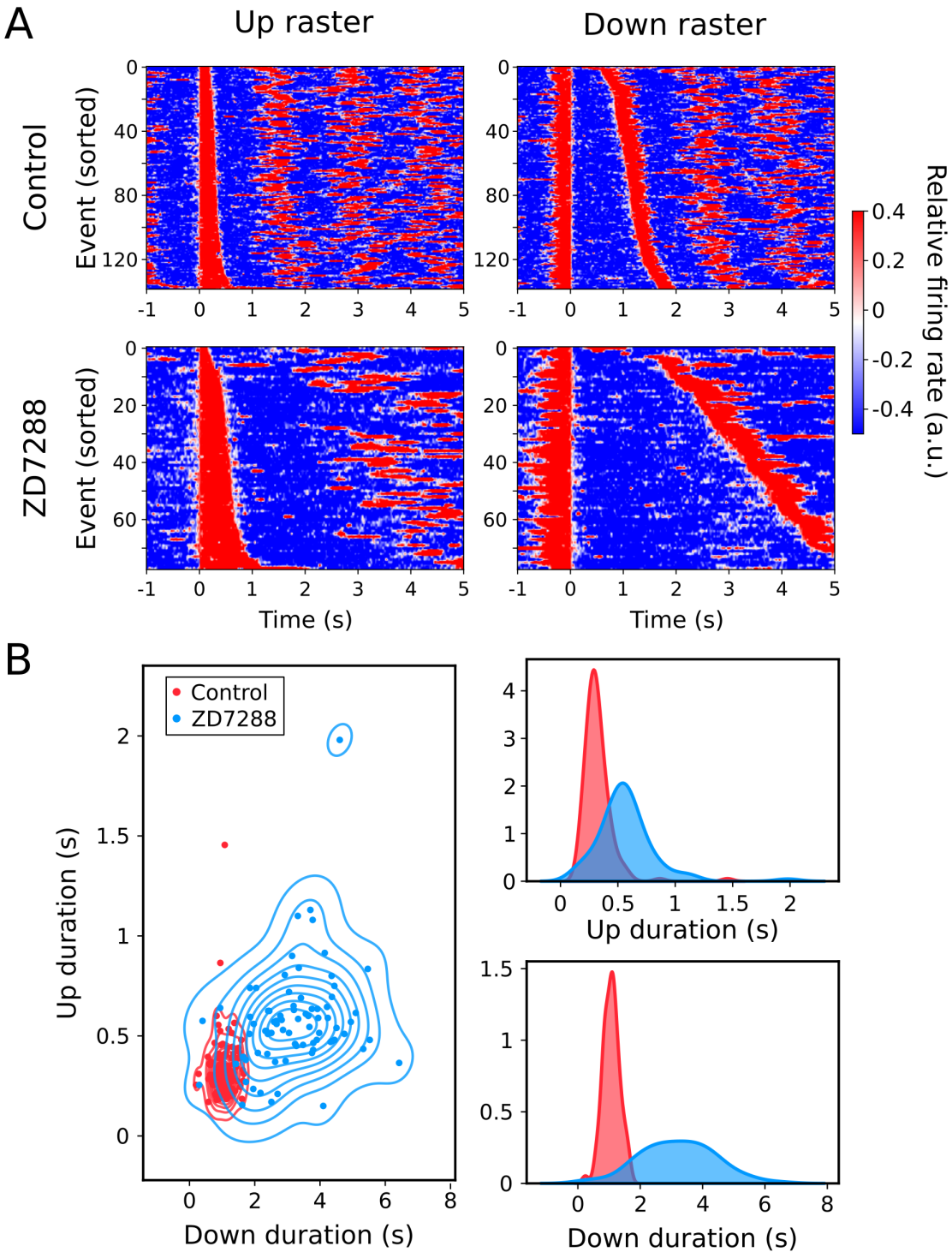

Figure 29 – Modulation of Up and Down states through the blockage of H-current. (A) Raster plots of relative firing rate (LogMUA) of all Up and Down states detected in control (top row) and blockage of H-current (bottom row). (B), Scatter plot of Up and Down durations. Irregular ellipses stand for the bivariate (2D) kernel density estimated (KDE). For details see Methods Sec. 3.4.

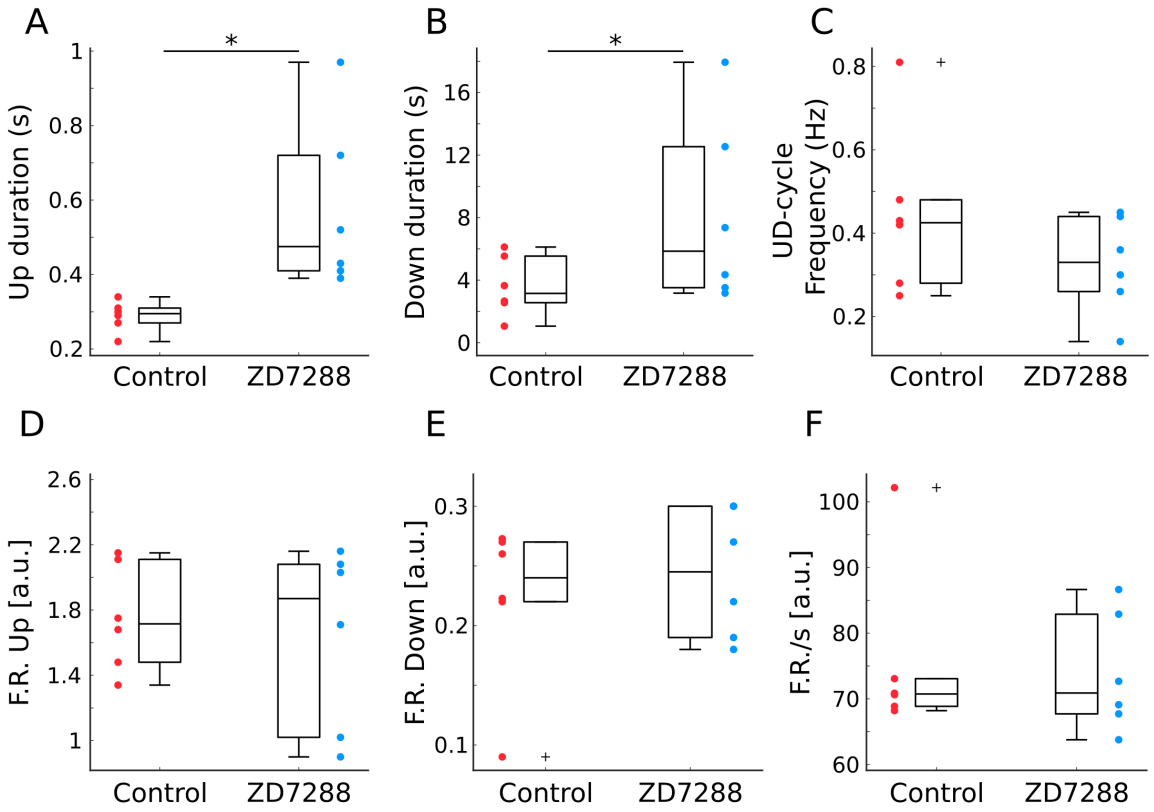

Figure 30 – Relative changes of Up and Down state properties during the H-current blockage. (A), Up state duration. (B), Down state duration. (C), Frequency of the Up and Down cycle (UD-cycle). (D), Relative firing during Up states. (E), Relative firing during Down states (F), Relative firing rate per second. Relative firing rate is defined as the mean LogMUA across time. * stands for a p-value p<0.05 (two-sided Wilcoxon signed rank test).

is able to reproduce many features of slow oscillations observed *in vitro* [Compte et al., 2003, Compte et al., 2009, Sanchez-Vives et al., 2010]. Nevertheless, it does not account for the H-current. By adjusting the ionic current's maximal conductances we introduced a model of H-current described in [Hill and Tononi, 2005]. Importantly, only 30% of the pyramidal neurons were modeled with the presence of H-current (see Methods 3.1.1.4 for details). Thus, when we refer to blockage of H-current it means that we are decreasing the maximal conductance of H-current on the 30% of neurons that are modelled with it.

Our model was able to display the periods of persistent activity (Up states) followed by quiescent periods (Down states) (Fig. 31A and B, left). Also, it reproduces the dynamic activity under blockage of H-current (Fig. 31A and B, right). We explored the H-current effect on the cortical network model by parametrically decreasing its maximal channel conductance (g_H) from 100% to 10% in the pyramidal cells that account for the H-current (see Methods 3.1.1.4). The periodic alternation between Up and Down states during control slow oscillations remained after the blockage of H-current, although

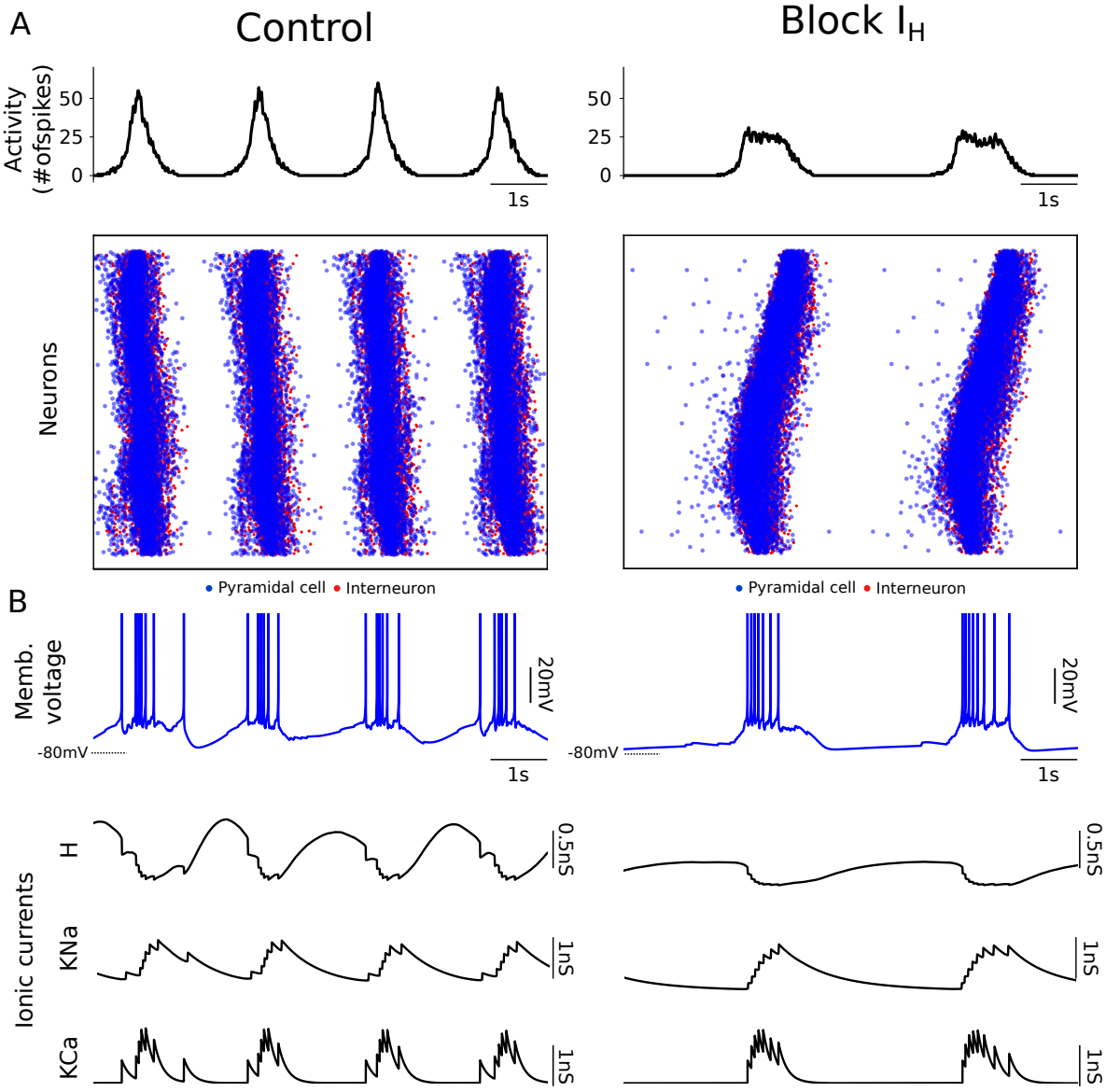

Figure 31 – Impact of H-current on the cortical network model. (A) left, Slow oscillatory activity in the form of Up and Down states in a control network (slow oscillations, SO) visualized as the sum of network activity (top) and raster plot (bottom). (A) right, Effect of H-current bloackge (80%) on the slow oscillatory activity. (B), Representative membrane potential of pyramidal cell as well the intrinsic channel conductances for H, sodium (KNa) and calcium (KCa) dependent potassium currents for control (left column) and under partially blockage of H-current (right). Blue and red dots in (A) stand for pyramidal cells and interneurons, respectively.

it showed larger Up and Down states duration (Fig. 31A). By looking into the single pyramidal cells voltage membrane we observed how the intrinsic properties changed over time (Fig. 31B). For the control SO we observed a typical dynamics pyramidal cells during SO observed *in vitro* and *in vivo* preparations [Sanchez-Vives and McCormick,

2000, Steriade et al., 1993b]. The hyperpolarization-activated cation current (H-current) was activated during periods of quiescence while afterhyperpolarization currents were inactivated (Fig. 31B, left). After the blockage (20%) of H-current, through the reduction of g_H, we observed a longer period of silence (Down states) followed by longer periods of depolarization (Up states), where the H-current was active for a longer period (Fig. 31B, right).

To better understand the relationship between SO and the expression H-current we performed a parametric variation of H-current in the network model. The mean pyramidal firing rate decreased when the H-current expression was lowered (Control: 2.91 Hz, 80% H-blockage: 2.06 Hz) as well as the mean interneurons firing rate (Control: 7.04 Hz, 80% H-blockage: 4.46 Hz; Fig. 32A and B). The interspike interval (ISI) distribution showed an absence of intermediate values for the blockage of H-current, due to the longer period of afterhyperpolarization (Fig. 31B and Fig. 32C). The presence of longer quiescent periods (Down states) could reflect a more synchronous regime in the network. We next proceed to measure the network synchronization evaluating spiking correlations and fluctuations of the membrane potential. The mean spiking correlation indicated a less pronounced synchrony of the network after lowering the expression of H-current (Control: 0.90 ± 0.06, 80% H-blockage: 0.86 ± 0.10 Hz; Fig. 32D). However by evaluating the synchronization through membrane potential fluctuations a more synchronous regime was found when the network expressed less concentration of H-current (Fig. 32D, inset). Regarding the firing rate and Up and Down state relationship, we observed an anticorrelated increment with the firing rate, such that the lower the expression, the lower the firing rate and the longer the duration of Up and Down states (Fig. 31E and F).

4.5 Spatiotemporal complexity on cortical states

The cerebral cortex exhibits a rich dynamic repertoire of activity ranging from highly synchronized to asynchronous states. Each of these states, either physiological or pathologic, can be characterized by its spatiotemporal complexity. An approach used in the clinic to quantify cortical complexity is the perturbational complexity index (PCI), which quantifies the causal interactions that follow an exogenous perturbation of the cortex [Casali et al., 2013]. It consists of estimating the Lempel-Ziv [Ziv and Lempel, 1977, Ziv and Lempel, 1978] complexity of the spatiotemporal matrix of cortical activation after perturbation. However, how cellular, synaptic and network parameters modulate cortical spatiotemporal complexity are not clear. It is known that cortical processing there is co-occurrence of excitation and inhibition both during spontaneous activity and in response to stimulation. Here, we sought to investigate the relevance of fast inhibition, GABA-A receptors-mediated, and slow inhibition, mediated by GABA-B-Rs,

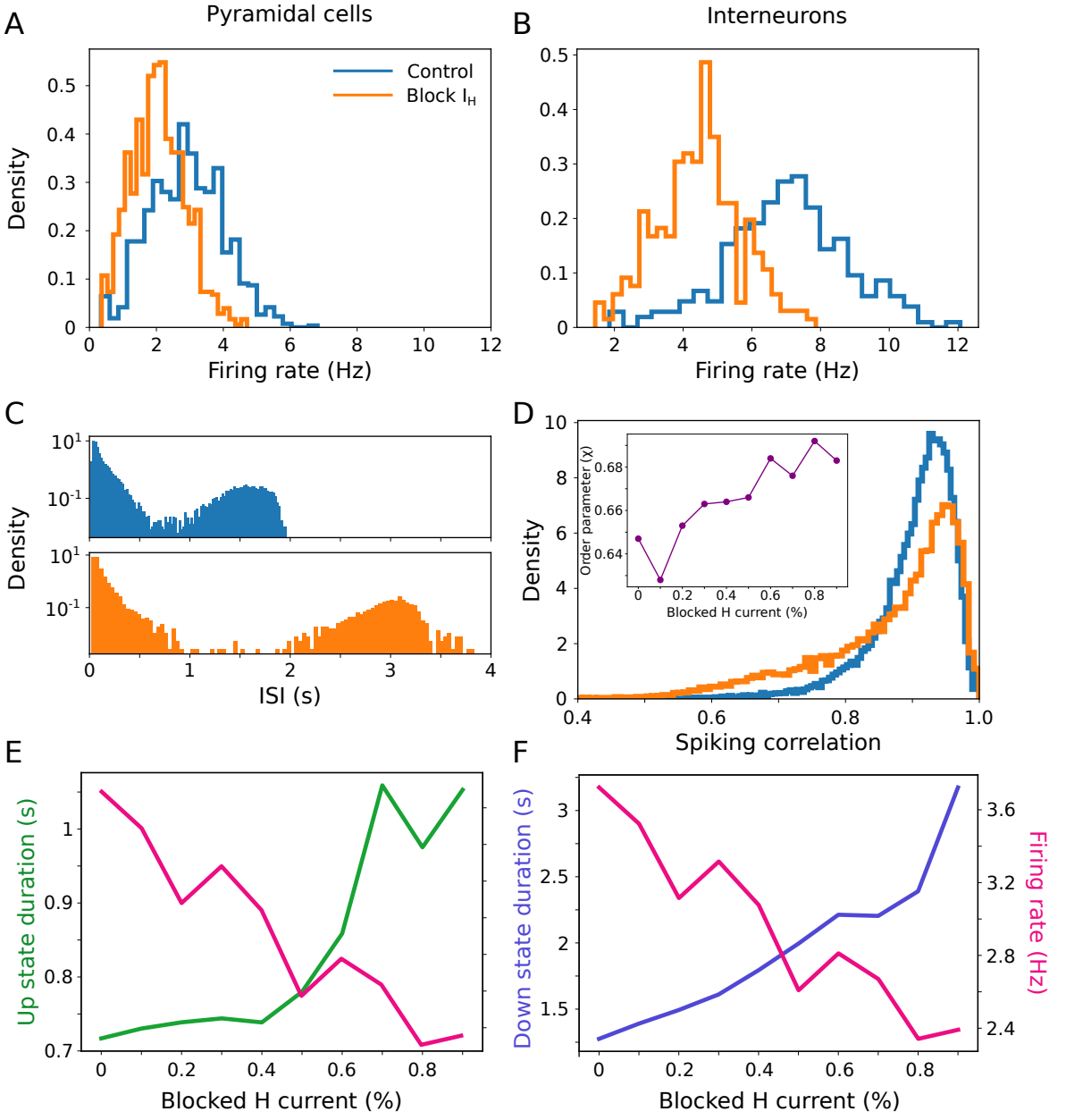

Figure 32 – Network features under H-current blockage in the cortical model. (A) and (B), Neuronal firing rate distribution during control (slow oscillations, SO) and blockage (80%) of H-current for pyramidal cells and interneurons, respectively. (C), Interspike interval distribution for pyramidal cells during SO and H-current blockage. (D), Pairwise spiking correlation distribution as a function of H-current expression. Inset: normalized average voltage fluctuations (χ) order parameter. (E) and (F), Up and Down state duration and mean neuronal firing as a function of H-current expression, respectively. Up and Down state were detected arbitrarily thresholding the network activity.

on cortical complexity. This section is based on our publication Barbero-Castillo et al. [Barbero-Castillo et al., 2021] and Dalla Porta and Sanchez-Vives [DALLA PORTA

and Sanchez-Vives, 2021].

4.5.1 Impact of slow and fast inhibition on perturbational complexity in cortical slices

In vitro extracellular 16−channel local field potentials (LFPs) were recorded from ferret primary visual cortex (V1) coronal slices (n = 58) during two different regimes of spontaneous activity: i) synchronous activity consisting in spontaneous Up and Down states organized in slow oscillations (SO) (Fig. 33 A, left); and (ii) asynchronous activity (Fig. 33 A, right).

In our experimental paradigm, cortical slices displayed spontaneous SO similar to the ones occurring *in vivo* during slow wave sleep (SWS) [Sanchez-Vives and McCormick, 2000]. Oscillatory frequencies in the different slices ranged from 0.2 to 0.92 Hz (mean 0.476 ± 0.02 Hz, n= 58). While the synchronous slow oscillatory activity replicates the dynamics of SWS, asynchronous activity in the slice can mimic that of awake states . In cortical slices, asynchronous states can be mimicked by adding neurotransmitters, through bath application of noradrenaline (NE) and acetylcholine (ACh), present in awake states [McCormick, 1992, Brumberg et al., 2000, Jones, 2005, D'Andola et al., 2018]. Even when cholinergic and noradrenergic agonists are reported to block SO through the blockade of afterhyperpolarizations [Steriade et al., 1993a], we still observe synchronization at a frequency higher than spontaneous SO, at ∼ .4 Hz (see Fig. 33 A−C). In order to obtain a more asynchronous (desynchronized) activity, we used additional strategies based on previous studies, recording at 32°C [Reig et al., 2010] and lowering calcium in the bath from 1˜1.2 mM to 0.8˜0.9 mM [Markram et al., 2015] to enhance excitability (see Fig. 33 A−C).

Aiming to quantify the complexity of network responses to single-pulse electrical stimulation (ES), we used an adapted version of the PCI [Casali et al., 2013] for slice recordings (sPCI) [D'Andola et al., 2018]. During ongoing SO, ES evoked a response followed by a sudden decrease in activity, Down state (Fig. 33 D, left) or what, in humans, has been referred to as "off-periods" [Rosanova et al., 2018], resembling reported findings for LFP recordings in humans [Pigorini et al., 2015, Rosanova et al., 2018]. According to the sPCI algorithm by [D'Andola et al., 2018] and to quantify the spatiotemporal patterns of response to ES, we converted the raw LFP traces obtained from multielectrode array recordings to firing rate signals (specifically to LogMUA) and computed the binary matrices of significant activity (Fig. 33 D; see Methods Sec. 3.4.5 for details). We then compressed the spatiotemporal binary matrices of significant sources with a Lempel-Ziv algorithm and normalized them by the source entropy to finally obtain the sPCI. Under synchronous, SO activity, the sPCI was 0.1 ± 0.002 (range 0.07 − 0.14, n= 58), similar to what has been previously reported[D'Andola et al., 2018, Dasilva et al., 2021b].

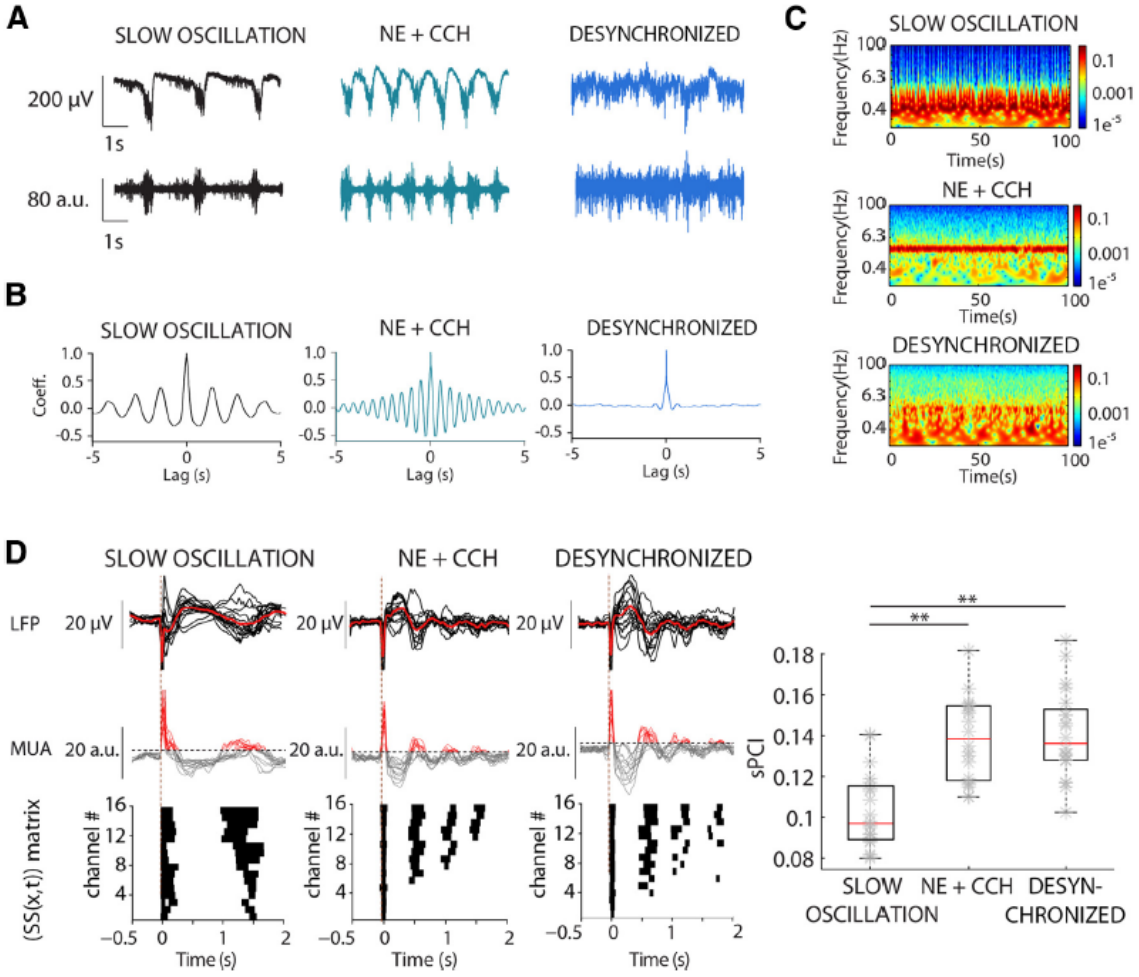

Figure 33 – Network complexity increased from spontaneous synchronous slow oscillations to asynchronous activity (desynchronized). (A), Local field potential (LFP, top) and multiunit activity (MUA, bottom) recording of 5 s of spontaneous slow oscillations (SO, left), noradrenaline and carbachol (NE+CCh, middle) and asynchronous activity (right). (B) and (C), Autocorrelograms and spectrograms of LFPs recording shown in (A), respectively. (D), Averaged LFP (top) and MUA (bottom) responses to electrical stimulation (ES) during spontaneous SO (left), NE+CCh (middle), and asynchronous activity (right). Binary matrices of significant sources of activity $[SS(x,t)]$ following ES delivered to neocortical slices (bottom). Population slice perturbational complexity index (sPCI; n=20) measured during control SO, NE+CCh, and asynchronous activity ($^{**}p < 0.01$).

We next calculated sPCI in the two described conditions: (1) NE+CCh; and (2) asynchronous (desynchronized) state (Fig. 33). As said above, following the bath application of NE+CCh the regime of Up/Down states was transformed (Fig. 33A, middle), the network went on to generate a higher frequency (~ 2.4 Hz; Fig. 33C, middle). The sPCI following the ES revealed a significant increase of the sPCI with respect to that in SO (Fig. 33D, right), similar to what was reported previously [D'Andola et al.,

2018]. In the asynchronous state, the mean sPCI was also significantly larger than that in SO, but not higher than in NE+CCh, despite being more desynchronized (SO: 0.103 ± 0.004; desynchronized: 0.141 ± 0.005, p= 1.301×10^{-6}, n= 20; Fig. 33D, right). When cortical complexity was calculated by means of sPCI, there was a significant increase in complexity following the blockade of network Up/Down state bistability, which is a highly synchronous state. However, the more subtle change in dynamics taking place between NE+CCh and desynchronized conditions did not convey a complexity increase as detected by sPCI. From this point on, we used two departing points or baselines that we compared: (1) the slow oscillatory, synchronous state; and (2) the asynchronous (desynchronized) state. These two extremes of the dynamics mimic awake versus slow wave sleep, or awake versus deep anesthesia, respectively.

4.5.1.1 Role of $GABA_A$-Rs on cortical complexity

Blocking of $GABA_A$-Rs in the desynchronized state

To investigate the GABAergic role in cortical complexity we explored how a progressive blockade of inhibition affected sPCI while departing from two different dynamic states, either (1) the asynchronous (desynchronized) state or (2) the synchronous, slow oscillatory state (Fig. 34A). We first induced the asynchronous (desynchronized) state (Fig. 34A) and next we blocked fast inhibition by application of the selective $GABA_A$-R blocker GBZ (Fig. 34; 50˜200 nM). When $GABA_A$-Rs were blocked, desynchronized dynamics progressively shifted toward pre-epileptiform dynamics as described in [Sanchez-Vives et al., 2010] (Fig. 6D). Such modification of spontaneous dynamics was also reflected in the spatiotemporal pattern of responses to perturbation (Fig. 34A, middle), that were used for the calculation of sPCI (Fig. 34A, right).

As shown above, from slow oscillatory regime to desynchronized regime, there was an increase in sPCI. However, following the maximum sPCI reached in the desynchronized state, the progressive blockade of $GABA_A$-Rs resulted in a progressive decline of sPCI (n= 10; Fig. 34A, right). Interestingly, whereas the sPCI was significantly reduced compared with the desynchronized state for concentrations above 50 nM GBZ (GBZ 100 nM: p= 0.003; GBZ 150 nM: p= 1.588×10^{-4}; GBZ 200 nM: p= 4.128×10^{-8}; n= 10; Fig. 34A, right), it was only at the highest concentration of GBZ that the sPCI significantly decayed below control levels (p= 7.525×10^{-4}, n= 10; Fig. 34A, right). In summary, these results indicate that blockade of $GABA_A$-Rs in the desynchronized state decreases perturbational complexity in cortical slices, or conversely, physiological $GABA_A$-mediated inhibition contributes to cortical complexity during desynchronized dynamics. Furthermore, highly synchronous epileptiform discharges (in 200 nM GBZ) display decreased complexity. A decreased information content and complexity in

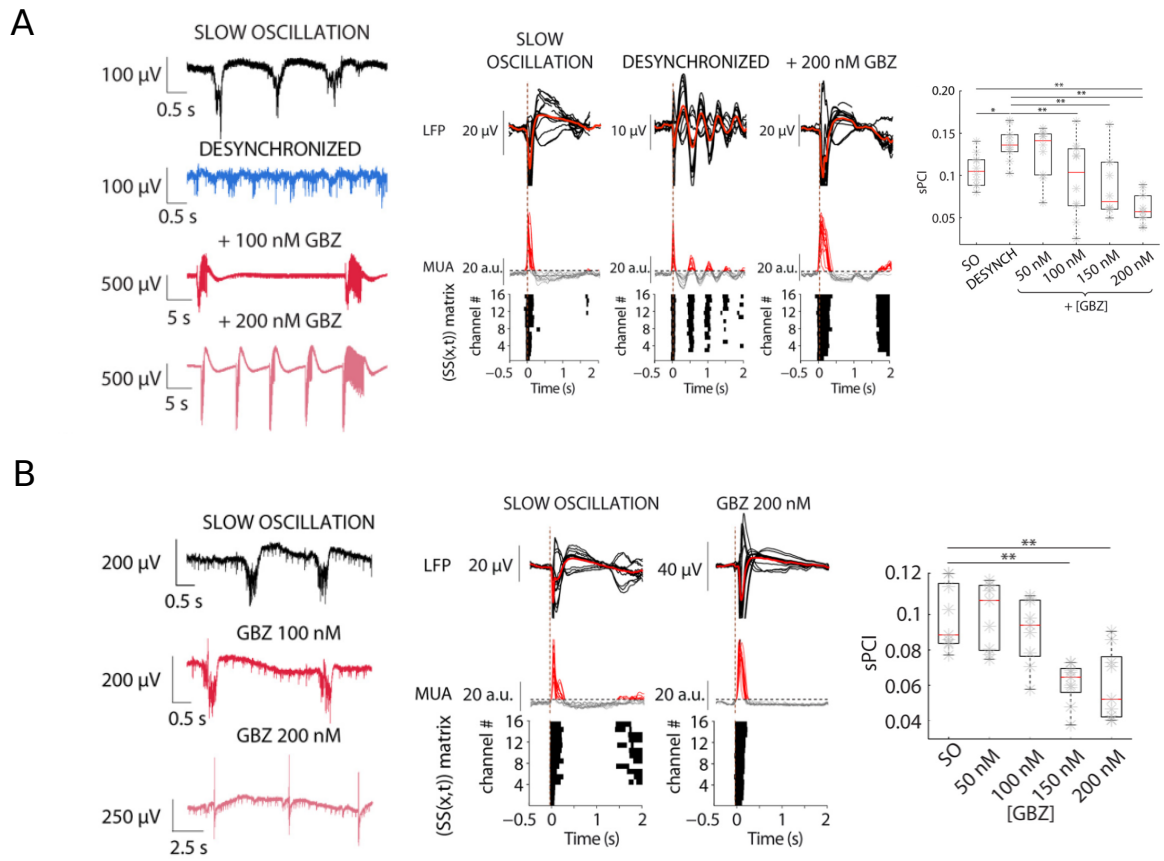

Figure 34 – Progressive blockade of $GABA_A$-Rs reduces sPCI during desynchronized and slow oscillations activity. (A)-left, Raw local field potential (LFP) recordings of spontaneous activity in neocortical slices, during slow oscillation (SO), desynchronized activity and blockade of $GABA_A$-Rs by bath application of increasing concentrations of GBZ demonstrated progressively shifted toward preepileptiform dynamics; (A)-middle, Averaged LFP (top) and multiunit activity (MUA; middle) to electrical stimulation (ES) during distinct regimes of activity. Binary matrices of significant sources of activity [SS(x,t)] following ES delivered to neocortical slices (bottom). (A)-right, Population sPCI (n= 10) demonstrated that presence of large Down-states breaks the causal interactions and decreased the complexity of the response ($^*p< 0.05$, $^{**}p< 0.01$). (B)-left, Raw LFP recordings of spontaneous activity in control SOs and blockade of $GABA_A$-Rs by bath application of increasing concentrations of GBZ induced shortening of evoked Up states. (B)-middle, Averaged LFP and MUA and binary matrices of significant sources of activity [SS(x,t)] following ES. (B)-right, Population sPCI (n= 9) demonstrated that presence of large Down states breaks the causal interactions and correlates with low complexity states ($^{**}p< 0.01$).

synchronous, epileptic discharges has also been described in both animal models and humans [Lehnertz and Elger, 1995, Artinian et al., 2011, Trevelyan et al., 2013].

Blocking of $GABA_A$-Rs in the slow oscillatory state

We next investigated the effect of $GABA_A$-R blockade on complexity but departing from synchronous slow oscillations (Fig. 34B). We bath-applied increasing concentrations of GBZ (50, 100, 150, and 200 nM) and recorded network responses to electrical stimulation. Raising GBZ concentrations induced a gradual shortening of evoked Up states and augmented Up-state amplitude, as previously described [Sanchez-Vives et al., 2010](Fig. 34B, left). Such an increase in Up-state amplitude corresponded to a linear increase in the firing rate during Up states with the removal of inhibition because of an enhanced excitatory reverberation [Sanchez-Vives et al., 2010]. Up states of larger amplitude resulted in binary matrices with shorter significant periods of activity (Fig. 34B, middle). sPCI was significantly decreased with increasing GBZ concentrations (n= 9). In particular, the sPCI reduction with respect to the SO condition was significant above 100 nM GBZ (GBZ 150 nM: $p= 1.94 \times 10^{-4}$; GBZ 200 nM: $p= 1.36 \times 10^{-4}$; n= 9; Fig. 34B, right).

Thus, these results indicate that removal of fast inhibition reduces perturbational complexity in cortical slices. Enhanced excitability during Up states because of excitatory recurrency in cortical circuits induced stereotypical responses to stimulation that resulted in lower sPCI values. Balanced $GABA_A$-R-mediated inhibition in cortical activity provides richness in the emergent patterns, contributing to the complexity of causal interactions. Later, in our computer model, we explored the limits of the relationship between inhibition and complexity, in a range that is unattainable experimentally.

4.5.1.2 Role of $GABA_B$-Rs on cortical complexity

Blocking of $GABA_B$-Rs in the desynchronized state

Next, we followed a similar approach (as described above) to investigate the effects of progressive $GABA_B$-R blockade during desynchronized activity in cortical slices (Fig. 35). Departing from slow oscillatory spontaneous activity, we induced desynchronized activity. The transformation of the activity is illustrated in the raw recordings (Fig. 35A-left). We then bath-applied increasing concentrations of CGP55845, a specific antagonist of $GABA_B$-Rs. Such application had a progressive effect enhancing the synchronization in the network (Fig. 35A-left; compare raw traces of desynchronized with +1μM CGP activity). However, it did not turn activity into epileptiform activity as $GABA_A$-R blockade did (Fig. 34A-left). We proceed then to compute the sPCI for each condition and significant differences were found (Fig. 35A-middle and right; p= 0.029; n= 7). Although sPCI significantly increased during desynchronized condition compared with SO, *post hoc* tests did not reveal significant differences, neither between control versus CGP condition (CGP 100 nM: p= 0.348; CGP 200 nM: p= 0.837; CGP

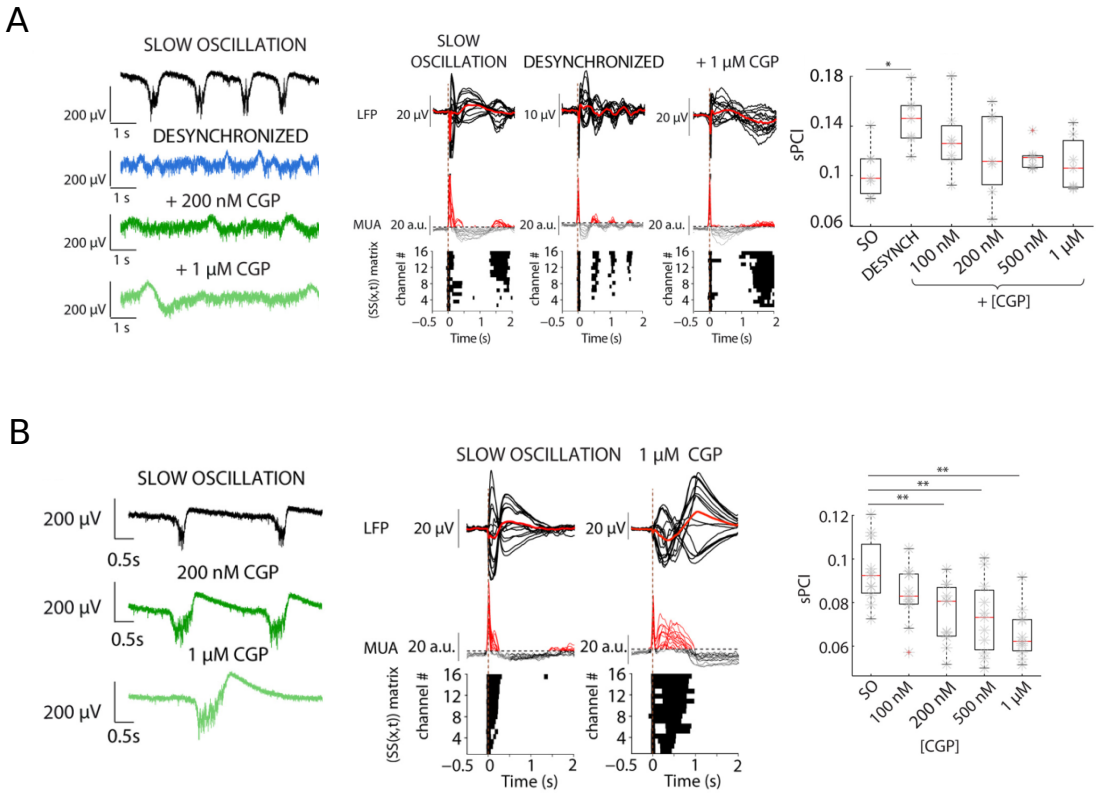

Figure 35 – Progressive blockade of $GABA_A$-Rs reduces sPCI during desynchronized and slow oscillations activity. (A)-left, Raw local field potential (LFP) recordings of spontaneous activity in neocortical slices, during slow oscillation (SO), desynchronized activity and blockade of $GABA_A$-Rs by bath application of increasing concentrations of GBZ demonstrated progressively shifted toward preepileptiform dynamics; (A)-middle, Averaged LFP (top) and multiunit activity (MUA; middle) to electrical stimulation (ES) during distinct regimes of activity. Binary matrices of significant sources of activity [SS(x,t)] following ES delivered to neocortical slices (bottom). (A)-right, Population sPCI (n= 10) demonstrated that presence of large Down-states breaks the causal interactions and decreased the complexity of the response ($^*p< 0.05$, $^{**}p< 0.01$). (B)-left, Raw LFP recordings of spontaneous activity in control SOs and blockade of $GABA_A$-Rs by bath application of increasing concentrations of GBZ induced shortening of evoked Up states. (B)-middle, Averaged LFP and MUA and binary matrices of significant sources of activity [SS(x,t)] following ES. (B)-right, Population sPCI (n= 9) demonstrated that presence of large Down states breaks the causal interactions and correlates with low complexity states ($^{**}p< 0.01$).

500 nM: p= 0.941; CGP 1μM: p= 0.996; n= 7, Fig. 35A-right) nor desynchronized versus CGP groups (CGP 100 nM: p= 0.768; CGP 200 nM: p= 0.281; CGP 500 nM: p= 0.171; CGP 1μM: p= 0.072; n= 7, Fig. 35A-right). In summary, these results indicate that blockade of $GABA_B$-Rs during desynchronized activity showed a trend toward a decreased sPCI

but did not reach significance. Thus, the contribution of $GABA_B$-mediated inhibition to causal complexity in the awake state is less relevant than that of $GABA_A$-mediated inhibition.

Blocking of $GABA_B$-Rs in the slow oscillatory state

During slow oscillations, $GABA_B$-Rs have been found to play a role in Up-state termination since their blockade results in longer persistent activity [Mann et al., 2009, Perez-Zabalza et al., 2020, Sanchez-Vives et al., 2021]. In order to further investigate the role of $GABA_B$-R-mediated inhibition in emergent activity and cortical complexity, we gradually blocked $GABA_B$-Rs while departing from slow oscillatory activity (Fig. 35B-left). Progressive blockade of $GABA_B$- Rs induced Up states of longer duration followed by prominent Down states that decreased the frequency of Up states and increased their regularity, as described in [Perez-Zabalza et al., 2020] (Fig.6A,B). The sPCI decreased following $GABA_B$-R blockade ($p= 1.97 \times 10^{-5}$; n= 11; Fig. 35B-middle and right). Significant sPCI reductions were confirmed by *post hoc* analysis for the three tested conditions (CGP 200 nM: p= 0.004; CGP 500 nM: p= 0.002; CGP 1μM: $p= 1.45 \times 10^{-5}$; n= 11; Fig. 35B-right). Interestingly, the removal of slow inhibition by bath-application of increasing concentrations of CGP55845 significantly increased the firing rate during Up states, although to a lesser extent than $GABA_A$-R blockade did (compare Fig.6C with Fig.4C in [Barbero-Castillo et al., 2021]). Finally, we showed that blockade of $GABA_B$-Rs, while in SO, reduced perturbational complexity, confirming that $GABA_B$-R-mediated inhibition contributes to the richness of activity patterns, spatiotemporal variability, and cortical complexity during the slow oscillatory regime.

4.5.2 Impact of slow and fast inhibition on perturbational complexity in a cortical network model

In order to further investigate the cellular and network mechanisms involved in the spatiotemporal dynamics of spontaneous and induced cortical complexity, here we proposed a modified version of a biophysically detailed neuronal model [Compte et al., 2003] - that follows the Hodgkin-Huxley formalism - in a two-dimensional network. The model consists of pyramidal and inhibitory conductance-based neurons synaptically connected within a local range. Pyramidal cells have a larger range of connectivity than inhibitory neurons, which are more locally connected (Fig. 36A; see Methods Sec. 3.1.2). Our neuronal model includes $GABA_A$ as in Compte et al. [Compte et al., 2003] and additionally accounts for $GABA_B$ inhibitory synapses, as well as potassium leakage current which is modulated by acetylcholine (ACh) and noradrenaline (NE) [Bazhenov et al., 2002, Li et al., 2017]. We simulated population local field potentials LFPs (sLFP), and recorded from 20 different locations organized in a matrix (see Methods Sec. 3.1.2). The

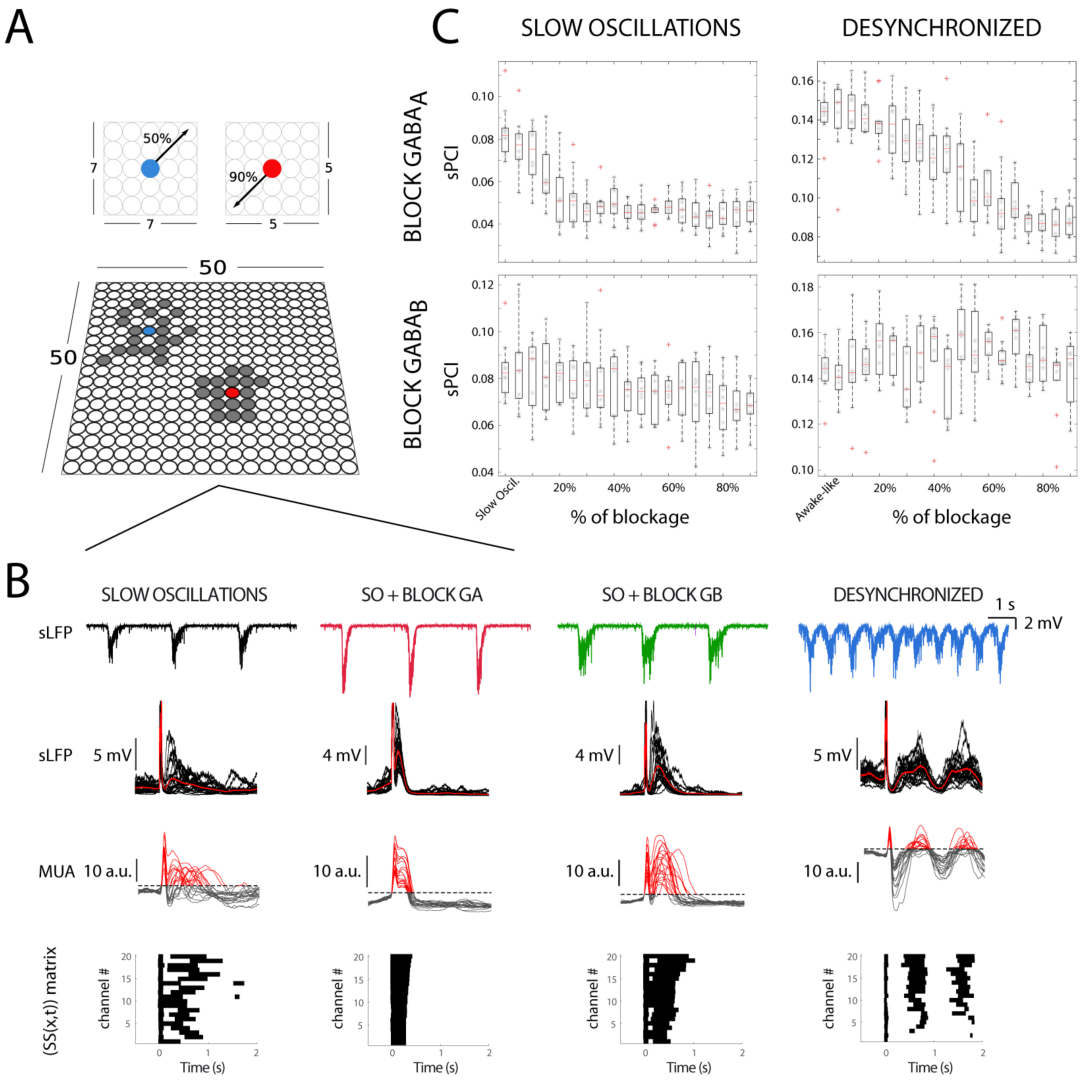

Figure 36 – A network cortical model to reproduce the sPCI measured during different regimes of network activity. (A), The model consists of pyramidal (blue) and inhibitory neurons (red) arranged in a 50×50 square lattice. The excitatory neurons may connect locally to a 50% fraction of its neighbors (gray circles) within a 7×7 square, while the inhibitory neurons to a 90% fraction within a 5×5 square (see Methods Sec. 3.1.2). (B) The model reproduces similar spontaneous and evoked neuronal activity, as observed experimentally during (from left to right) SOs, SOs + blocking $GABA_A$ (SO+BLOCK G_A), SOs + blocking $GABA_B$ (SO+BLOCK G_B) and desynchronized activity. Single spontaneous sLFP (top), averaged sLFP (middle top), MUA (middle bottom), and binary matrices of significant sources of activity [SS(x,t)] following stimulation delivered in a cortical model. (C), Population sPCI for different cortical activity, SOs with GABA A (left-top) and GABA B (left-bottom) progressively blockade, the same for desynchronized activity (right column).

sLFP signal was analyzed with exactly the same techniques as the ones experimentally recorded in the cortical slices.

The model is able to reproduce slow oscillatory dynamics and desynchronized activity as observed *in vitro*, as well as the cortical activity under blockade of $GABA_A$-Rs and $GABA_B$-Rs (Fig. 36B). The transition from synchronized toward desynchronized activity was modeled by blocking the potassium leak current, mimicking the action of ACh and NE [McCormick, 1992], a strategy that has been used in thalamocortical models to this end [Bazhenov et al., 2002, Li et al., 2017] (see Methods Sec. 3.1.2). We then evaluated the perturbational complexity in the cortical network model. For SO and desynchronized activity, the sPCI showed similar values to those observed *in vitro*: 0.08 ± 0.01 and 0.10 ± 0.01, respectively. We next tested the effects of the progressive blockade of $GABA_A$ and $GABA_B$ during both different dynamics corresponding to the conditions of SO and desynchronized states. The maximal effect of $GABA_A$ blockade on the sPCI during SO occurred by reducing the receptor availability by 20%, when we obtained values of sPCI 0.05 ± 0.01 that remained unchanged for lower availability (Fig. 36C top left). On the other hand, the sPCI during desynchronized dynamics progressively decreased with the $GABA_A$-R blockade, reaching a plateau for blockade of $> 80\%$ of receptors, 0.08 ± 0.01 (Fig. 36C, top right). Interestingly, for large $GABA_A$ blockade during desynchronized activity, the sPCI values approach those observed during SO, as observed experimentally. For the $GABA_B$-Rs blockade, we observed a progressive slow decay of the sPCI values from SO conditions (Fig. 36C, bottom left), while for desynchronized dynamics we did not observe any trend in sPCI (Fig. 36C, bottom right). To a lesser extent, the $GABA_B$ effects were also similar to those observed experimentally.

Since $GABA_A$ modulation presented a stronger effect on the perturbational complexity in both conditions (i.e., SO and desynchronized dynamics), we next proceeded to evaluate the network dynamics in two scenarios: i) in a disinhibited network and ii) in an inhibited network (see Methods Sec. 3.1.2). As observed experimentally during SO, when we blocked $GABA_A$ (i.e., disinhibited the network) the spontaneous activity presented a shorter Up state with higher firing rate (Fig. 36B, compare top left and top middle left). In the model, we observed that the dynamics of spontaneous activity in a disinhibited network during SO is fully integrated, while weakly segregated, giving rise to activation waves that rapidly span the whole network (Fig. 37A, right; see Movie 1). Conversely, when the network is inhibited, the spontaneous activity is highly segregated and weakly integrated, and the activation waves propagate more locally and do not span over the whole network (Fig. 37A, left; Movie 1). Nonetheless, when there is a balance between integration and segregation, the activation waves span over the whole network recruiting their nearest neighbors (Fig. 37A, middle; Movie 1). Finally, we evaluated the perturbational complexity networks where the inhibition was not only decreased (as in the experiments), but also increased. While departing from the slow oscillatory regime, we found that increasing inhibition by +20% further increased sPCI (0.10 ± 0.01),

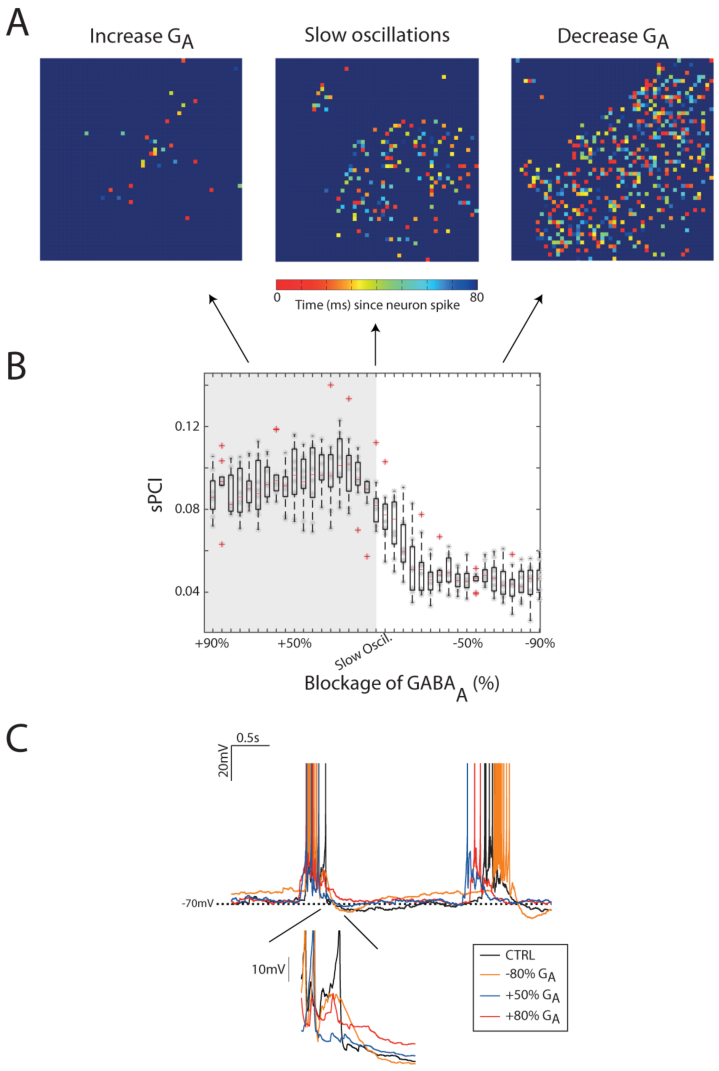

Figure 37 – sPCI for an inhibited and disinhibited cortical network model. (A), Example snapshot of cortical network activity for three networks with different inhibition ($GABA_A$) concentration (E/I balance). The color scale indicates the time since each neuron last spiked, thus illustration the temporal dynamics of activity propagation. Right, Networks with low inhibition blockade (−80%) show high integration, while with high inhibition blockade (+80%) show high segregation (left). Middle, Networks with an intermediate segregation/integration balance. See the simulations in Movie 1. (B), Population sPCI for inhibited and disinhibited cortical networks. The shadow area represents the model predictions. (C), Membrane potential traces for three neurons in the cortical network model during SOs (CTRL), disinhibited (orange), slightly inhibited (red), and high inhibited (blue) cortical network activity. Notice the increase and decrease afterhyperpolarization (AHP) following the up state for slightly inhibited and high inhibited neurons, respectively.

remaining high during SO for highly inhibited networks (+90%, 0.09 ± 0.02; Fig. 37B). In summary, these results indicate that there is a close link between integration and segregation with E/I balance, as suggested by [Lord et al., 2017], and that higher/lower

sPCI values are not the consequence of merely increasing/decreasing excitability.

4.5.3 Cortical complexity of spontaneous activity

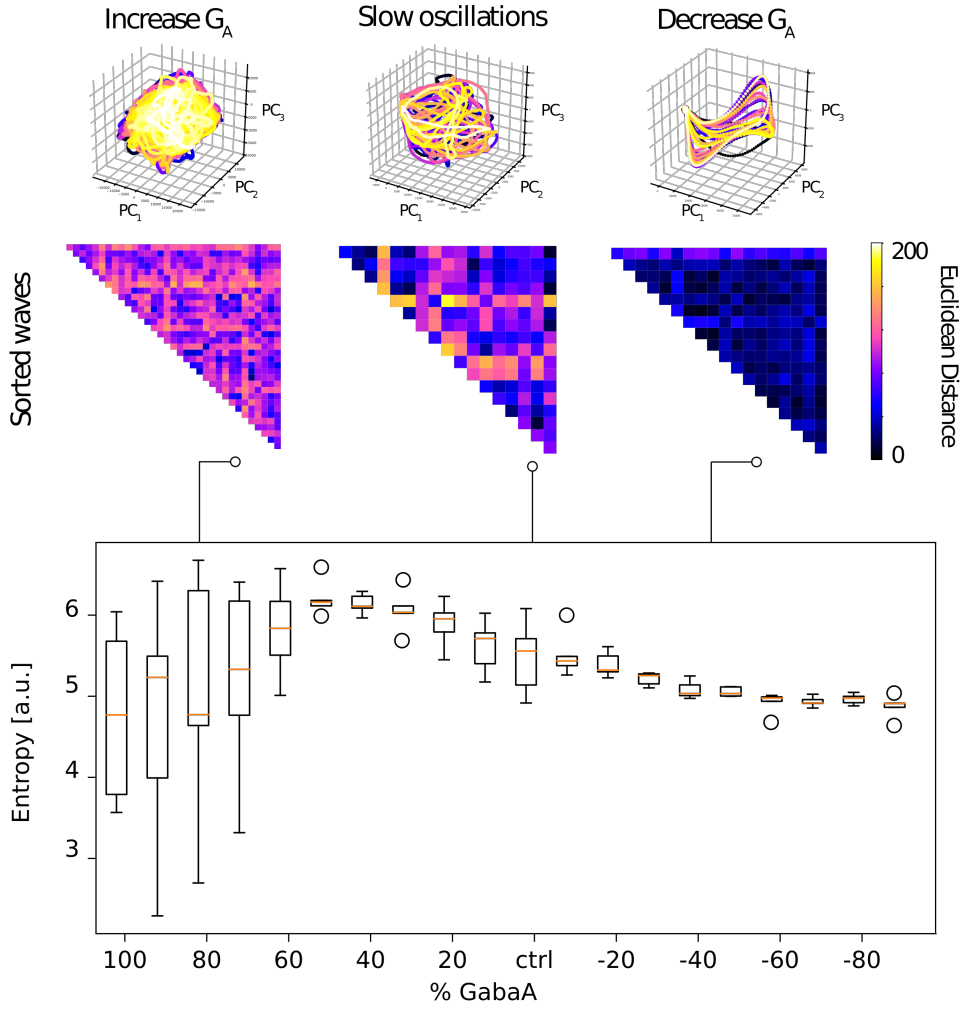

Figure 38 – Spontaneous cortical waves complexity in a cortical network model. Top, Energy trajectory of cortical activity in the three-dimensional space defined by the first three principal components for three networks with different inhibition ($GABA_A$, G_A) concentration (E/I balance). Left, Network with high inhibition blockade (+80%); Middle, Network under control slow oscillations; Right, Network with low inhibition blockade (−80%). Middle, Matrices of Euclidean distance (Distance Matrix, DM) between waves' trajectories. Bottom, Shannon entropy on the distribution of the values contained in each DM as a function of $Gaba_A$ concentration.

In the previous chapter, we have characterized the cortical complexity quantifying the causal interaction that follows an exogenous perturbation of the cortex. We have shown that there is a close link between perturbational complexity with E/I balance. Here, we sought to further characterized the spatiotemporal dynamics of SO, although

exploring the spontaneous complexity of the network. We used a method proposed by [Camassa et al., 2021b] in order to estimate the complexity of spontaneously generated slow oscillations (different from sPCI that consists in perturbation of the cortex). The method, called the Energy-based Hierarchical Waves Clustering method (EHWC), consists of the following steps: i) detect the occurrence of global waves; ii) reduce the data dimensionality via single value decomposition; iii) cluster hierarchically the singled out waves; iv) compute the matrices of pairwise Euclidean distance between waves (distance matrix, DM) and v) compute the entropy of the probability distribution from DM.

We evaluated the network complexity in two scenarios (similar to that done in 37B): i) in a disinhibited network, i.e., decrease $GABA_A$ (G_A) conductance, and, ii) in an inhibited network, i.e., increasing G_A conductance (see Methods Sec. 3.1.2). As previously observed the dynamics of spontaneous activity in a disinhibited network (decreased G_A) is fully integrated, while weakly segregated, giving rise to activation waves that rapidly span the whole network (Movie 1). The energy trajectories of these spontaneous waves were regular (Fig. 38 top right) giving rise to a homogeneous DM and subsequently a low entropy state, or less complex state (Fig. 38, bottom). On the other hand, in a inhibited network (increase G_A), we observed that the trajectories are more independent of each other (Fig. 38 top left), which in turn generates a homogeneous DM with larger distances, resulting also in a less complex state (Fig. 38, bottom). Both cases are different from the control network, where a rich matrix of distance can be observed (Fig. 38, top-center), meaning that there are an interplay between local and global waves propagation, giving rise then to a more complex state (Fig. 38 bottom). These results strengthen the fact that there is a close link between integration and segregation with E/I balance.

4.6 From spiking neurons to mean-field model

We have previously used a biophysically detailed model to shade light on the mechanisms of cortical activity. Although this kind of model are extremely useful to understand the impact of intrinsic mechanism on network activity, it can be not appropriate to study large scale networks, as the whole brain mouse for example. In order to join the gap between detailed neuronal models and mean-field (also called neural mass models) we used a mean-field approach of complex neurons, using three types of them, to show how from the network activity we can extract a mean-field equation models. We show in this section one approach to connect Hodgkin Huxley models with mean-field formalism. This section is based on our publication [Carlu et al., 2020]. It is also noteworthy that this research resulted from student project during the Spring School of European Institute of Theoretical Neuroscience `http://eitn.org`.

4.6.1 Mean-field formalism

We use here the master equation formalism proposed by [El Boustani and Destexhe, 2009], appropriate for a second-order mean-field description of network activity. This approach has some assumptions: i) it assumes the network dynamics as a Markovian process[§] on an infinitesimal scale ($\sim$ 20 ms); ii) it assumes the neurons to emit no more than one spike over the Markovian step T. Consequently, this theory assumes relatively low firing rate, as it is the case in the asynchronous regimes here studied (Methods Sec. 3.2).

4.6.2 Transfer function for simple and complex neuronal models

We present here the results of a comparison between mean-field predictions and direct simulations for the three models studied: AdEx, Hodgkin-Huxley, and Morris-Lecar. We start by estimating the transfer function of single cell and then proceed to test with large networks of neurons.

The transfer function for a simple AdEx neuron is well approximated by a sigmoidal function but its specific parameters follow from a complex combination of microscopic information, e.g., neuron resting potential (Fig. 39. See black and gray dots for comparison). Two main spiking patterns can be observed in the neuronal dynamics. One is characterized by a low firing rate, where spikes mainly result from the membrane voltage fluctuations (Fig. 39 bottom inset)). The second is characterized by a highly deterministic and regular firing rate (larger than 50 Hz, Fig. 39 top inset). The semi-analytic approach corresponded well with values reported from direct simulations

[§] A Markov process is a random process in which the future depends on the present, ignoring the late history of the process. In other words, in a discrete form, $P(X_n = x_n | X_{n-1} = x_{n-1}, ..., X_0 = x_0) = P(X_n = x_n | X_{n-1} = x_{n-1})$

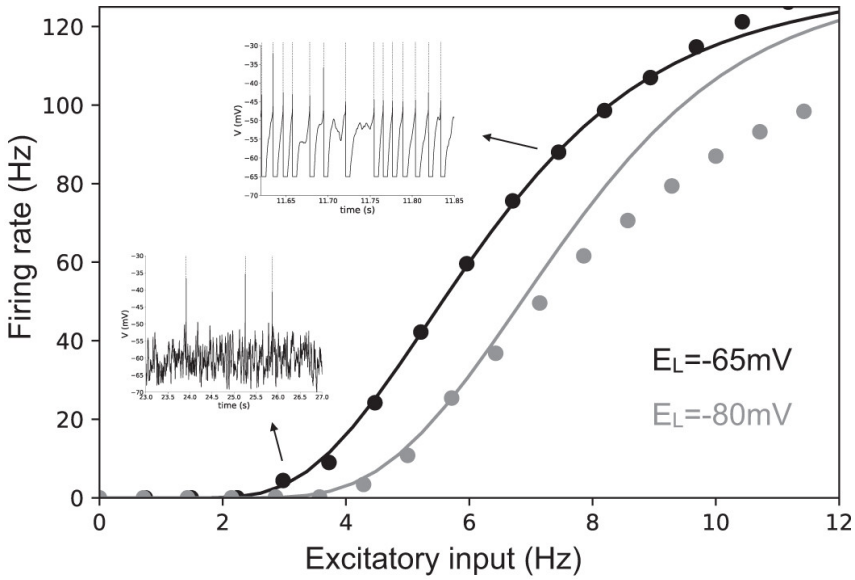

Figure 39 – Transfer function (TF) for an Exponential Integrate-and-Fire model (AdEx). Dots stand for numerical simulations while continuous line for the semi-analytic approach for the TF. The inhibitory Poissonian spike train has a fixed rate of 8 Hz, while we show neuron average output firing rate as the fiction of the Poissonian rate of excitatory input spike train. Inset: excitatory membrane potential for two combination of parameters. Color stands for different values of the leakage reversal potential as indicated in the figure.

as shown previously by other groups [El Boustani and Destexhe, 2009, Zerlaut et al., 2016]. For high firing rates the semi-analytic approach differs from the direct simulation. It is a direct consequence of the approach , once it assumes that neurons fire in an irregular manner strongly driven by fluctuation around the mean membrane voltage. Therefore, we only consider the case where the neuronal neuron activity is low, irregular and strongly fluctuation driven.

More complex models, such as Hodgkin-Huxley (HH) and Morris-Lecar (ML), permit to describe the details of sodium and potassium channel dynamics neglected in the simple AdEx model. The semi-analytic approach proposed for AdEx models can be applied exactly in the same way. Excitatory cells (regular spiking) were modeled as lower gain while inhibitory cells (fast spiking) were modeled with a higher gain. A lower/higher gain of the transfer function can be achieved by changing the cell's excitability, by means of resting membrane potential or by adaptation strength. Indeed, when comparing the semi-analytical approach to the direct simulation we obtained a good fit (of excitatory RS and inhibitory FS cells)for both HH and ML type models (Fig. 40 B and C).

Notice that the ML model shows a decrease of firing rate at frequencies higher than ~ 8 Hz, eventually reaching to no firing. Such dynamics is a consequence of the depolarization block observed at high input frequencies (high average external current)

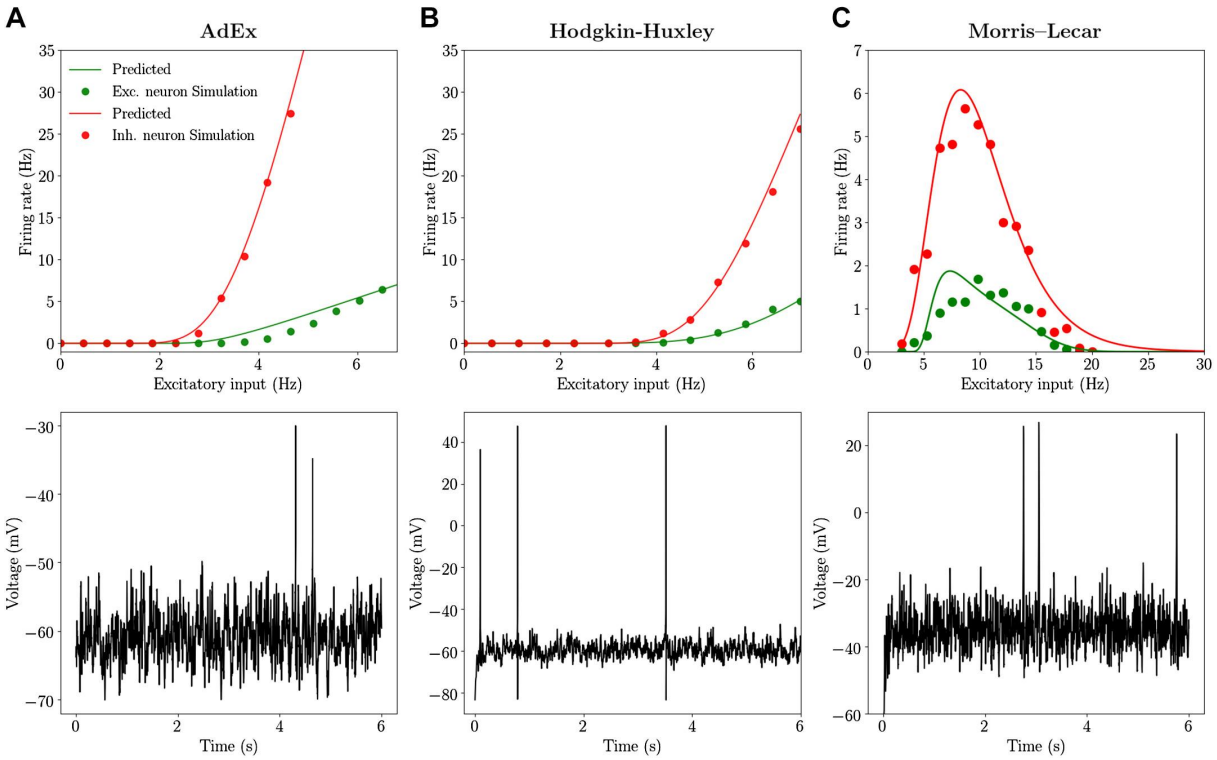

Figure 40 – Transfer function for single cells. Regular-spiking (RS, excitatory neurons, green) and fast-spiking (FS, inhibitory neurons, red) for: (A) AdEx, (B) Hodgkin-Huxley, and (C) Morris-Lecar model. Dots stand for numerical simulations while continuous line for the semi-analytic approach for the transfer function. Bottom row excitatory membrane potential for the three models, (A), (B), and (C), respectively.

and has been described previously by Kim and Nykamp [Kim and Nykamp, 2017]. Accordingly, we obtained a bell-shaped transfer function that was well predicted by our semi-analytical formalism.

Our results show that even if the details of the mechanism that generate a specific transfer function are very different, is is possible to adjust neuron parameters (e.g.,excitability) in a way allowing to obtain similar transfer function (at least in the region before entering a depolarization block). As a consequence, according to the mean-field theory where what matters for the population dynamics is only the transfer function, we expect different models to have a comparable emergent dynamics at the population (collective) scale.

4.6.3 Collective dynamics and mean-field predictions for spontaneous and evoked activity

In this section we used networks of neurons (AdEx, HH and ML model) to compare mean-field prediction with direct simulations. Specifically, we simulated

a sparse network of regular-spiking (RS, excitatory neurons) and fast-spiking (FS, inhibitory neurons) cells (Fig. 41) coupled through conductance base interactions (see Methods Sec. 3.2.1).

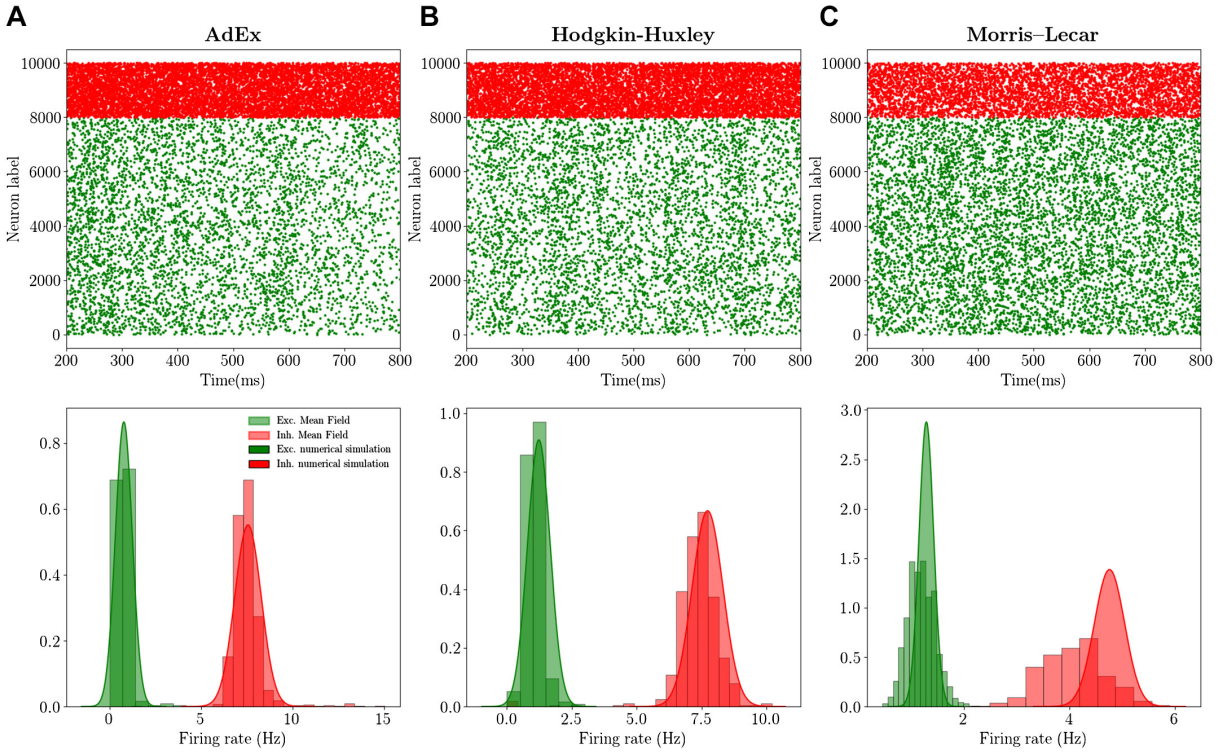

Figure 41 – Transfer function for single cells. Regular-spiking (RS, excitatory neurons, green) and fast-spiking (FS, inhibitory neurons, red) for: (A) AdEx, (B) Hodgkin-Huxley, and (C) Morris-Lecar model. Dots stand for numerical simulations while continuous line for the semi-analytic approach for the transfer function. Bottom row excitatory membrane potential for the three models, (A), (B), and (C), respectively. Inset of (B): the transfer function estimated over very large values of input rates.

We observed that in the different networks the dynamics stabilizes on an asynchronous regime. In all cases, this regime is characterized by irregular microscopic dynamics (i.e., neuron's spiking statistics are Poissonian) and displays the typical spiking patterns observed during awake states in cortical regions. Furthermore, as expected, inhibitory FS cells fired at a higher frequency with respect to excitatory RS cells. Through the mean-field model it is possible to measure both the average population rate and its covariance (see Methods Sec. 3.2.3). In Fig. 41 we show that the mean-field model gave a good quantitative prediction of both quantities. The higher discrepancy observed for the complex neuronal models (in our case HH and ML models) was related to a higher mismatch of the transfer function linked to the higher complexity of the model.

To complete the comparison between the mean-field model and the network dynamics, we explored the response of the system to external stimuli. Specifically, we considered an Poissonian train of spikes characterized by time-varying frequency and

targeting both RS and FS cells according to the following equation:

$$v(t) = A\left(\Theta(t_0 - t)e^{\frac{-(t-t_0)^2}{T_1^2}} + \Theta(t - t_0)e^{\frac{-(t-t_0)^2}{T_2^2}}\right), \tag{4.1}$$

where Θ is the Heaviside function and T_1 and T_2 are the rise and decay time constants, respectively.

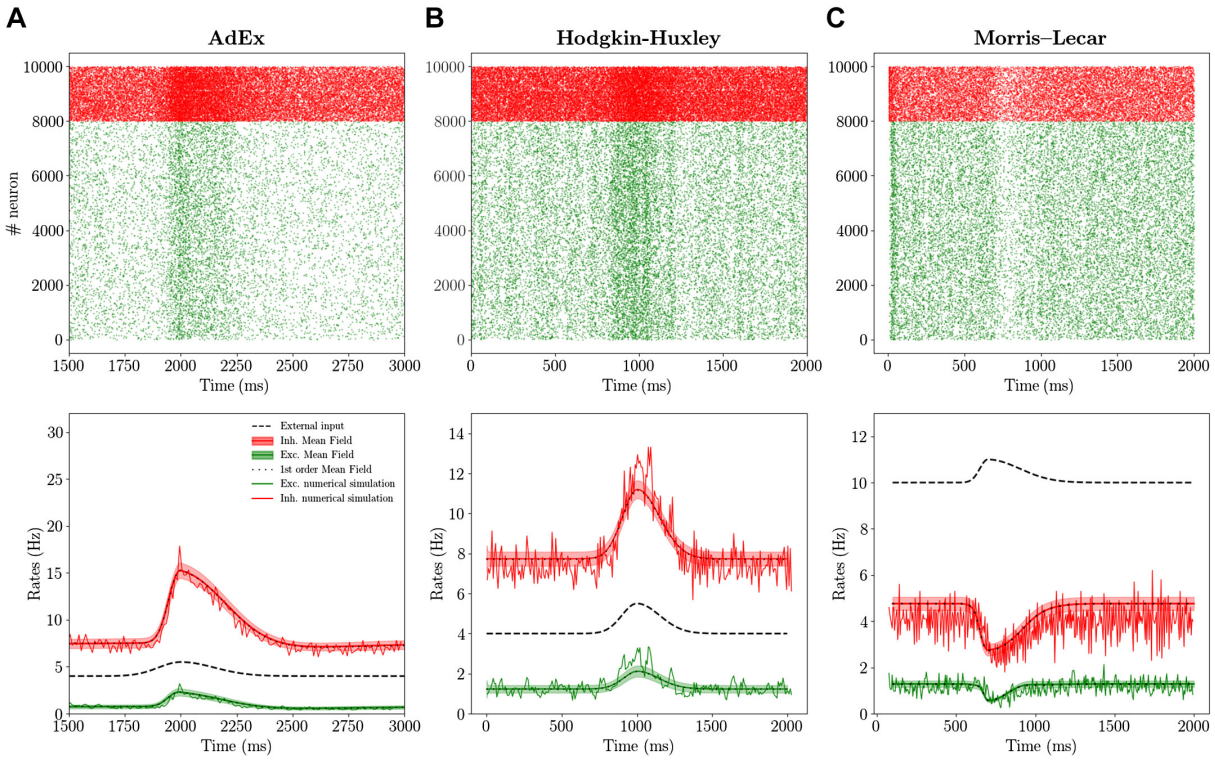

Figure 42 – Transfer function for single cells. Regular-spiking (RS, excitatory neurons, green) and fast-spiking (FS, inhibitory neurons, red) for: (A) AdEx, (B) Hodgkin-Huxley, and (C) Morris-Lecar model. Dots stand for numerical simulations while continuous line for the semi-analytic approach for the transfer function. Bottom row excitatory membrane potential for the three models, (A), (B), and (C), respectively. Inset of (B): the transfer function estimated over very large values of input rates.

In Fig. 42 we show the comparison between the mean-field prediction and the network dynamics given an external stimuli. Considering AdEx and HH models, we observed that both mean-field models under investigation compared favorably with their corresponding network dynamics. We also verified, as it has been shown in ref. [Di Volo et al., 2019a], that the faster the input dynamics is, the worse the agreement becomes. Indeed, for the Markovian hypothesis to hold, we need the time scale T to be much larger than the autocorrelation time in the spontaneous activity $T \sim \tau \sim 10$ ms.

For the Morris-Lecar model, we observed that a relatively strong input would bring singles neurons to a depolarization block, which appeared at relatively low activity

levels (Fig. 40 C). Given this difference between ML and AdEx and HH models, we expected to obtain different population dynamics properties in response to external perturbations. Indeed, as we show in Fig. 42 C, the response to an external stimuli differed from the one observed in the HH and AdEx models (compare Fig. 42 A and B against C). In this case the external excitatory stimuli turned out to inhibit both population activities. Such anticorrelation between external stimuli and network response as well its time course was well captured by the mean-field model (Fig. 42 C bottom). These results showed that also for a more complex and highly nonlinear setup the mean-field model was capable of predicting the ongoing activity and the time course of the response of a network of neurons operating in the asynchronous dynamical regime.

Finally, we compared the results of the first and second order mean field on average population rates. In Fig. 42 we superimposed the continuous green (red) line for excitatory (inhibitory) rate obtained with the second order mean field with the results obtained with the first order (black dots). We observed that the two quantities almost overlapped (the difference is too small to be appreciated at this scale). Nevertheless, it is worth noticing that the second order mean field permits to obtain nontrivial information on the population dynamics and its fluctuations in time, with good quantitative predictions of the covariance of population rates.

Chapter 5

Discussion

This thesis has investigated the emergence of activity generated by the cortical network, its mechanisms and properties, by combining experiments and a computational modelling approach. A large part of the focus has been on the study of slow oscillations, the coordinated activity of large populations of neurons consisting of an alternation of active periods (Up states) and silent periods (Down states, also referred to as off-periods). These oscillations occur with a slow frequency ($\leq$ 1 Hz) in the corticothalamocortical network during slow wave sleep and deep anesthesia, and they spontaneously occur also in cortical slices. This rhythmic activity emerges in the cortical network when there are no other driving inputs and it can be considered its default activity [Sanchez-Vives and Mattia, 2014]. During the active periods, or Up states, neocortical neurons (both excitatory and inhibitory) are depolarized, receive barrages of synaptic inputs and fire action potentials. During Down states neurons remain hyperpolarized and the synaptic activity is almost non-existent. This ”on and off” synaptic activity results in a bimodal distribution of the membrane potential values, an intracellular signature of slow oscillations. Here, I will first discuss the role of ionic current in the generation of this rhythmic pattern and how they also participate - by modulation through neurotransmitters - on the transition to other brain states, in particular to wakefulness. Then, I will discuss the impact of fast ($GABA_A$) and slow ($GABA_B$) inhibition on the spatiotemporal complexity of cortical networks. Finally, I will discuss a computational method that seeks to derive mean-field equations from spiking networks.

5.1 Impact of ion channels on cortical dynamics

5.1.1 SK calcium-activated potassium channels (KCa)

We have investigated the role of apamin-sensitive SK calcium-activated potassium channel (KCa) on spontaneous emergent activity in the form of slow oscillations. By doing this we attempted to connect the role of specific ionic channels types on the emergent patterns generated by the cortical network. We found that during physiological activity, KCa contributes to the modulation of neuronal firing and maintenance of Up states, and its blockage results in a shorter Up duration and higher neuronal firing. In our cortical network model, we parametrically explore the impact of KCa channels on network dynamics.

The KCa channel mediates the afterhyperpolarization that follows a train of action potential [Pennefather et al., 1985]. In other words, I_{KCa} is a spike-frequency adaptation current [McCormick and Williamson, 1989]. Due to its slow time course (order of 100 ms) during the hyperpolarization period (Down state), KCa has been suggested to be involved on the termination of Up states [Steriade et al., 1993c, Compte et al., 2003, Neske, 2016]. This suggestion also relays on the fact that KCa is modulated by acetylcholine via muscarinic receptors[McCormick and Williamson, 1989, McCormick, 1992], therefore suggesting the role of the KCa block in the transition from sleep to awake[Stocker et al., 1999].

Here, in order to investigate how KCa channel impact the cortical SO, we resorted to its blockage. KCa channel blocker apamin was applied to cortical slices resulting in an significant increase in the population firing rate during the Up state and a shortening of this period (Fig. 10). Indeed both properties are mechanistically related, since it has been proposed that the termination mechanism of the Up state is the recruitment of activity-dependent adaptation, thus dependent on the firing rate during the Up states [Compte et al., 2003]. We also observed that the KCa channel is involved on the recruitment of the local network, i.e., its blockage resulted in a steeper slope in the Down to Up transition (Fig. 10C).

Finally, our network model allowed us to bridge the gap between intrinsic mechanisms and emergent activity of brain networks. We implemented the Compte et al. [Compte et al., 2003] network model that was originally tuned based on experimental observations of cortical SOs, and further studies have validated that it reproduces diverse features of excitability and oscillations [Sancristóbal et al., 2016], and of cortical emergent properties such as β and γ frequencies [Compte et al., 2008]. We were able to reproduce the physiological Up and Down dynamics of SO as well as systematically explore the effects under blockage of KCa channel. We have shown how the KCa controls the neuronal firing during Up states, not only of the pyramidal neurons (that were

simulated containing the KCa channel) but also, indirectly, the inhibitory neuronal firing rate. By parametrically blocking the KCa channel, we showed that there was a anticorrelation between the duration of Up states with the firing rate, such that the lower the expression of the channel, the lower the duration of Up states and the higher the firing rate (Fig. 27) during the block. Also, KCa channel had a significant role on the network synchronization and membrane fluctuation, such that the lower the expression, the higher the synchronization and the lower the membrane fluctuation (Fig.13). Finally, we reproduced the steeper transition form Down to Up observed experimentally, and showed that the faster recruitment results in faster propagating waves (Fig.14). In summary, we suggested that activation of KCa channel determines the firing pattern and firing rate during Up states as well as its duration (Fig.15).

How to explain the observed changes and what does it tell us about the role of KCa? A main conclusion is that KCa, due to its properties and time course, is well fit to regulate firing rates during excitation and thus, during Up states, given that it is activated by the calcium that enters the cell with the firing [Sah and Faber, 2002]. For this reason, it also regulates the recruitment of the local network, acting as a ”brake” that slows down recruitment, and therefore as a control for hyperexcitability and epileptiform discharges. For this reason, its block results into higher firing rates and steeper activation. Such Up states with higher firing rates are not consistently followed by longer Down states, as it is the case when blocking $GABA_A$ [Sanchez-Vives et al., 2010]. Higher firing rates recruit activity dependent mechanisms of hyperpolarization, like sodium-dependent potassium currents. Of course, if we are blocking KCa, then this mechanism is no longer available [Wang et al., 2003] in order to induce an elongation of the Down state. The dominant effect (prolongation o shortening of the Down state) will depend on the departing point and the global level of excitability, for example, if the Down state had some dependence on KCa, then it can be shorter, but longer if it relies on KNa current.

5.1.2 Calcium and sodium -dependent potassium channels

An open question is how does a ionic current that is present in only a group of cortical cells influences network activity. We explored up to what point the network is sensitive to ionic currents present within only a fraction of neurons by parametrically changing the expression of I_{KCa} or I_{KNa} (calcium and sodium -dependent potassium currents, respectively). We found that while we gradually vary such currents from random neurons in different proportions, several properties of the network were affected, such as Up state duration, oscillation frequency or synchrony in the state transition, demonstrating the large impact that ionic channels had at the network level, even if present in only $< 40\%$ of neurons. Furthermore, we observed that neurons without those specific currents were indistinguishable from the remaining ones at both their

extracellular and intracellular spontaneous activity. Finally, we showed these potassium dependent channels were involved in the off-periods that followed network perturbation.

Considerable progress has been made towards a detailed understanding of the mechanisms controlling SO. For instance, in a thalamocortical model, Hill and Tononi [Hill and Tononi, 2005] suggested that ionic currents (I_H and I_{NaP}) are responsible for the initiation of Up states. Conversely, Holcman and Tsodyks [Holcman and Tsodyks, 2006] have suggested that high level of recurrency may be responsible for Up and Down dynamics. Both ideas are not mutually exclusive. Indeed, experimental and theoretical studies have suggested a joint mechanism, integrating both intrinsic cellular properties and network recurrent connectivity as the driving force fot the generation of Up states [Sanchez-Vives and McCormick, 2000, Compte et al., 2003]. The proposed mechanism suggests an interplay between neuronal firing amplified by recurrent excitation and a negative feedback due to slow activity-dependent K^+ currents. In other words, the Down state is generated by the failure of the network to maintain persistent activity due to the negative feedback provided by activity-dependent K^+ currents, which drives the sudden transition from the Up to the Down state. Once in the Down state, the slow afterhyperpolarization slowly decreases in amplitude, allowing the network to, through recurrent excitation, generate another Up state.

To investigate how intrinsic mechanisms in the form of depended K^+ currents impact collective phenomena we have parametrically varied the fraction of neurons that include ionic currents such as Na^+-dependent K-current or Ca^{2+}-dependent K-current. Lowering the expression of KCa currents was not enough to break-off the Up and Down network dynamics. Instead it promoted shorter Up states with more neuronal firing (Fig. 18, in agreement with the effects of apamin blockage previously discussed). We also observed and elongation of Down states, although it may be due to the high activation of KNa current, once it has a longer time scale than KCa current.

Exploring the dependence of the network dynamics on the expression of neurons containing KNa current, we observed a high impact on the network dynamics. By lowering the KNa expression we observed a transition from a high synchronized network, to a low synchronized one (Fig. 19), resembling the awake state. This impact on network dynamics generated by I_{KNa} has been previously described by Compte et al., although there they lowered the maximal channel conductance (g_{KNa}) instead of it expression, as we did here [Compte et al., 2003]. This result is in agreement with experimental observations that suggested that activation of I_{KNa} current play an important role in the termination of Up states [Sanchez-Vives and McCormick, 2000, Neske, 2016]. Interestingly, when comparing those neurons that contained the KNa current versus those that did not, were indistinguishable from their extracellular and intracellular spontaneous activity. We have shown, by analyzing isolated neurons, that

KNa current controls the excitability of single neurons, as previously described [Schwindt et al., 1989], but that the recurrency from the network keeps the neurons, with and without KNa current, in the same dynamical regime (Fig.21).

Finally, we evaluated the effect of KNa and KCa currents on the off-periods (a period of suppressed firing after an stimulation; Fig. 22). As we previously discussed, KCa acts slowing down the fast network recruitment, thus its blockage after stimulation is not enough to avoid the presence of off-periods. Conversely, KNa seems to be the main responsible for the off-periods, since its blockage after stimulation resulted in an active reverberating-like state, without falling into silence. By blocking both, KCa and KNa, we have shown that the off-periods are abolished, being replaced by an asynchronous-like activity. Together our results are a first step into describing how different adaptation K+ currents may contribute to the off-periods. Also, our results are in agreement with the work from Rosanova and collaborators, who have suggested that the tendency of neurons to go to an off-period is due an enhancement of adaptation K+ currents, since it is the main mechanism responsible for cortical bistability [Rosanova et al., 2018].

5.1.3 Voltage gated K^+ channel 7: the M-current

M-current is a time and voltage-dependent K+ current, non-inactivating and non-rectifying, which exerts a clamping effect of the membrane potential [Brown and Adams, 1980]. The molecular basis of this current were identified by [Wang et al., 1998], corresponding to the KCNQ2 and KCNQ3 potassium channels. Being the M-current a powerful stabiliser of the membrane potential, controlling subthreshold activity and synaptic responses, abnormal function of neuronal KCNQ channels have been associated to diseases related to hyperexcitability: just a loss of 25% of KCNQ2 or KCNQ3 channels are the cause of benign familial neonatal seizures ([Schroeder et al., 1998]; for a review see [Jentsch, 2000]). The control of neuronal excitability by M-current has also been exploited as a therapeutic strategy, enhancing this current for the treatment of epilepsy [Tatulian et al., 2001] of to reduce the stroke related brain injury [Bierbower et al., 2015].

In the current work we investigated the effect of reducing M-current over a physiological network activity of the cerebral cortex: slow oscillations. Slow occur in slow wave sleep and in deep anesthesia (for a review see [Neske, 2016, Sanchez-Vives et al., 2017]) but also in isolated cortical tissue, such as isolated cortical gyri, cortical slabs [Timofeev et al., 2000], cortical slices [Sanchez-Vives and McCormick, 2000], or tissue isolated by injury [Sarasso et al., 2020]. Such pervasive activity acts as a default activity of the cortical circuitry [Sanchez-Vives and Mattia, 2014], integrating intrinsic properties of neurons such as ionic channels, cellular and synaptic properties and connectivity. We have carried out this study in cortical slices expressing spontaneous

slow oscillatory activity *in vitro*, allowing us to study the isolated effect of M-current on the cortical network, and without the influence of other connected brain areas. The block of M-current was originally described in bullfrog sympathetic neurons [Adams et al., 1982]. Specific blockade was caused by muscarinic and by other agents, resulting in an inward rectification causing depolarization, increased input resistance, reduced outward rectification and increased excitability. Such an increase of excitability reflected in the emergent network activity, has also been observed in our study, in which we have used XE991 dihydrochloride (100μM) as a specific M-current blocker [Wang et al., 2000] to explore the transformation of the slow oscillations. We found that M-current has an important role in the mechanisms controlling the Up state, specifically modulating its persistence and termination. Blocking the M-current resulted in a prominent elongation ($\sim$ 3 times) of the periods of activation (Up states) of the cortical network, while the Down states or silent periods hardly varied in duration (Fig. 24). The population firing rate was also significantly increased during the Up and also in Down states, also reflecting the hyperexcitability of the circuit. It should be noted that this excitability includes depolarization of the membrane potential, but also an increase of the input resistance, such that the synaptic inputs evoke larger responses.

Given that Up states are driven by bursts of synaptic inputs from neighboring neurons [Steriade et al., 1993c], the global activity is enhanced. The effect on Up states if very prominent, prolonging them to the point that they remind of the so-called microarousals that occur during slow wave sleep as a result of activation of the arousal systems [Halasz et al., 1979], and that also appear along with slow oscillations in the transition slow wave dominated, deep anesthesia, towards light anesthesia [Tort-Colet et al., 2021]. Interestingly, the blockade of M-current in the isolated neocortical network does not result into epilepsy, as it occurs in the case of newborns with deficits in the current [Schroeder et al., 1998]. We can suggest that the recurrent connections with more epileptogenic areas in this circumstances, such as the hippocampus [Hu et al., 2007, Peña and Alavez-Pérez, 2006] can drive the neocortex *in vivo* into epileptic discharges. However, such epileptic discharges do not seem to be originated through this mechanism in the cortical network, not even in highly excitable cortical areas like the entorhinal cortex [Yoshida and Alonso, 2007].

In order to do a systematic exploration of the role of M-current on the network, being able to vary its expression parametrically, we reproduced a conductance-based computational model of the cortical network that expresses slow oscillations [Compte et al., 2003]. In it, the M-current was integrated in the excitatory neurons following the model in [McCormick et al., 1993] and locating it in the somatic compartment [Wang, 1999]. In this new implementation of the model we were able to reproduce the physiological Up and Down dynamics of the slow oscillations as well as the experimental effects of blocking the M-current. As observed in the experiments, in the model the block of

the M-current resulted in an increase of the firing rate. Interestingly, even when only the excitatory neurons expressed M-current, the increase of the firing rate did also occur in the inhibitory neurons, by virtue of the recurrent connectivity. By parametrically blocking the M-current (from 0 to 100%), we found a correlation between the elongation of the Up states and the increase in the firing rate, such that the lower the expression, the higher the duration of Up states and the firing rate (Fig. 27D). We also found that the presence of M-current induced a higher global synchrony and more periodicity in the network (Fig. 26A), which was reduced by blocking the channel. Higher excitability lead a less regular rhythmic pattern, which was reflected in the autocorrelogram of the population activity. Further, the calculation of the synchrony order parameter as in [Golomb, 2007], reflected a nonlinear decay with the reduction of the M-current, reflecting a less synchronized network. In contrast, we can say that M-current contributes to the synchronous firing in the network, with higher correlation across spikes (Fig. 27E) and more synchronous and regular Up states.

The role of the block of the M-current in the modulation of firing and synchronization of the network is highly relevant if we consider that this current owns its name to "muscarine": Brown and Adams [Brown and Adams, 1980] discovered a novel voltage-sensitive K+ current that was suppressed by muscarine, and that they called M-current. Indeed, since McCormick and Prince [McCormick and Prince, 1986], a majority of the studies of M-current in the cerebral cortex have been carried out in the context of the studies of the effects of cholinergic innervation. Acetylcholine is one of the main neurotransmitters inducing the transition from slow wave sleep to wakefulness. Particularly, the cholinergic action in the cerebral cortex takes place largely through muscarinic rather than nicotinic receptors, and as shown here, an important actor - but not the only one - is by blocking the M-current. As generated in our computational model in the individual neuron level (Fig. 26), just the reduction of this current induces quite a radical change in the network dynamics, going from regular and synchronous slow oscillations to more prolonged and irregular firing periods. However, this is not yet the asynchronous, persistent activated state that it is associated to wakefulness [Constantinople and Bruno, 2011], because there are other potassium channels (sodium and calcium dependent potassium currents) that remain open, repolarizing the membrane potential towards Down states (Fig. 5). The similarity of this activity pattern with those described in the transition periods towards wakefulness that are achieved by light (versus deep) levels of anesthesia, when microarousals occur, is remarkable (Fig. 5A in [Deco et al., 2009]). In conclusion, our experimental results together with our computational model, supports a highly relevant role of M-current on cortical network dynamics. This effect is even more relevant if we consider that probably only a fraction of the neurons express this channels, but its effects reverberate through the recurrent connectivity. The block of M-current induces a significant increased excitability, with longer and less

synchronous periods of activity or Up states, that also express higher firing rates. Since cholinergic action in the cerebral cortex critical to induce the transition from slow wave sleep to wakefulness, our observations suggest a relevant role of the M-current block by muscarinic action into this transition. On the contrary, the physiological activation of the M-current plays an important role maintaining hyperpolarized the neuronal membrane potential and facilitating, in the absence of cholinergic inputs, that the cortical network expresses slow waves.

5.1.4 Hyperpolarization-activated cation current: the H-current

We explored the role of the hyperpolarization-activated cation current (H-current, for a review see [Pape, 1996]) on the spontaneous generated activity of slow oscillations. We found that H-current a relevant role on the maintenance of Up and Down states. The bath applied 10μM of ZD7288, a selective blocker of HCN channels (hyperpolarization-activated cyclic nucleotide–gated) that generates the H-current, resulted in larger periods of activation (Up states) and also in large periods of inactivation (Down states) (Fig. 28). In our detailed conductance-based model of SO, we implemented the H-current and explored more extensively the relationship between this ionic current and its impact on the network dynamics.

The hyperpolarization-activated cation current (H-current) is suggested to be involved in the generation of slow periodic rhythms, such as spindle waves, in the thalamocortical system [Lüthi and McCormick, 1998b, Lüthi and McCormick, 1999]. In thalamocortical single cell dynamics, it is known that the H-current has an important role, such as, modulating the resting membrane potential, controlling the response to hyperpolarization, and contributing to oscillatory frequency [Lüthi and McCormick, 1998a]. Conversely, it's role on network dynamics, a global effect emerging from the interaction of single neurons, was mainly studied in thalamic networks [McCormick and Pape, 1990, Pape, 1996, Lüthi and McCormick, 1998a, Yue and Huguenard, 2001]. Despite of all these studies regarding H-current, it is still not clear how its impact on cortical slow rhythmic oscillations (see [Lüthi and McCormick, 1998a, Neske, 2016] for a review). One exception is the work from Mao and collaborators [Mao et al., 2001] have shown that, at single cell resolution, spontaneous activity is delayed when H-current is blocked, albeit this study was not done in slow oscillatory activity.

Here, we have resorted to H-current blockage during network slow oscillations to better understand its effects at a population level. H-current blockage resulted in an significant increment on the Up and Down state duration (Fig. 29). Although neither the network periodicity nor in its neuronal firing were significant affected (Fig. 30). In our cortical network model of SO, we implemented in a subset of pyramidal neurons the H-current. We successfully reproduced the physiological Up and Down dynamics of

slow oscillations as well as the effects under H-current blockage (Fig. 31). We have shown that there was a modulation on the firing rate of the pyramidal cells and interneurons such that lower the concentration higher the firing rate (Fig. 32). Furthermore, by parametrically blocking the H-current, we showed that there was a correlation between the duration of Up states and Down with the firing rate, such that the lower the expression, the higher the duration of Up and Down states and the firing rate (Fig. 32). The increment in the duration of Down states is consistent with a previous modelling study of the thalamocortical system [Hill and Tononi, 2005]. Finally, we showed how the presence of H-current induced a higher global synchrony in the network (Fig. 26), reflected in a higher order parameter. Our model suggests that the increased firing rates during the Up states and their longer duration, result into a larger accumulation of sodium and a slower time course of the KNa current, that keeps the Down states longer. HCN channels are a target of noradrenaline, which maintains the channels open [Pape and McCormick, 1989]. Since noradrenaline is one of the activating neurotransmitters contributing to the transition from slow wave sleep to awake, the shortening of Down states that is due to H-current could contribute to the transition to arousal. Future studies should model our simulations of cholinergic with noradrenergic action to investigate in depth the mechanisms of this transition.

5.2 Impact of slow and fast inhibition on cortical complexity

We have investigated the role of $GABA_A$-R-mediated and $GABA_B$-R-mediated inhibition on cortical emergent activity and complexity, in particular on complexity measured by means of perturbing the network with stimulation. By doing this we have attempted to bridge a macroscale clinical measure (PCI), with the synaptic and cellular components of the local cortical circuits. We found that during physiological activity, both types of inhibition, fast and slow, contribute to the generation of richness of spatiotemporal activity patterns and cortical complexity, and the progressive blockade of fast or slow inhibition results in enhanced synchronization and breakdown of complexity. However, the contribution of $GABA_A$-R-mediated and $GABA_B$-R-mediated inhibition is different in the desynchronized and in the slow oscillatory (SO) regimes, and this is discussed below. In our computational model, we explore areas of the parameter space that cannot be reached experimentally, exploring more extensively the relationship between excitatory and inhibitory balance, network dynamics, and cortical complexity.

The PCI [Casali et al., 2013] is a measure of cortical complexity that has been used to quantify consciousness levels, in awake/sleep, in anesthesia [Hudetz, 2012, Sarasso et al., 2015] and in patients with disorders of consciousness [Rosanova et al., 2018, Casarotto et al., 2016]. This measure consists in the perturbation of the brain network by means of cortical stimulation to engage the cortico-thalamocortical circuit in causal

interactions, and then capturing the spatiotemporal properties of the response in an index that reflects cortical complexity. It is based on the hypothesis that for consciousness to occur, simultaneous integration and segregation of information in the network are needed, resulting in high complexity in the awake state [Tononi and Edelman, 1998]. This perturbational approach presents advantages with respect to an observational one (based on spontaneous activity) because it is less affected by noise or isolated processes, and only assesses information generated through deterministic interactions, which also gives advantages that are useful clinically [Casali et al., 2013]. Given that there is accumulating evidence that brain complexity is a relevant property that informs about the brain state and consciousness levels [Massimini et al., 2005, Pigorini et al., 2015, Sarasso et al., 2015, Casarotto et al., 2016, Dasilva et al., 2021b], we sought to link this measure to the properties of cells and circuits, to understand how the different mechanisms may sculpt the resulting complexity. This understanding is also important to eventually devise strategies to recover complexity in pathologic situations.

To investigate how inhibition contributes to complexity, we resorted to the progressive blockade of GABAergic receptors. However, network complexity in humans has been found to be different in the synchronized, slow oscillatory state (low complexity) and in the awake state (high complexity) [Massimini et al., 2005, Casali et al., 2013, Rosanova et al., 2018]. For this reason, we conducted the GABAergic blockade while departing from these two extreme conditions, to understand the different role GABAergic inhibition plays in both regimes, i.e., during synchronized and desynchronized states. Our preparation reproduced several features of these different dynamics. Bath application of NE+CCh shifted SO to low-frequency 1− to 5−Hz oscillations (Fig. 33; as in [D'Andola et al., 2018]), which in part resemble the cortical activity observed during wakefulness. Further, we lowered the temperature by 2°C to 32°C, which we have demonstrated previously diminishes cortical synchronization [Reig et al., 2010], and increases excitability by increasing electrical compactness and synaptic summation [J. Trevelyan and Jack, 2002]. We also lowered $[Ca^{2+}]_o$ levels to enhance excitability (0.8 − 0.9 mM; [Markram et al., 2015]). Both manipulations resulted in larger desynchronization as illustrated in the autocorrelograms (Fig. 33B) and spectrograms (Fig. 33C). Both manipulations led to higher sPCI values (Fig. 33D) as well as increased SampEn with respect to the SO regime, which is consistent with the idea of different cortical dynamics. Our experimental model thus allows the study of transitions between different cortical dynamics, SO to desynchronized states.

Departing from SO as well as from desynchronized activity, $GABA_A$-R blockade resulted in Up states of higher amplitude and shorter duration than those observed in control conditions (Fig. 34B). This property has been described [Sanchez-Vives et al., 2010], but only for the evolution of Up states in SO. Interestingly, when departing from desynchronized activity, it is also possible to induce rhythmicity in low frequencies by

partially blocking $GABA_A$-Rs (Fig. 34A). It should be noticed that this is not epileptiform activity, although progressive inhibition would eventually lead to epileptiform discharges (Fig. 34A). Disinhibition causes higher firing rates that induces a hypersynchronization of the network, as we also find in our computer model simulations. In the simulations, the activation of potassium channels is critical to induction of the silent periods. Such hypersynchronization of the network results in a decrease in complexity.

$GABA_B$-R blockade during SOs increased Up-state duration [Mann et al., 2009, Perez-Zabalza et al., 2020], resulting in highly regular oscillatory patterns and prominent bistable responses to electrical perturbation (Fig. 35B). This finding is revealing of the role of $GABA_B$-Rs in increasing richness of activity patterns and irregularity in the Up and Down states [Perez-Zabalza et al., 2020]. This is also translated in a consistently decreased sPCI with $GABA_B$-R blockade. A different situation takes place when departing from the desynchronized state (Fig. 35A). In this situation, the blockade of $GABA_B$-Rs tends to induce, but does not fully induce, a bistable oscillatory regime, nor significantly decreases sPCI. These findings suggest that the role of $GABA_B$-Rs in the desynchronized state for introducing richness of activity patterns and thus complexity, is not as relevant as it is for the SO regime. It is probably the case that the intense firing of neurogliaform neurons necessary for the activation of $GABA_B$-Rs is more commonly achieved in synchronized than in desynchronized states (for review, see [Sanchez-Vives et al., 2021]).

Local network excitability, bistability, and the integration-segregation balance in brain slices

A straightforward explanation of our observation of increased sPCI during desynchronized states is that the sPCI merely reflects network excitability. In other words, the sPCI scored higher just because bath-application of modulators such as CCh or NE increased the excitability of the slice. However, if that were the case, any experimental manipulation increasing the excitability of the slice would result in higher sPCI values compared with those obtained under the SO regime. However, previous studies already demonstrated the opposite, showing that either bath-application of a glutamate receptor agonist (kainate) [D'Andola et al., 2018] or electric field modulation [Barbero-Castillo et al., 2019] in cortical slices increased network excitability without affecting sPCI. Finally, the authors did not find a relationship between network excitability and sPCI [D'Andola et al., 2018]. Here, we further explored the relationship between excitability, inhibition and connectivity in our experiments and our newly implemented network model and provided a number of novel insights. On one hand, the progressive reduction of fast inhibition gradually increased the firing rate (Fig. 34), even leading to epileptiform discharges in some cases. We found that excessive excitability can in fact reduce the sPCI, and statistical analysis indicated that following $GABA_A$-R blockade, the sPCI was

significantly reduced while the relative firing rate increased (Fig. 34). On the other hand, $GABA_B$-R blockade also reduced the sPCI without significantly increasing the firing rate (Fig. 35), supporting the idea of the independence of firing rates or excitability and complexity.

Finally, our network model (Fig. 9) allowed us to investigate areas of the parameter space that were not visited experimentally. The model that has been used for these simulations, as described, is a biologically inspired, Hodgkin and Huxley model [Hodgkin and Huxley, 1952], in which pyramidal neurons have two compartments: somatic and dendritic (see Methods Sec. 3.1), where excitatory synapses target the dendritic compartment and inhibitory synapses are localized on the somatic compartment of postsynaptic pyramidal neurons [Compte et al., 2003]. The Compte et al. [Compte et al., 2003] network model was originally tuned based on experimental observations of cortical SOs, and further studies have validated that it reproduces diverse features of excitability and oscillations [Sancristóbal et al., 2016], and of cortical emergent properties such as β and γ frequencies [Compte et al., 2008]. Activation of GABAergic receptors in the soma compartment hyperpolarizes the membrane potential and decreases the input resistance, while those in dendrites modulate NMDA potentials [Doron et al., 2017], calcium spikes, block back-propagation of action potentials and neuronal bursting, all without modifying the membrane potential in the soma [Larkum et al., 1999, Pouille and Scanziani, 2004, Breton and Stuart, 2012, Palmer et al., 2012]. Previous study have demonstrated that this model could reproduce at the cellular and network level the transformation of the SOs when $GABA_A$-Rs were progressive blocked [Sanchez-Vives et al., 2010]. In the current study, we implemented a new version (see Methods Sec. 3.1.2) of the cortical network model aimed to reproduce population features that we observed while blocking as well $GABA_B$-R: an elongation of the Up states (as in [Mann et al., 2009, Perez-Zabalza et al., 2020], and the spatiotemporal response to stimulation (or perturbation), which results in a decrease in the resulting sPCI with GABAergic block. Somatic GABAergic receptors located in the soma in our model were sufficient to reproduce both spontaneous and evoked population responses observed in cortical slices, although a further exploration of a more detailed somatic versus dendritic influence on network dynamics could be a valuable future development. In the model we explored parametrically the variation of $GABA_A$-R blockade and found the rate of decrease of sPCI reached a minimum for about a 25% decrease in inhibition (Fig. 36). Interestingly, we were also able to enhance inhibition, and found that there is a window of excitatory/inhibitory balance, around the physiological values, in which complexity is maximal, but either enhancing or decreasing inhibitions diminishes complexity (Fig. 37). However, when we look at the spatial patterns (see Movie 1) we can see how the spatiotemporal pattern to reach decreased complexity can be very different, from a highly disaggregated activity in enhanced inhibition, to hypersynchronization in low inhibition.

Furthermore, given the spontaneous spatial patterns observed in the model, we applied a different measure of cortical complexity based on the wave propagation [Camassa et al., 2021b], differently from sPCI that is based on cortical response to stimulation. In agreement with the results obtained for sPCI (Fig. 37), the entropy of wave propagation also showed high complexity values for a window where excitatory/inhibitory balance is kept around physiological values (Fig. 38). These finds bridge the activity of receptors with the activation of the network at the mesocortical level and connects circuit properties with large-scale causal interactions in the cortical network. Furthermore, it suggests that there is a close link between integration and segregation with E/I balance and that higher/lower sPCI values and wave propagation entropy are not the consequence of merely increasing/decreasing excitability.

5.3 Mean-field approach to the dynamics of networks of complex neurons

We reviewed and applied a formalism to derive mean-field (MF) models and showed that it can be applied for simple and complex neuronal models such as Adaptive Exponential Integrate-and-Fire (AdEx), Hodking-Huxley (HH) and Morris-Lecar (ML). The key aspect to achieve biologically plausible MF models is to be able to obtain the transfer function (TF) of the desired neuronal model. Our approach followed a MF formalism based on a master equation, which is applicable to every neuron, once the TF is known [El Boustani and Destexhe, 2009]. Recently, Zerlaut et al. [Zerlaut et al., 2016] have shown that the usual mathematical form of the TF, known analytically for the Integrate-and-Fire model, can be applied to more complex neuronal models. This gave rise to a semianalytic approach, where the TF can be parameterized and fitted numerically to the neuron model, while the MF remains analytic. This approach has been applied to the AdEx model [Zerlaut et al., 2018, Di Volo et al., 2019a], and here we applied it to more complex models, namely the Morris–Lecar and the Hodgkin–Huxley model.

We studied the predictions of the considered MF models on neuronal networks of excitatory (modelled as regular spiking neurons) and inhibitory (modelled as fast spiking neurons) cell populations during the asynchronous regime, typical of awake-like cortical regime. In order to explore different cortical regimes where neurons can exhibit different patterns of activity, e.g. bursting, a different methodology must by employed [Ostojic and Brunel, 2011, Di Volo et al., 2019b]. Nevertheless, in the context of tonic neuronal activity, as assumed here, the method is shown to be able to capture the response function of highly realistic models. Our results positively compare in the case of ML and HH models for both the average and the variance of network population

activity.

We have shown that the MF predictions are strongly dependent on the goodness of the fitting procedure for single neurons TF. Even if such procedure works very well for neurons working in a low rate regime, whenever the firing rate becomes very high (> 100 Hz) the quantitative agreement gets worse. A more refined technique for the evaluation of the transfer function in different states (low and high rates activity) is an important topic for future research [recent work has addressed this issue in AdEx model [Capone et al., 2019a]]. A step forward in this direction can be important when dealing with neurons entering depolarization block at high firing rates, a mechanism playing an important role in focal seizures [Meijer et al., 2015] or in dopaminergic neurons under normal condition or under drugs assumption [Dovzhenok and Kuznetsov, 2012, Di Volo et al., 2019b]. In both the ML and HH models, the semianalytic fitting was found to give quite good predictions on the presence of depolarization block, especially in the ML case as this setup does not consider very high spiking frequencies. Even if work remains to be done to extend this framework to obtain a more reliable quantitative prediction on the depolarization block at very high frequencies, these preliminary results indicate the possibility to use these MF techniques to connect the physiology at the cellular scale with pathological states at the population level, as the case of focal seizures.

We also reported that, in the framework of the asynchronous regime here considered, corrections to first order mean field due to second order terms (see Eqs. 3.34 and 3.35) were relatively small but gave a good quantitative indication on the covariance of population rates (see histograms in Fig. 41). Nevertheless, in the case of dynamical regimes with higher neuronal correlation with respect to the ones here considered, we expect the second order mean field (explicitly taking into account the dynamics of covariances) to play an important role in the prediction of population average collective dynamics. The goodness of the MF prediction depends indeed also on the emergent dynamics of the network, i.e., in a highly synchronous dynamical regime the Markovian hypothesis fails and the MF model cannot give accurate predictions. Nevertheless, even if light synchronization is considered, e.g., during slow-wave sleep, the MF models have been shown to correctly predict such collective oscillations [Di Volo et al., 2019b]. In this case it is, however, necessary to consider a MF model that includes the slow dynamics of spike frequency adaptation, e.g., the M current in the case of Hodgkin–Huxley model. The possibility to include a conductance based adaptation to this formalism, e.g., by considering the slow dynamics of M current, is a stimulating perspective for future works and will permit to obtain mean-field models for realistic neuronal models beyond the asynchronous irregular regime.

Moreover, beyond the input-output transfer function used here, a more complex

transfer function has been used to take into account other features of neuron response, e.g., response in frequency [Ostojic and Brunel, 2011]. The addition of variables to account for a richer spiking pattern is an interesting direction, in case one is interested in modeling brain regions characterized by nontonic firing of neurons (e.g., bursting cells in the thalamus). The general framework presented here could be extended in this direction, as it has been done to account for spike frequency adaptation yielding slow oscillations at the population scale [Di Volo et al., 2019b]. Another possible extension is to apply the same formalism to complex neuronal models that include dendrites. A first attempt has been made in this direction [Zerlaut and Destexhe, 2017] by considering simple "ball and stick" neuron models, where some analytic approximation is possible. In principle, it should be possible to apply this approach to models based on morphologically reconstructed neurons and to calculate the transfer function of such models. This will lead to mean-field models based on morphologically realistic neuronal models. However, the presence of dendritic voltage-dependent currents complicates this approach and should be integrated in the formalism. This suggests an exciting future development of our approach.

Finally, the positive results obtained here for complex models, by showing the generality of our approach, motivate the future step of the application of this technique directly to experimental data. To this end, neurons must be recorded intracellularly in the absence of network activity (as typically *in vitro*), and many combinations of excitatory and inhibitory inputs must be injected as conductances (using the dynamic-clamp technique). The first attempt of this sort was realized on the layer 5 neurons from mouse primary visual cortex [Zerlaut et al., 2016], where the transfer function could be reconstructed for a few dozen neurons. The same dynamic-clamp experiments should be done in the future to characterize the transfer function of inhibitory interneurons. Based on such experiments, it will be possible to obtain a mean-field model based on the properties of real neurons. Such a model will evidently be more realistic than the models we have presented here, which must be considered as a first step toward a quantitative population modeling of cerebral cortex and other brain regions.

Chapter 6

Conclusions

1. Computational models accompanied by experimental data are a powerful tool to obtain mechanistic insights of network dynamics.

2. Departing from a biophysical-detailed model, this thesis has allowed for its modification in terms of newly incorporated ionic channels and more realistic topology. Thus, allowing for a more detailed exploration of cortical activity mechanisms.

3. SK calcium-activated potassium channel (KCa), during slow oscillations, acts as a control for hyperexcitability controlling the neuronal firing rate during Up states. Also, KCa regulates the recruitment of the local network, where its blockage results in steeper transition from Down to Up states and faster wave propagation, thus reflecting its role on neuronal synchronization.

4. Ionic currents present within only a fraction of neurons are able to modulate the collective behaviour. Due to the network recurrent connectivity neurons with and without the specific ionic currents are indistinguishable at both their extracellular and intracellular spontaneous activity.

5. The sodium-dependent potassium channel (KNa) is crucial to the maintenance of slow oscillations in the cortical network model due to its slow time course with a duration in the range of that of the Down states.

6. The off-periods or Down states caused by potassium currents (KCa and KNa) share properties with those described in the brain of unresponsive wakefulness syndrome patients that have been found to disrupt causality and complexity.

7. M-current has an important role on the generation of rhythmic slow oscillatory activity. It controls the Up state termination and the network synchronization. Its blockage results in larger Up states and more excitable Up and Down states.

Our results suggest that the cholinergic blockade of this current is a relevant mechanism in the transition towards wakefulness.

8. H-current has an important role on the frequency of emergent cortical slow oscillations. Its blockage induce larger Up and Down states. In the cortical network model, H-current blockage increase duration of Up and Down states and reduces the neuronal firing rate.

9. Fast ($GABA_A$) and slow ($GABA_B$) synaptic inhibition are both required for spatiotemporal cortical complexity. The reduction of gabergic inhibitions results in a reduced cortical complexity.

10. Fast ($GABA_A$) synaptic inhibition is necessary for the balance between neuronal segregation and integration in the cortical network model.

11. A two-dimensional computational model is able to reproduce the experimental observations during the study of perturbational complexity. Perturbation and spontaneous estimation of cortical complexity revealed that complexity is maximized when there is a balance between excitation and inhibition.

12. From a master equation formalism, mean-field models can be derived from different complex neuronal models being able to describe its temporal dynamics.

Bibliography

[Adams et al., 1982] Adams, P. R., Brown, D., and Constanti, A. (1982). Pharmacological inhibition of the m-current. *The Journal of Physiology*, 332(1):223–262. Cited on page 103.

[Alkire et al., 2008] Alkire, M. T., Hudetz, A. G., and Tononi, G. (2008). Consciousness and anesthesia. *Science*, 322(5903):876–880. Cited on page 19.

[Amit and Brunel, 1997] Amit, D. J. and Brunel, N. (1997). Model of global spontaneous activity and local structured activity during delay periods in the cerebral cortex. *Cerebral cortex (New York, NY: 1991)*, 7(3):237–252. Cited on page 24.

[Arena et al., 2021] Arena, A., Comolatti, R., Thon, S., Casali, A. G., and Storm, J. F. (2021). General anesthesia disrupts complex cortical dynamics in response to intracranial electrical stimulation in rats. *eneuro*, 8(4). Cited on page 19.

[Artinian et al., 2011] Artinian, J., Peret, A., Marti, G., Epsztein, J., and Crépel, V. (2011). Synaptic kainate receptors in interplay with inap shift the sparse firing of dentate granule cells to a sustained rhythmic mode in temporal lobe epilepsy. *Journal of Neuroscience*, 31(30):10811–10818. Cited on page 83.

[Barbero-Castillo et al., 2021] Barbero-Castillo, A., Mateos-Aparicio, P., DALLA PORTA, L., Camassa, A., Perez-Mendez, L., and Sanchez-Vives, M. V. (2021). Impact of gabaa and gabab inhibition on cortical dynamics and perturbational complexity during synchronous and desynchronized states. *Journal of Neuroscience*, 41(23):5029–5044. Cited 5 times on page 9, 15, 66, 79, and 86.

[Barbero-Castillo et al., 2019] Barbero-Castillo, A., Weinert, J. F., Camassa, A., Perez-Mendez, L., Caldas-Martinez, S., Mattia, M., and Sanchez-Vives, M. V. (2019). Proceedings# 31: cortical network complexity under different levels of excitability controlled by electric fields. *Brain Stimulation: Basic, Translational, and Clinical Research in Neuromodulation*, 12(2):e97–e99. Cited 2 times on page 19 and 108.

[Bazhenov et al., 2008] Bazhenov, M., Rulkov, N. F., and Timofeev, I. (2008). Effect of synaptic connectivity on long-range synchronization of fast cortical oscillations. *Journal of neurophysiology*, 100(3):1562–1575. Cited on page 33.

[Bazhenov et al., 2002] Bazhenov, M., Timofeev, I., Steriade, M., and Sejnowski, T. J. (2002). Model of thalamocortical slow-wave sleep oscillations and transitions to activated states. *Journal of neuroscience*, 22(19):8691–8704. Cited 3 times on page 24, 86, and 88.

[Benita et al., 2012] Benita, J. M., Guillamon, A., Deco, G., and Sanchez-Vives, M. V. (2012). Synaptic depression and slow oscillatory activity in a biophysical network model of the cerebral cortex. *Frontiers in computational neuroscience*, 6:64. Cited on page 18.

[Berger, 1938] Berger, H. (1938). Über das elektrenkephalogramm des menschen. xiv. *Archiv für Psychiatrie und Nervenkrankheiten*. Cited on page 14.

[Betzel and Bassett, 2017] Betzel, R. F. and Bassett, D. S. (2017). Multi-scale brain networks. *Neuroimage*, 160:73–83. Cited on page 21.

[Bhattacharjee and Kaczmarek, 2005] Bhattacharjee, A. and Kaczmarek, L. K. (2005). For k+ channels, na+ is the new ca2+. *Trends in neurosciences*, 28(8):422–428. Cited on page 58.

[Bierbower et al., 2015] Bierbower, S. M., Choveau, F. S., Lechleiter, J. D., and Shapiro, M. S. (2015). Augmentation of m-type (kcnq) potassium channels as a novel strategy to reduce stroke-induced brain injury. *Journal of Neuroscience*, 35(5):2101–2111. Cited on page 102.

[Breton and Stuart, 2012] Breton, J.-D. and Stuart, G. J. (2012). Somatic and dendritic gabab receptors regulate neuronal excitability via different mechanisms. *Journal of neurophysiology*, 108(10):2810–2818. Cited on page 109.

[Brette and Gerstner, 2005] Brette, R. and Gerstner, W. (2005). Adaptive exponential integrate-and-fire model as an effective description of neuronal activity. *Journal of neurophysiology*, 94(5):3637–3642. Cited 2 times on page 23 and 36.

[Brown and Adams, 1980] Brown, D. and Adams, P. (1980). Muscarinic suppression of a novel voltage-sensitive k+ current in a vertebrate neurone. *Nature*, 283(5748):673–676. Cited 2 times on page 102 and 104.

[Brown, 2010] Brown, D. A. (2010). Muscarinic acetylcholine receptors (machrs) in the nervous system: some functions and mechanisms. *Journal of molecular neuroscience*, 41(3):340–346. Cited 2 times on page 18 and 66.

[Brown et al., 2012] Brown, R. E., Basheer, R., McKenna, J. T., Strecker, R. E., and McCarley, R. W. (2012). Control of sleep and wakefulness. *Physiological reviews*. Cited on page 15.

[Brumberg et al., 2000] Brumberg, J. C., Nowak, L. G., and McCormick, D. A. (2000). Ionic mechanisms underlying repetitive high-frequency burst firing in supragranular cortical neurons. *Journal of Neuroscience*, 20(13):4829–4843. Cited on page 80.

[Buice et al., 2010] Buice, M. A., Cowan, J. D., and Chow, C. C. (2010). Systematic fluctuation expansion for neural network activity equations. *Neural computation*, 22(2):377–426. Cited on page 39.

[Butz et al., 2004] Butz, M., Gross, J., Timmermann, L., Moll, M., Freund, H.-J., Witte, O. W., and Schnitzler, A. (2004). Perilesional pathological oscillatory activity in the magnetoencephalogram of patients with cortical brain lesions. *Neuroscience letters*, 355(1-2):93–96. Cited on page 15.

[Buzsaki, 2006] Buzsaki, G. (2006). *Rhythms of the Brain*. Oxford university press. Cited on page 14.

[Buzsaki and Draguhn, 2004] Buzsaki, G. and Draguhn, A. (2004). Neuronal oscillations in cortical networks. *science*, 304(5679):1926–1929. Cited on page 14.

[Buzsáki et al., 2013] Buzsáki, G., Logothetis, N., and Singer, W. (2013). Scaling brain size, keeping timing: evolutionary preservation of brain rhythms. *Neuron*, 80(3):751–764. Cited on page 14.

[Camassa et al., 2021a] Camassa, A., Galluzzi, A., Mattia, M., and Sanchez-Vives, M. V. (2021a). Metastability of Down states in the cerebral cortex: dynamics and modulation. *Zenodo*. Cited 2 times on page 18 and 19.

[Camassa et al., 2021b] Camassa, A., Mattia, M., and Sanchez-Vives, M. V. (2021b). Energy-based hierarchical clustering of cortical slow waves in multi-electrode recordings. In *2021 43rd Annual International Conference of the IEEE Engineering in Medicine Biology Society (EMBC)*, pages 198–203. Cited 2 times on page 91 and 110.

[Capone et al., 2019a] Capone, C., Di Volo, M., Romagnoni, A., Mattia, M., and Destexhe, A. (2019a). State-dependent mean-field formalism to model different activity states in conductance-based networks of spiking neurons. *Physical Review E*, 100(6):062413. Cited on page 111.

[Capone et al., 2019b] Capone, C., Rebollo, B., Muñoz, A., Illa, X., Del Giudice, P., Sanchez-Vives, M. V., and Mattia, M. (2019b). Slow waves in cortical slices: how spontaneous activity is shaped by laminar structure. *Cerebral cortex*, 29(1):319–335. Cited on page 24.

[Carlu et al., 2020] Carlu, M., Chehab, O., Dalla Porta, L., Depannemaecker, D., Héricé, C., Jedynak, M., Köksal Ersöz, E., Muratore, P., Souihel, S., Capone, C., et al. (2020).

A mean-field approach to the dynamics of networks of complex neurons, from nonlinear integrate-and-fire to hodgkin–huxley models. *Journal of Neurophysiology*, 123(3):1042–1051. Cited 2 times on page 9 and 92.

[Casali et al., 2013] Casali, A. G., Gosseries, O., Rosanova, M., Boly, M., Sarasso, S., Casali, K. R., Casarotto, S., Bruno, M.-A., Laureys, S., Tononi, G., et al. (2013). A theoretically based index of consciousness independent of sensory processing and behavior. *Science translational medicine*, 5(198):198ra105–198ra105. Cited 7 times on page 19, 20, 45, 78, 80, 106, and 107.

[Casarotto et al., 2016] Casarotto, S., Comanducci, A., Rosanova, M., Sarasso, S., Fecchio, M., Napolitani, M., Pigorini, A., G. Casali, A., Trimarchi, P. D., Boly, M., et al. (2016). Stratification of unresponsive patients by an independently validated index of brain complexity. *Annals of neurology*, 80(5):718–729. Cited 3 times on page 19, 106, and 107.

[Castle et al., 1989] Castle, N., Haylett, D., and Jenkinson, D. (1989). Toxins in the characterization of potassium channels. *Trends in neurosciences*, 12(2):59–65. Cited on page 47.

[Catterall et al., 2012] Catterall, W. A., Raman, I. M., Robinson, H. P., Sejnowski, T. J., and Paulsen, O. (2012). The hodgkin-huxley heritage: from channels to circuits. *Journal of Neuroscience*, 32(41):14064–14073. Cited on page 22.

[Chauvette et al., 2011] Chauvette, S., Crochet, S., Volgushev, M., and Timofeev, I. (2011). Properties of slow oscillation during slow-wave sleep and anesthesia in cats. *Journal of Neuroscience*, 31(42):14998–15008. Cited on page 15.

[Chauvette et al., 2010] Chauvette, S., Volgushev, M., and Timofeev, I. (2010). Origin of active states in local neocortical networks during slow sleep oscillation. *Cerebral cortex*, 20(11):2660–2674. Cited on page 16.

[Chemla et al., 2019] Chemla, S., Reynaud, A., Di Volo, M., Zerlaut, Y., Perrinet, L., Destexhe, A., and Chavane, F. (2019). Suppressive traveling waves shape representations of illusory motion in primary visual cortex of awake primate. *Journal of Neuroscience*, 39(22):4282–4298. Cited on page 24.

[Comolatti et al., 2019] Comolatti, R., Pigorini, A., Casarotto, S., Fecchio, M., Faria, G., Sarasso, S., Rosanova, M., Gosseries, O., Boly, M., Bodart, O., et al. (2019). A fast and general method to empirically estimate the complexity of brain responses to transcranial and intracranial stimulations. *Brain stimulation*, 12(5):1280–1289. Cited on page 19.

[Compte et al., 2008] Compte, A., Reig, R., Descalzo, V. F., Harvey, M. A., Puccini, G. D., and Sanchez-Vives, M. V. (2008). Spontaneous high-frequency (10 – 80hz)

oscillations during up states in the cerebral cortex in vitro. *Journal of Neuroscience*, 28(51):13828–13844. Cited 5 times on page 25, 49, 69, 99, and 109.

[Compte et al., 2009] Compte, A., Reig, R., and Sanchez-Vives, M. V. (2009). Timing excitation and inhibition in the cortical network. In *Coherent Behavior in Neuronal Networks*, pages 17–46. Springer. Cited 4 times on page 16, 26, 51, and 76.

[Compte et al., 2003] Compte, A., Sanchez-Vives, M. V., McCormick, D. A., and Wang, X.-J. (2003). Cellular and network mechanisms of slow oscillatory activity (< 1Hz) and wave propagations in a cortical network model. *Journal of neurophysiology*, 89(5):2707–2725. Cited 19 times on page 16, 18, 24, 25, 27, 28, 31, 32, 49, 56, 58, 69, 74, 76, 86, 99, 101, 103, and 109.

[Constantinople and Bruno, 2011] Constantinople, C. M. and Bruno, R. M. (2011). Effects and mechanisms of wakefulness on local cortical networks. *Neuron*, 69(6):1061–1068. Cited on page 104.

[Contreras et al., 1996] Contreras, D., Timofeev, I., and Steriade, M. (1996). Mechanisms of long-lasting hyperpolarizations underlying slow sleep oscillations in cat corticothalamic networks. *The Journal of physiology*, 494(1):251–264. Cited 2 times on page 16 and 18.

[Dalla Porta et al., 2021] Dalla Porta, L., Castro, D. M., Copelli, M., Carelli, P. V., and Matias, F. S. (2021). Feedforward and feedback influences through distinct frequency bands between two spiking-neuron networks. *Physical Review E*, 104(5):054404. Cited 2 times on page 10 and 23.

[DALLA PORTA and Copelli, 2019] DALLA PORTA, L. and Copelli, M. (2019). Modeling neuronal avalanches and long-range temporal correlations at the emergence of collective oscillations: Continuously varying exponents mimic M/EEG results. *PLOS Computational Biology*, 15(4):1–26. Cited on page 33.

[Dalla Porta et al., 2019] Dalla Porta, L., Matias, F. S., Dos Santos, A. J., Alonso, A., Carelli, P. V., Copelli, M., and Mirasso, C. R. (2019). Exploring the phase-locking mechanisms yielding delayed and anticipated synchronization in neuronal circuits. *Frontiers in systems neuroscience*, page 41. Cited on page 9.

[DALLA PORTA and Sanchez-Vives, 2021] DALLA PORTA, L. and Sanchez-Vives, M. V. (2021). Fast and slow inhibition on cortical spatiotemporal complexity in a computational model of the cerebral cortex. In *JOURNAL OF COMPUTATIONAL NEUROSCIENCE*, volume 49, pages S166–S167. SPRINGER VAN GODEWIJCKSTRAAT 30, 3311 GZ DORDRECHT, NETHERLANDS. Cited 2 times on page 9 and 80.

[D'Andola et al., 2018] D'Andola, M., Rebollo, B., Casali, A. G., Weinert, J. F., Pigorini, A., Villa, R., Massimini, M., and Sanchez-Vives, M. V. (2018). Bistability, causality, and complexity in cortical networks: an in vitro perturbational study. *Cerebral Cortex*, 28(7):2233–2242. Cited 8 times on page 20, 21, 45, 46, 80, 82, 107, and 108.

[Dasilva et al., 2021a] Dasilva, M., Camassa, A., Navarro-Guzman, A., Pazienti, A., Perez-Mendez, L., Zamora-López, G., Mattia, M., and Sanchez-Vives, M. V. (2021a). Modulation of cortical slow oscillations and complexity across anesthesia levels. *Neuroimage*, 224:117415. Cited on page 19.

[Dasilva et al., 2021b] Dasilva, M., Camassa, A., Navarro-Guzman, A., Pazienti, A., Perez-Mendez, L., Zamora-López, G., Mattia, M., and Sanchez-Vives, M. V. (2021b). Modulation of cortical slow oscillations and complexity across anesthesia levels. *Neuroimage*, 224:117415. Cited 3 times on page 19, 80, and 107.

[Dayan and Abbott, 2001] Dayan, P. and Abbott, L. F. (2001). *Theoretical Neuroscience: Computational and Mathematical Modeling of Neural Systems*. The MIT Press. Cited on page 34.

[Deco et al., 2009] Deco, G., Martí, D., Ledberg, A., Reig, R., and Sanchez Vives, M. V. (2009). Effective reduced diffusion-models: a data driven approach to the analysis of neuronal dynamics. *PLoS computational biology*, 5(12):e1000587. Cited on page 104.

[Destexhe, 2009] Destexhe, A. (2009). Self-sustained asynchronous irregular states and up–down states in thalamic, cortical and thalamocortical networks of nonlinear integrate-and-fire neurons. *Journal of computational neuroscience*, 27(3):493–506. Cited on page 45.

[Destexhe et al., 1996] Destexhe, A., Bal, T., McCormick, D. A., and Sejnowski, T. J. (1996). Ionic mechanisms underlying synchronized oscillations and propagating waves in a model of ferret thalamic slices. *Journal of neurophysiology*, 76(3):2049–2070. Cited 2 times on page 31 and 32.

[Destexhe et al., 2003] Destexhe, A., Rudolph, M., and Paré, D. (2003). The high-conductance state of neocortical neurons in vivo. *Nature reviews neuroscience*, 4(9):739–751. Cited on page 38.

[Di Santo et al., 2018] Di Santo, S., Villegas, P., Burioni, R., and Muñoz, M. A. (2018). Landau–ginzburg theory of cortex dynamics: Scale-free avalanches emerge at the edge of synchronization. *Proceedings of the National Academy of Sciences*, 115(7):E1356–E1365. Cited on page 44.

[Di Volo et al., 2019a] Di Volo, M., Morozova, E. O., Lapish, C. C., Kuznetsov, A., and Gutkin, B. (2019a). Dynamical ventral tegmental area circuit mechanisms of alcohol-dependent dopamine release. *European Journal of Neuroscience*, 50(3):2282–2296. Cited 2 times on page 96 and 110.

[Di Volo et al., 2019b] Di Volo, M., Romagnoni, A., Capone, C., and Destexhe, A. (2019b). Biologically realistic mean-field models of conductance-based networks of spiking neurons with adaptation. *Neural computation*, 31(4):653–680. Cited 3 times on page 110, 111, and 112.

[Doron et al., 2017] Doron, M., Chindemi, G., Muller, E., Markram, H., and Segev, I. (2017). Timed synaptic inhibition shapes nmda spikes, influencing local dendritic processing and global i/o properties of cortical neurons. *Cell reports*, 21(6):1550–1561. Cited on page 109.

[Dovzhenok and Kuznetsov, 2012] Dovzhenok, A. and Kuznetsov, A. S. (2012). Exploring neuronal bistability at the depolarization block. *PLOS ONE*, 7(8):1–12. Cited on page 111.

[El Boustani and Destexhe, 2009] El Boustani, S. and Destexhe, A. (2009). A master equation formalism for macroscopic modeling of asynchronous irregular activity states. *Neural computation*, 21(1):46–100. Cited 6 times on page 24, 38, 39, 92, 93, and 110.

[Estarellas et al., 2020] Estarellas, C., Masoliver, M., Masoller, C., and Mirasso, C. R. (2020). Characterizing signal encoding and transmission in class i and class ii neurons via ordinal time-series analysis. *Chaos: An Interdisciplinary Journal of Nonlinear Science*, 30(1):013123. Cited on page 22.

[Fontenele et al., 2019] Fontenele, A. J., de Vasconcelos, N. A., Feliciano, T., Aguiar, L. A., Soares-Cunha, C., Coimbra, B., Dalla Porta, L., Ribeiro, S., Rodrigues, A. J., Sousa, N., et al. (2019). Criticality between cortical states. *Physical review letters*, 122(20):208101. Cited on page 45.

[Fröhlich and McCormick, 2010] Fröhlich, F. and McCormick, D. A. (2010). Endogenous electric fields may guide neocortical network activity. *Neuron*, 67(1):129–143. Cited on page 24.

[Gerstner et al., 2014] Gerstner, W., Kistler, W. M., Naud, R., and Paninski, L. (2014). *Neuronal dynamics: From single neurons to networks and models of cognition*. Cambridge University Press. Cited 2 times on page 22 and 23.

[Ginzburg and Sompolinsky, 1994] Ginzburg, I. and Sompolinsky, H. (1994). Theory of correlations in stochastic neural networks. *Physical review E*, 50(4):3171. Cited on page 39.

[Gloor et al., 1977] Gloor, P., Ball, G., and Schaul, N. (1977). Brain lesions that produce delta waves in the eeg. *Neurology*, 27(4):326–326. Cited on page 15.

[Gollo et al., 2014] Gollo, L. L., Mirasso, C., Sporns, O., and Breakspear, M. (2014). Mechanisms of zero-lag synchronization in cortical motifs. *PLoS computational biology*, 10(4):e1003548. Cited on page 23.

[Golomb, 2007] Golomb, D. (2007). Neuronal synchrony measures. *Scholarpedia*, 2(1):1347. revision #128277. Cited 2 times on page 45 and 104.

[Golomb and Rinzel, 1993] Golomb, D. and Rinzel, J. (1993). Dynamics of globally coupled inhibitory neurons with heterogeneity. *Physical review E*, 48(6):4810. Cited on page 45.

[Golomb et al., 2006] Golomb, D., Shedmi, A., Curtu, R., and Ermentrout, G. B. (2006). Persistent synchronized bursting activity in cortical tissues with low magnesium concentration: a modeling study. *Journal of neurophysiology*, 95(2):1049–1067. Cited 3 times on page 45, 55, and 71.

[Górski et al., 2021] Górski, T., Depannemaecker, D., and Destexhe, A. (2021). Conductance-based adaptive exponential integrate-and-fire model. *Neural Computation*, 33(1):41–66. Cited on page 23.

[Halasz et al., 1979] Halasz, P., Kundra, O., Rajna, P., Pal, I., and Vargha, M. (1979). Micro-arousals during nocturnal sleep. *Acta physiologica Academiae Scientiarum Hungaricae*, 54(1):1–12. Cited on page 103.

[Hansel and Sompolinsky, 1992] Hansel, D. and Sompolinsky, H. (1992). Synchronization and computation in a chaotic neural network. *Physical Review Letters*, 68(5):718. Cited on page 45.

[Harris et al., 2020] Harris, C. R., Millman, K. J., van der Walt, S. J., Gommers, R., Virtanen, P., Cournapeau, D., Wieser, E., Taylor, J., Berg, S., Smith, N. J., Kern, R., Picus, M., Hoyer, S., van Kerkwijk, M. H., Brett, M., Haldane, A., del Río, J. F., Wiebe, M., Peterson, P., Gérard-Marchant, P., Sheppard, K., Reddy, T., Weckesser, W., Abbasi, H., Gohlke, C., and Oliphant, T. E. (2020). Array programming with NumPy. *Nature*, 585(7825):357–362. Cited on page 45.

[Helmchen et al., 1996] Helmchen, F., Imoto, K., and Sakmann, B. (1996). Ca2+ buffering and action potential-evoked ca2+ signaling in dendrites of pyramidal neurons. *Biophysical journal*, 70(2):1069–1081. Cited on page 56.

[Hendry et al., 1987] Hendry, S. H., Schwark, H., Jones, E., and Yan, J. (1987). Numbers and proportions of gaba-immunoreactive neurons in different areas of monkey cerebral cortex. *Journal of Neuroscience*, 7(5):1503–1519. Cited on page 32.

[Hill and Tononi, 2005] Hill, S. and Tononi, G. (2005). Modeling sleep and wakefulness in the thalamocortical system. *Journal of neurophysiology*, 93(3):1671–1698. Cited 6 times on page 19, 24, 33, 76, 101, and 106.

[Hodgkin and Huxley, 1952] Hodgkin, A. L. and Huxley, A. F. (1952). A quantitative description of membrane current and its application to conduction and excitation in nerve. *The Journal of physiology*, 117(4):500–544. Cited 5 times on page 21, 23, 28, 37, and 109.

[Holcman and Tsodyks, 2006] Holcman, D. and Tsodyks, M. (2006). The emergence of up and down states in cortical networks. *PLoS computational biology*, 2(3):e23. Cited 2 times on page 18 and 101.

[Hopfield, 1984] Hopfield, J. J. (1984). Neurons with graded response have collective computational properties like those of two-state neurons. *Proceedings of the national academy of sciences*, 81(10):3088–3092. Cited on page 24.

[Hu et al., 2007] Hu, H., Vervaeke, K., and Storm, J. F. (2007). M-channels (kv7/kcnq channels) that regulate synaptic integration, excitability, and spike pattern of ca1 pyramidal cells are located in the perisomatic region. *Journal of Neuroscience*, 27(8):1853–1867. Cited on page 103.

[Hudetz, 2012] Hudetz, A. G. (2012). General anesthesia and human brain connectivity. *Brain connectivity*, 2(6):291–302. Cited on page 106.

[Hudetz et al., 2016] Hudetz, A. G., Liu, X., Pillay, S., Boly, M., and Tononi, G. (2016). Propofol anesthesia reduces lempel-ziv complexity of spontaneous brain activity in rats. *Neuroscience letters*, 628:132–135. Cited on page 19.

[Hughes et al., 1999] Hughes, S. W., Cope, D. W., Tóth, T. I., Williams, S. R., and Crunelli, V. (1999). All thalamocortical neurones possess a t-type ca2+ 'window'current that enables the expression of bistability-mediated activities. *The Journal of physiology*, 517(3):805–815. Cited on page 73.

[Izhikevich, 2003] Izhikevich, E. M. (2003). Simple model of spiking neurons. *IEEE Transactions on neural networks*, 14(6):1569–1572. Cited on page 23.

[J. Trevelyan and Jack, 2002] J. Trevelyan, A. and Jack, J. (2002). Detailed passive cable models of layer 2/3 pyramidal cells in rat visual cortex at different temperatures. *The Journal of physiology*, 539(2):623–636. Cited on page 107.

[Jentsch, 2000] Jentsch, T. J. (2000). Neuronal kcnq potassium channels: physislogy and role in disease. *Nature Reviews Neuroscience*, 1(1):21–30. Cited on page 102.

[Jercog et al., 2017] Jercog, D., Roxin, A., Bartho, P., Luczak, A., Compte, A., and de la Rocha, J. (2017). Up-down cortical dynamics reflect state transitions in a bistable network. *Elife*, 6:e22425. Cited on page 24.

[Jones, 2005] Jones, B. E. (2005). From waking to sleeping: neuronal and chemical substrates. *Trends in pharmacological sciences*, 26(11):578–586. Cited 2 times on page 17 and 80.

[Kim and Nykamp, 2017] Kim, C. M. and Nykamp, D. Q. (2017). The influence of depolarization block on seizure-like activity in networks of excitatory and inhibitory neurons. *Journal of computational neuroscience*, 43(1):65–79. Cited on page 94.

[Koch et al., 2016] Koch, C., Massimini, M., Boly, M., and Tononi, G. (2016). Neural correlates of consciousness: progress and problems. *Nature Reviews Neuroscience*, 17(5):307–321. Cited on page 16.

[Koch and Segev, 1998] Koch, C. and Segev, I. (1998). *Methods in neuronal modeling: from ions to networks*. MIT press. Cited on page 22.

[Larkum et al., 1999] Larkum, M. E., Zhu, J. J., and Sakmann, B. (1999). A new cellular mechanism for coupling inputs arriving at different cortical layers. *Nature*, 398(6725):338–341. Cited on page 109.

[Lehnertz and Elger, 1995] Lehnertz, K. and Elger, C. (1995). Spatio-temporal dynamics of the primary epileptogenic area in temporal lobe epilepsy characterized by neuronal complexity loss. *Electroencephalography and clinical Neurophysiology*, 95(2):108–117. Cited on page 83.

[Li et al., 2017] Li, G., Henriquez, C. S., and Fröhlich, F. (2017). Unified thalamic model generates multiple distinct oscillations with state-dependent entrainment by stimulation. *PLoS computational biology*, 13(10):e1005797. Cited 2 times on page 86 and 88.

[Liu et al., 2019] Liu, Y., Milton, J., and Campbell, S. A. (2019). Outgrowing seizures in childhood absence epilepsy: time delays and bistability. *Journal of Computational Neuroscience*, 46(2):197–209. Cited on page 31.

[Lord et al., 2017] Lord, L.-D., Stevner, A. B., Deco, G., and Kringelbach, M. L. (2017). Understanding principles of integration and segregation using whole-brain computational connectomics: implications for neuropsychiatric disorders. *Philosophical Transactions of the Royal Society A: Mathematical, Physical and Engineering Sciences*, 375(2096):20160283. Cited on page 89.

[Lorente de No, 1938] Lorente de No, R. (1938). Cerebral cortex: architecture, intracortical connections, motor projections. *Physiology of the nervous system*, pages 288–313. Cited on page 16.

[Lüthi and McCormick, 1998a] Lüthi, A. and McCormick, D. A. (1998a). H-current: properties of a neuronal and network pacemaker. *Neuron*, 21(1):9–12. Cited 2 times on page 74 and 105.

[Lüthi and McCormick, 1998b] Lüthi, A. and McCormick, D. A. (1998b). Periodicity of thalamic synchronized oscillations: the role of ca2+-mediated upregulation of ih. *Neuron*, 20(3):553–563. Cited 3 times on page 19, 73, and 105.

[Lüthi and McCormick, 1999] Lüthi, A. and McCormick, D. A. (1999). Modulation of a pacemaker current through ca2+-induced stimulation of camp production. *Nature neuroscience*, 2(7):634–641. Cited 3 times on page 19, 73, and 105.

[Mann et al., 2009] Mann, E. O., Kohl, M. M., and Paulsen, O. (2009). Distinct roles of gabaa and gabab receptors in balancing and terminating persistent cortical activity. *Journal of Neuroscience*, 29(23):7513–7518. Cited 6 times on page 16, 18, 51, 86, 108, and 109.

[Mao et al., 2001] Mao, B.-Q., Hamzei-Sichani, F., Aronov, D., Froemke, R. C., and Yuste, R. (2001). Dynamics of spontaneous activity in neocortical slices. *Neuron*, 32(5):883–898. Cited on page 105.

[Markram et al., 1995] Markram, H., Helm, P. J., and Sakmann, B. (1995). Dendritic calcium transients evoked by single back-propagating action potentials in rat neocortical pyramidal neurons. *The Journal of physiology*, 485(1):1–20. Cited on page 56.

[Markram et al., 2015] Markram, H., Muller, E., Ramaswamy, S., Reimann, M. W., Abdellah, M., Sanchez, C. A., Ailamaki, A., Alonso-Nanclares, L., Antille, N., Arsever, S., et al. (2015). Reconstruction and simulation of neocortical microcircuitry. *Cell*, 163(2):456–492. Cited 3 times on page 21, 80, and 107.

[Markram et al., 2004] Markram, H., Toledo-Rodriguez, M., Wang, Y., Gupta, A., Silberberg, G., and Wu, C. (2004). Interneurons of the neocortical inhibitory system. *Nature reviews neuroscience*, 5(10):793–807. Cited on page 32.

[Massimini et al., 2005] Massimini, M., Ferrarelli, F., Huber, R., Esser, S. K., Singh, H., and Tononi, G. (2005). Breakdown of cortical effective connectivity during sleep. *Science*, 309(5744):2228–2232. Cited on page 107.

[Massimini et al., 2004] Massimini, M., Huber, R., Ferrarelli, F., Hill, S., and Tononi, G. (2004). The sleep slow oscillation as a traveling wave. *Journal of Neuroscience*, 24(31):6862–6870. Cited 2 times on page 14 and 19.

[Mattia and Del Giudice, 2002] Mattia, M. and Del Giudice, P. (2002). Population dynamics of interacting spiking neurons. *Physical Review E*, 66(5):051917. Cited on page 43.

[Mattia and Sanchez-Vives, 2012] Mattia, M. and Sanchez-Vives, M. V. (2012). Exploring the spectrum of dynamical regimes and timescales in spontaneous cortical activity. *Cognitive neurodynamics*, 6(3):239–250. Cited 3 times on page 16, 17, and 21.

[McCormick and Prince, 1986] McCormick, D. and Prince, D. (1986). Mechanisms of action of acetylcholine in the guinea-pig cerebral cortex in vitro. *The Journal of physiology*, 375(1):169–194. Cited on page 104.

[McCormick, 1992] McCormick, D. A. (1992). Neurotransmitter actions in the thalamus and cerebral cortex and their role in neuromodulation of thalamocortical activity. *Progress in neurobiology*, 39(4):337–388. Cited 3 times on page 80, 88, and 99.

[McCormick and Huguenard, 1992] McCormick, D. A. and Huguenard, J. R. (1992). A model of the electrophysiological properties of thalamocortical relay neurons. *Journal of neurophysiology*, 68(4):1384–1400. Cited on page 73.

[McCormick and Pape, 1990] McCormick, D. A. and Pape, H.-C. (1990). Properties of a hyperpolarization-activated cation current and its role in rhythmic oscillation in thalamic relay neurones. *The Journal of physiology*, 431(1):291–318. Cited 2 times on page 73 and 105.

[McCormick et al., 1993] McCormick, D. A., Wang, Z., and Huguenard, J. (1993). Neurotransmitter control of neocortical neuronal activity and excitability. *Cerebral cortex*, 3(5):387–398. Cited 3 times on page 33, 69, and 103.

[McCormick and Williamson, 1989] McCormick, D. A. and Williamson, A. (1989). Convergence and divergence of neurotransmitter action in human cerebral cortex. *Proceedings of the National Academy of Sciences*, 86(20):8098–8102. Cited 2 times on page 17 and 99.

[McCormick and Yuste, 2006] McCormick, D. A. and Yuste, R. (2006). *UP states and cortical dynamics*, chapter 16, pages 327–346. MIT Press. Cited 2 times on page 16 and 17.

[Meijer et al., 2015] Meijer, H. G., Eissa, T. L., Kiewiet, B., Neuman, J. F., Schevon, C. A., Emerson, R. G., Goodman, R. R., McKhann, G. M., Marcuccilli, C. J., Tryba, A. K., et al. (2015). Modeling focal epileptic activity in the wilson–cowan model with depolarization block. *The Journal of Mathematical Neuroscience (JMN)*, 5(1):1–17. Cited on page 111.

[Metherate and Ashe, 1993] Metherate, R. and Ashe, J. H. (1993). Ionic flux contributions to neocortical slow waves and nucleus basalis-mediated activation: whole-cell recordings in vivo. *Journal of Neuroscience*, 13(12):5312–5323. Cited on page 16.

[Morris and Lecar, 1981] Morris, C. and Lecar, H. (1981). Voltage oscillations in the barnacle giant muscle fiber. *Biophys. J.*, 35:193–213. Cited 2 times on page 22 and 38.

[Muller and Destexhe, 2012] Muller, L. and Destexhe, A. (2012). Propagating waves in thalamus, cortex and the thalamocortical system: experiments and models. *Journal of Physiology-Paris*, 106(5-6):222–238. Cited on page 23.

[Néda et al., 2000] Néda, Z., Ravasz, E., Brechet, Y., Vicsek, T., and Barabási, A.-L. (2000). The sound of many hands clapping. *Nature*, 403(6772):849–850. Cited on page 14.

[Neske, 2016] Neske, G. T. (2016). The slow oscillation in cortical and thalamic networks: mechanisms and functions. *Frontiers in neural circuits*, 9:88. Cited 7 times on page 18, 58, 74, 99, 101, 102, and 105.

[Ohira and Cowan, 1993] Ohira, T. and Cowan, J. D. (1993). Master-equation approach to stochastic neurodynamics. *Physical Review E*, 48(3):2259. Cited on page 39.

[Ostojic and Brunel, 2011] Ostojic, S. and Brunel, N. (2011). From spiking neuron models to linear-nonlinear models. *PLoS computational biology*, 7(1):e1001056. Cited 2 times on page 110 and 112.

[Palmer et al., 2012] Palmer, L. M., Schulz, J. M., Murphy, S. C., Ledergerber, D., Murayama, M., and Larkum, M. E. (2012). The cellular basis of gabab-mediated interhemispheric inhibition. *Science*, 335(6071):989–993. Cited on page 109.

[Pape, 1996] Pape, H.-C. (1996). Queer current and pacemaker: the hyperpolarization-activated cation current in neurons. *Annual review of physiology*, 58:299–327. Cited on page 105.

[Pape and McCormick, 1989] Pape, H.-C. and McCormick, D. A. (1989). Noradrenaline and serotonin selectively modulate thalamic burst firing by enhancing a hyperpolarization-activated cation current. *Nature*, 340(6236):715–718. Cited on page 106.

[Peña and Alavez-Pérez, 2006] Peña, F. and Alavez-Pérez, N. (2006). Epileptiform activity induced by pharmacologic reduction of m-current in the developing hippocampus in vitro. *Epilepsia*, 47(1):47–54. Cited on page 103.

[Pennefather et al., 1985] Pennefather, P., Lancaster, B., Adams, P. R., and Nicoll, R. A. (1985). Two distinct ca-dependent k currents in bullfrog sympathetic ganglion cells. *Proceedings of the National Academy of Sciences*, 82(9):3040–3044. Cited on page 99.

[Perez-Zabalza et al., 2020] Perez-Zabalza, M., Reig, R., Manrique, J., Jercog, D., Winograd, M., Parga, N., and Sanchez-Vives, M. V. (2020). Modulation of cortical slow oscillatory rhythm by gabab receptors: an in vitro experimental and computational study. *The Journal of physiology*, 598(16):3439–3457. Cited 5 times on page 16, 18, 86, 108, and 109.

[Pigorini et al., 2015] Pigorini, A., Sarasso, S., Proserpio, P., Szymanski, C., Arnulfo, G., Casarotto, S., Fecchio, M., Rosanova, M., Mariotti, M., Russo, G. L., et al. (2015). Bistability breaks-off deterministic responses to intracortical stimulation during non-rem sleep. *Neuroimage*, 112:105–113. Cited 3 times on page 63, 80, and 107.

[Pikovsky et al., 2002] Pikovsky, A., Rosenblum, M., and Kurths, J. (2002). Synchronization: a universal concept in nonlinear science. Cited on page 44.

[Poil et al., 2012] Poil, S.-S., Hardstone, R., Mansvelder, H. D., and Linkenkaer-Hansen, K. (2012). Critical-state dynamics of avalanches and oscillations jointly emerge from balanced excitation/inhibition in neuronal networks. *Journal of Neuroscience*, 32(29):9817–23. Cited on page 33.

[Pospischil et al., 2008] Pospischil, M., Toledo-Rodriguez, M., Monier, C., Piwkowska, Z., Bal, T., Frégnac, Y., Markram, H., and Destexhe, A. (2008). Minimal hodgkin–huxley type models for different classes of cortical and thalamic neurons. *Biological cybernetics*, 99(4):427–441. Cited 2 times on page 22 and 37.

[Pouille and Scanziani, 2004] Pouille, F. and Scanziani, M. (2004). Routing of spike series by dynamic circuits in the hippocampus. *Nature*, 429(6993):717–723. Cited on page 109.

[Radnikow and Feldmeyer, 2018] Radnikow, G. and Feldmeyer, D. (2018). Layer-and cell type-specific modulation of excitatory neuronal activity in the neocortex. *Frontiers in neuroanatomy*, 12:1. Cited on page 66.

[Reig et al., 2010] Reig, R., Mattia, M., Compte, A., Belmonte, C., and Sánchez-Vives, M. V. (2010). Temperature modulation of slow and fast cortical rhythms. *Journal of neurophysiology*, 103(3):1253–1261. Cited 3 times on page 43, 80, and 107.

[Reig et al., 2015] Reig, R., Zerlaut, Y., Vergara, R., Destexhe, A., and Sanchez-Vives, M. V. (2015). Gain modulation of synaptic inputs by network state in auditory cortex in vivo. *Journal of Neuroscience*, 35(6):2689–2702. Cited 2 times on page 15 and 24.

[Renart et al., 2010] Renart, A., De La Rocha, J., Bartho, P., Hollender, L., Parga, N., Reyes, A., and Harris, K. D. (2010). The asynchronous state in cortical circuits. *science*, 327(5965):587–590. Cited on page 45.

[Rinzel and Ermentrout, 1998] Rinzel, J. and Ermentrout, G. B. (1998). Analysis of neural excitability and oscillations. *Methods in neuronal modeling*, 2:251–292. Cited on page 22.

[Robinson and Siegelbaum, 2003] Robinson, R. B. and Siegelbaum, S. A. (2003). Hyperpolarization-activated cation currents: from molecules to physiological function. *Annual review of physiology*, 65(1):453–480. Cited on page 33.

[Rosanova et al., 2018] Rosanova, M., Fecchio, M., Casarotto, S., Sarasso, S., Casali, A., Pigorini, A., Comanducci, A., Seregni, F., Devalle, G., Citerio, G., et al. (2018). Sleep-like cortical off-periods disrupt causality and complexity in the brain of unresponsive wakefulness syndrome patients. *Nature communications*, 9(1):1–10. Cited 6 times on page 19, 63, 80, 102, 106, and 107.

[Russo et al., 2021] Russo, S., Pigorini, A., Mikulan, E., Sarasso, S., Rubino, A., Zauli, F. M., Parmigiani, S., d'Orio, P., Cattani, A., Francione, S., et al. (2021). Focal lesions induce large-scale percolation of sleep-like intracerebral activity in awake humans. *NeuroImage*, 234:117964. Cited on page 15.

[Sah and Faber, 2002] Sah, P. and Faber, E. L. (2002). Channels underlying neuronal calcium-activated potassium currents. *Progress in neurobiology*, 66(5):345–353. Cited 2 times on page 47 and 100.

[Sanchez-Vives and Compte, 2005] Sanchez-Vives, M. and Compte, A. (2005). Structural statistical properties of the connectivity could underlie the difference in activity propagation velocities in visual and olfactory cortices. In *International Work-Conference on the Interplay Between Natural and Artificial Computation*, pages 133–142. Springer. Cited on page 26.

[Sanchez-Vives and Mattia, 2014] Sanchez-Vives, M. and Mattia, M. (2014). Slow wave activity as the default mode of the cerebral cortex. *Arch. Ital. Biol*, 152(2-3):147–155. Cited 3 times on page 15, 98, and 102.

[Sanchez-Vives, 2012] Sanchez-Vives, M. V. (2012). Spontaneous rhythmic activity in the adult cerebral cortex in vitro. In *Isolated central nervous system circuits*, pages 263–284. Springer. Cited on page 51.

[Sanchez-Vives et al., 2021] Sanchez-Vives, M. V., Barbero-Castillo, A., Perez-Zabalza, M., and Reig, R. (2021). Gabab receptors: modulation of thalamocortical dynamics and synaptic plasticity. *Neuroscience*, 456:131–142. Cited 4 times on page 16, 18, 86, and 108.

[Sanchez-Vives et al., 2017] Sanchez-Vives, M. V., Massimini, M., and Mattia, M. (2017). Shaping the default activity pattern of the cortical network. *Neuron*, 94(5):993–1001. Cited 3 times on page 15, 17, and 102.

[Sanchez-Vives et al., 2010] Sanchez-Vives, M. V., Mattia, M., Compte, A., Perez-Zabalza, M., Winograd, M., Descalzo, V. F., and Reig, R. (2010). Inhibitory modulation of cortical up states. *Journal of neurophysiology*, 104(3):1314–1324. Cited 12 times on page 16, 18, 25, 43, 56, 69, 76, 82, 84, 100, 107, and 109.

[Sanchez-Vives and McCormick, 2000] Sanchez-Vives, M. V. and McCormick, D. A. (2000). Cellular and network mechanisms of rhythmic recurrent activity in neocortex. *Nature neuroscience*, 3(10):1027–1034. Cited 14 times on page 15, 16, 17, 21, 24, 41, 51, 56, 58, 71, 78, 80, 101, and 102.

[Sancristóbal et al., 2016] Sancristóbal, B., Rebollo, B., Boada, P., Sanchez-Vives, M. V., and Garcia-Ojalvo, J. (2016). Collective stochastic coherence in recurrent neuronal networks. *Nature Physics*, 12(9):881–887. Cited 5 times on page 26, 35, 58, 99, and 109.

[Sarasso et al., 2015] Sarasso, S., Boly, M., Napolitani, M., Gosseries, O., Charland-Verville, V., Casarotto, S., Rosanova, M., Casali, A. G., Brichant, J.-F., Boveroux, P., et al. (2015). Consciousness and complexity during unresponsiveness induced by propofol, xenon, and ketamine. *Current Biology*, 25(23):3099–3105. Cited 3 times on page 19, 106, and 107.

[Sarasso et al., 2020] Sarasso, S., D'Ambrosio, S., Fecchio, M., Casarotto, S., Viganò, A., Landi, C., Mattavelli, G., Gosseries, O., Quarenghi, M., Laureys, S., et al. (2020). Local sleep-like cortical reactivity in the awake brain after focal injury. *Brain*, 143(12):3672–3684. Cited 2 times on page 15 and 102.

[Sarasso et al., 2014] Sarasso, S., Rosanova, M., Casali, A. G., Casarotto, S., Fecchio, M., Boly, M., Gosseries, O., Tononi, G., Laureys, S., and Massimini, M. (2014). Quantifying cortical eeg responses to tms in (un) consciousness. *Clinical EEG and neuroscience*, 45(1):40–49. Cited on page 20.

[Schroeder et al., 1998] Schroeder, B. C., Kubisch, C., Stein, V., and Jentsch, T. J. (1998). Moderate loss of function of cyclic-amp-modulated kcnq2/kcnq3 k+ channels causes epilepsy. *Nature*, 396(6712):687–690. Cited 2 times on page 102 and 103.

[Schwindt et al., 1989] Schwindt, P., Spain, W., and Crill, W. (1989). Long-lasting reduction of excitability by a sodium-dependent potassium current in cat neocortical neurons. *Journal of neurophysiology*, 61(2):233–244. Cited 2 times on page 17 and 102.

[Steriade, 2000] Steriade, M. (2000). Corticothalamic resonance, states of vigilance and mentation. *Neuroscience*, 101(2):243–276. Cited on page 19.

[Steriade et al., 1993a] Steriade, M., Amzica, F., and Nunez, A. (1993a). Cholinergic and noradrenergic modulation of the slow (approximately 0.3 hz) oscillation in neocortical cells. *Journal of neurophysiology*, 70(4):1385–1400. Cited 4 times on page 15, 18, 58, and 80.

[Steriade et al., 1993b] Steriade, M., Nuñez, A., and Amzica, F. (1993b). Intracellular analysis of relations between the slow (< 1 hz) neocortical oscillation and other sleep rhythms of the electroencephalogram. *Journal of Neuroscience*, 13(8):3266–3283. Cited 3 times on page 15, 71, and 78.

[Steriade et al., 1993c] Steriade, M., Nunez, A., and Amzica, F. (1993c). A novel slow (< 1 hz) oscillation of neocortical neurons in vivo: depolarizing and hyperpolarizing components. *Journal of neuroscience*, 13(8):3252–3265. Cited 5 times on page 15, 16, 51, 99, and 103.

[Steriade et al., 2001] Steriade, M., Timofeev, I., and Grenier, F. (2001). Natural waking and sleep states: a view from inside neocortical neurons. *J. Neurophysiol.*, 85:1969–1985. Cited on page 14.

[Stocker et al., 1999] Stocker, M., Krause, M., and Pedarzani, P. (1999). An apamin-sensitive ca2+-activated k+ current in hippocampal pyramidal neurons. *Proceedings of the National Academy of Sciences*, 96(8):4662–4667. Cited on page 99.

[Strogatz and Stewart, 1993] Strogatz, S. H. and Stewart, I. (1993). Coupled oscillators and biological synchronization. *Scientific American*, 269(6):102–109. Cited on page 14.

[Sussillo and Abbott, 2009] Sussillo, D. and Abbott, L. F. (2009). Generating coherent patterns of activity from chaotic neural networks. *Neuron*, 63(4):544–557. Cited on page 24.

[Svoboda et al., 1997] Svoboda, K., Denk, W., Kleinfeld, D., and Tank, D. W. (1997). In vivo dendritic calcium dynamics in neocortical pyramidal neurons. *Nature*, 385(6612):161–165. Cited on page 56.

[Szczepański et al., 2003] Szczepański, J., Amigó, J. M., Wajnryb, E., and Sanchez-Vives, M. (2003). Application of lempel–ziv complexity to the analysis of neural discharges. *Network: Computation in Neural Systems*, 14(2):335. Cited on page 19.

[Tatulian et al., 2001] Tatulian, L., Delmas, P., Abogadie, F., and Brown, D. (2001). Activation of expressed kcnq potassium currents and native neuronal m-type potassium currents by the anti-convulsant drug retigabine. *Journal of Neuroscience*, 21(15):5535–5545. Cited on page 102.

[Taxidis et al., 2013] Taxidis, J., Mizuseki, K., Mason, R., and Owen, M. R. (2013). Influence of slow oscillation on hippocampal activity and ripples through cortico-hippocampal synaptic interactions, analyzed by a cortical-ca3-ca1 network model. *Frontiers in computational neuroscience*, 7:3. Cited on page 24.

[Timofeev et al., 2000] Timofeev, I., Grenier, F., Bazhenov, M., Sejnowski, T., and Steriade, M. (2000). Origin of slow cortical oscillations in deafferented cortical slabs. *Cerebral cortex*, 10(12):1185–1199. Cited 4 times on page 15, 19, 51, and 102.

[Timofeev et al., 2001] Timofeev, I., Grenier, F., and Steriade, M. (2001). Disfacilitation and active inhibition in the neocortex during the natural sleep-wake cycle: an intracellular study. *Proceedings of the National Academy of Sciences*, 98(4):1924–1929. Cited on page 71.

[Tononi and Edelman, 1998] Tononi, G. and Edelman, G. M. (1998). Consciousness and complexity. *science*, 282(5395):1846–1851. Cited on page 107.

[Tononi et al., 1994] Tononi, G., Sporns, O., and Edelman, G. M. (1994). A measure for brain complexity: relating functional segregation and integration in the nervous system. *Proceedings of the National Academy of Sciences*, 91(11):5033–5037. Cited on page 19.

[Tort-Colet et al., 2021] Tort-Colet, N., Capone, C., Sanchez-Vives, M. V., and Mattia, M. (2021). Attractor competition enriches cortical dynamics during awakening from anesthesia. *Cell Reports*, 35(12):109270. Cited on page 103.

[Trevelyan et al., 2013] Trevelyan, A. J., Bruns, W., Mann, E. O., Crepel, V., and Scanziani, M. (2013). The information content of physiological and epileptic brain activity. *The Journal of physiology*, 591(4):799–805. Cited on page 83.

[van Vreeswijk and Sompolinsky, 1998] van Vreeswijk, C. and Sompolinsky, H. (1998). Chaotic balanced state in a model of cortical circuits. *Neural computation*, 10(6):1321–1371. Cited on page 24.

[Wang et al., 2000] Wang, H.-S., Brown, B. S., McKinnon, D., and Cohen, I. S. (2000). Molecular basis for differential sensitivity of kcnq and iks channels to the cognitive enhancer xe991. *Molecular Pharmacology*, 57(6):1218–1223. Cited on page 103.

[Wang et al., 1998] Wang, H.-S., Pan, Z., Shi, W., Brown, B. S., Wymore, R. S., Cohen, I. S., Dixon, J. E., and McKinnon, D. (1998). Kcnq2 and kcnq3 potassium channel subunits: molecular correlates of the m-channel. *Science*, 282(5395):1890–1893. Cited on page 102.

[Wang, 1998] Wang, X.-J. (1998). Calcium coding and adaptive temporal computation in cortical pyramidal neurons. *Journal of Neurophysiology*. Cited on page 56.

[Wang, 1999] Wang, X.-J. (1999). Fast burst firing and short-term synaptic plasticity: a model of neocortical chattering neurons. *Neuroscience*, 89(2):347–362. Cited 2 times on page 33 and 103.

[Wang, 2010] Wang, X.-J. (2010). Neurophysiological and computational principles of cortical rhythms in cognition. *Physiological reviews*, 90(3):1195–1268. Cited on page 14.

[Wang et al., 2003] Wang, X.-J., Liu, Y., Sanchez-Vives, M. V., and McCormick, D. A. (2003). Adaptation and temporal decorrelation by single neurons in the primary visual cortex. *Journal of neurophysiology*, 89(6):3279–3293. Cited 3 times on page 24, 56, and 100.

[Ward, 2003] Ward, L. M. (2003). Synchronous neural oscillations and cognitive processes. *Trends in cognitive sciences*, 7(12):553–559. Cited on page 14.

[Waskom, 2021] Waskom, M. L. (2021). seaborn: statistical data visualization. *Journal of Open Source Software*, 6(60):3021. Cited on page 43.

[Williams et al., 1997] Williams, S. R., Toth, T. I., Turner, J. P., Hughes, S. W., and Crunelli, V. (1997). The 'window'component of the low threshold ca2+ current produces input signal amplification and bistability in cat and rat thalamocortical neurones. *The Journal of physiology*, 505(3):689–705. Cited on page 73.

[Wilson and Cowan, 1972] Wilson, H. R. and Cowan, J. D. (1972). Excitatory and inhibitory interactions in localized populations of model neurons. *Biophysical journal*, 12(1):1–24. Cited 2 times on page 23 and 24.

[Yoshida and Alonso, 2007] Yoshida, M. and Alonso, A. (2007). Cell-type–specific modulation of intrinsic firing properties and subthreshold membrane oscillations by the m (kv7)-current in neurons of the entorhinal cortex. *Journal of neurophysiology*, 98(5):2779–2794. Cited on page 103.

[Yue and Huguenard, 2001] Yue, B. W. and Huguenard, J. R. (2001). The role of h-current in regulating strength and frequency of thalamic network oscillations. *Thalamus & related systems*, 1(2):95–103. Cited on page 105.

[Zamora-López et al., 2016] Zamora-López, G., Chen, Y., Deco, G., Kringelbach, M. L., and Zhou, C. (2016). Functional complexity emerging from anatomical constraints in the brain: the significance of network modularity and rich-clubs. *Scientific reports*, 6(1):1–18. Cited on page 19.

[Zerlaut et al., 2018] Zerlaut, Y., Chemla, S., Chavane, F., and Destexhe, A. (2018). Modeling mesoscopic cortical dynamics using a mean-field model of conductance-based networks of adaptive exponential integrate-and-fire neurons. *Journal of computational neuroscience*, 44(1):45–61. Cited 3 times on page 40, 41, and 110.

[Zerlaut and Destexhe, 2017] Zerlaut, Y. and Destexhe, A. (2017). Heterogeneous firing responses predict diverse couplings to presynaptic activity in mice layer v pyramidal neurons. *PLoS computational biology*, 13(4):e1005452. Cited on page 112.

[Zerlaut et al., 2016] Zerlaut, Y., Teleńczuk, B., Deleuze, C., Bal, T., Ouanounou, G., and Destexhe, A. (2016). Heterogeneous firing rate response of mouse layer v pyramidal neurons in the fluctuation-driven regime. *The Journal of physiology*, 594(13):3791–3808. Cited 5 times on page 39, 41, 93, 110, and 112.

[Zhao et al., 2010] Zhao, M., Qiu, W.-H., and Liu, B.-S. (2010). Relative entropy evaluation method for multiple attribute decision making. *Control and Decision*, 25(7):1098–1100. Cited on page 19.

[Ziv and Lempel, 1977] Ziv, J. and Lempel, A. (1977). A universal algorithm for sequential data compression. *IEEE Transactions on Information Theory*, 23(3):337–343. Cited 2 times on page 20 and 78.

[Ziv and Lempel, 1978] Ziv, J. and Lempel, A. (1978). Compression of individual sequences via variable-rate coding. *IEEE Transactions on Information Theory*, 24(5):530–536. Cited 2 times on page 20 and 78.